NUMERICAL SIMULATION OF CRACK PROPAGATION IN REINFORCED CONCRETE DEEP BEAMS

GOH YEE HAO

UNIVERSITI TUNKU ABDUL RAHMAN

NUMERICAL SIMULATION OF CRACK PROPAGATION IN REINFORCED CONCRETE DEEP BEAMS

GOH YEE HAO

A project report submitted in partial fulfilment of the requirements for the award of Bachelor of Engineering (Honours) Civil Engineering
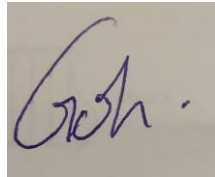
Lee Kong Chian Faculty of Engineering and Science
Universiti Tunku Abdul Rahman

May 2022

DECLARATION

I hereby declare that this project report is based on my original work except for citations and quotations which have been duly acknowledged. I also declare that it has not been previously and concurrently submitted for any other degree or award at UTAR or other institutions.

Signature   :

Name   :   Goh Yee Hao

ID No.   :   1801004

Date   :   13/5/2022

APPROVAL FOR SUBMISSION

I certify that this project report entitled **"NUMERICAL SIMULATION OF CRACK PROPAGATION IN REINFORCED CONCRETE DEEP BEAMS"** was prepared by **GOH YEE HAO** has met the required standard for submission in partial fulfilment of the requirements for the award of Bachelor of Engineering (Honours) Civil Engineering at Universiti Tunku Abdul Rahman.

Approved by,

Signature   :

Supervisor   :   Dr. Woon Kai Siong

Date   :   13/5/2022

The copyright of this report belongs to the author under the terms of the copyright Act 1987 as qualified by Intellectual Property Policy of Universiti Tunku Abdul Rahman. Due acknowledgement shall always be made of the use of any material contained in, or derived from, this report.

ACKNOWLEDGEMENT

I am overwhelmed in all humbleness to acknowledge my depth to my final year project supervisor Dr Woon Kai Siong who made this work possible. Dr Woon did sacrifice his precious time for hosting weekly meeting to provide a platform to us for sharing and discuss the problem we faced. He had given me uncountable precious guidance continuously in the progress of project. From the report skeleton setting, writing skill to modelling techniques of ABAQUS software, he has contributed his invaluable advice and guidance to me.

I would like to express my deep and sincere gratitude to my research moderator, Ir. Woon Yoke Bee. Ir Woon had provide valuable and constructive comments to my study. I would also appreciate to her attention and time paid while listening to my project presentation.

Finally, I am grateful to Mr Sai Yi Soon and Mr Eugene Kok Zhen Yin for their assistance, especially when I faced modelling problem. Their unconditional assistance is one of the most important factors that sustaining me to complete this study.

ABSTRACT

Reinforced concrete deep beam is a beam with a smaller shear span to depth ratio and is popular to be used as shear stress transfer component in high rise buildings. The cracking behaviour analysis of deep beam is a study aspect with high research value, but experimental analysis for cracking behaviour analysis can be costly. ABAQUS software helps simplify the parameter study of cracking behaviour for deep beam through Finite Element Analysis (FEA) method. In this study, an experimental result of deep beam published by Zhang and Tan (2007) was adopted for numerical modelling. Although failure load for numerical result reflected 20.6 % higher than experimental result, both results resembled well for the trend of the load-deflection curve and proven the reliability of numerical modelling technique. The verified model was used for performing the study of the parameter that affect the deep beam behaviour in term of strength and crack, which included shear span to depth ratio, longitudinal reinforcement diameter and position of shear link. The load-deflection curves were plotted to evaluate the strength behaviour of deep beam with changing of parameter while the von Mises stresses contour, plastic strain magnitude diagram and concrete tension damage contour were captured to evaluate the crack propagation and the changes of crack pattern with changing of parameter. As the result, smaller shear span to depth ratio showed an obvious enhancement ranging from 3.95 % to 10.13 % for deep beam shear capacity and less severe crack. Moreover, changing longitudinal reinforcement diameter brings very little enhancement effect with not more than 10 % in shear capacity and it decreases to 1.09 % when bar diameter goes beyond 20 mm, only the flexural behaviour of deep beam is affected instead of shear behaviour. Lastly, position of shear link is sensitive to deep beam behaviour. When it placed beyond the concrete compressive strut zone, it shows 7.6 % reduction in shear capacity as compared to control beam, and it shows 1.27 % enhancement when placed within the region. The reliability of numerical analysis for deep beam behaviour is proven and three insightful findings to different parameters that affecting deep beam behaviour are contributed.

TABLE OF CONTENTS

LIST OF TABLES

LIST OF FIGURES

LIST OF SYMBOLS / ABBREVIATIONS

ε_{cr} average tensile strain,mm/mm

ε strain, mm/mm

ε' ultimate strain, mm/mm

θ_s angle between the concrete compression strut, °

μ viscosity parameter

σ tensile stress on the descending limb, N/mm^2

σ_{t0} peak tensile stress, N/mm^2

Φ dilation angles

ω concrete density, kg/m^3

A_h areas of horizontal web reinforcement, mm^2

A_v areas of vertical web reinforcement, mm^2

E Young Modulus, GPa

E_c concrete Young Modulus, MPa

$K\ (K_c)$ ratio of the second stress invariant to the tensile Meridian

b_w width of deep beam, mm

d_c concrete compression damage factor

d_t concrete tensile damage factor

e   eccentricity

f'_c concrete compressive strength, N/mm^2

f_{bo}/f_{co} ratio of initial equi-biaxial compressive strength to initial uniaxial compressive strength

f'_c ultimate concrete compressive cylinder strength, MPa

f_{yh} yield strength of horizontal reinforcement, N/mm^2

f_{yv} yield strength of vertical reinforcement, N/mm^2

v concrete efficiency factor

w_s width of prismatic strut, mm

AFRP   aramid fibre reinforcement polymer

CDP   concrete damage plasticity

CFRP	carbon fiber reinforced polymer
FEA	finite element analysis
FEM	finite element method
FRP	fiber reinforced polymer
GFRP	glass fiber reinforced polymer
NSM	near surface mounted
RC	reinforced concrete
STM	strut and tie method

LIST OF APPENDICES

CHAPTER 1

INTRODUCTION

1.1   General Introduction

A building structure is built up with several components like a beam, column, and slabs etc. These components play an important role to ensure the integrity of the building structure and load transfer medium. The deep beam is one building component that can usually be found in a mega building structure like a high-rise building (Kim, Lee and Shin, 2011). The deep beam is a beam with a clear span that is four times lesser than overall member depth or a shear span to depth ratio less than 1.0 (Mohamed, Shoukry, and Saeed, 2014). According to Adinkrah-Appiah *et al* (2014), the lesser the span to depth ratio, the higher the shear strength. The characteristic of high shear strength makes the deep beam became a popular component of high rise buildings for playing a role in transfer girders, wall footings, foundation pile caps, floor diaphragms, and shear walls (Mohamed, Shoukry and Saeed, 2014.).

The normal design procedure which according to the Euler-Bernoulli hypothesis is not applied to deep beam design as this theory is determining the shear deformation and stress concentration under a condition that the transverse section remains a plane before and after the bending process, which also means the transverse shear is zero throughout bending process (Adinkrah-Appiah *et al*, 2014). It is completely different for deep beams as stress distribution for the deep beam is non-linear and there have a deformation happen in the transverse section.

The region of that plane remains unchanged and strain over the depth occurs linearly throughout the bending process is defined as B-region (Beam region), whereas the region that has a variety of strain is defined as D-region (Disturbed Region). D-region occurs at the part that has an abrupt change in geometry or the location of concentrated load (Shah, Haq, and Khan, 2011). D-region can always be found in the deep beam as it deals with a concentrated load. Since deep beam cannot be designed by linear elastic theory, the ACI code stated that deep beam should be designed via non-linear analysis or Strut-Tie model (STM) (Noh, Lee, and Lee, 2006). One of the methods for non-linear

analysis is the finite element method (FTM). The software that had been used for deep beam analysis ABAQUS, ANSYS, and CAST etc. ABAQUS and ANSYS are analysing under FTM while CAST is based on STM theory. The usage of software helps a lot on the tedious calculation step and perform modelling to give the user a better view of the analysis result.

1.2   Importance of the Study

A deep beam is a very useful element for the base support of the high rise building or tall building. Deep beam also plays a role in the load transferring and supporting for offshore gravity type structures (Chin and Doh, 2015). The internal structure of the deep beam can affect the reliability and the safety of the structure greatly as it is a critical structural element. According to Harsha and Raju (2019), the most common failure that happened to deep beams was the shear failure. The shear tension failure occurs due to a reduction in bond strength at flexural reinforcement while there is a horizontal cracking thus the load distribution among steel and concrete will be disturbed. When the reinforced bar is yielded but the load cannot be distributed along the beam, concrete will reach its ultimate strength and lead to crushing of concrete region, called shear compression failure.

From the research of Adinkrah-Appiah *et al* (2014), it is difficult to adopted the elastic solution to analyse the behaviour of deep beam after a crack occurred (i.e. diagonal crack). After loading, compressive stress and the shear stress will form a web pattern of complex stress field due to the small value of sectional area over depth ratio. This stress field makes a special arch behaviour to the deep beam which is different from an ordinary beam. Adinkrah-Appiah *et al* (2014) also mentioned that the shear strength of the deep beam may be 2 to 3 times smaller than the actual value if adopting to Euler-Bernoulli hypothesis for calculation. There will have major redistribution of strain and stress when the crack of the deep beam starts to elaborate, non-linear analysis become a vital measure to tackle this kind of analysis and stress flow prediction.

This phenomenon shows that the behaviour shear stress and strain distribution inside deep beam have a close relationship with the crack propagation. Engineers require to study the stress-strain distribution of deep beam to propose the reinforced design for crack control. ACI 318-14, Section

9.9.3.1 stated that the minimum reinforcement needs to provide for the aim to control the width and propagation of the inclined crack. By studying the stress-strain distribution of deep beams, an engineer may even try to propose an innovative design for deep beam reinforcement. For example, Metwally (2014) adopted the non-linear analysis to check with the deep beam with Glass Fibre Reinforce Polymer which is a newly introduced reinforcing method in terms of load-deflection behaviour, ultimate load capacity, crack pattern by using ABAQUS software and compared the result with the experimental result.

However, there is a downside for deep beam analysis to be carried out through experiments. An experimental test for deep beam analysis can be a costly project. It required a high-capacity test setup, more instrumentation and higher human and financial resource to simulate a scenario that is similar to real cases. Huge cost and critical experiment setup requirements make it infeasible to observe the behaviour of deep beam by experimenting (Rai, 2021),

Therefore, an alternative way to observe deep beam behaviour under loading needs to be identified. In this study, a numerical analysis will be carried to observe crack propagation of deep beam by using ABAQUS software and check the reliability of this method to replace the conventional experimental observing method.

1.3   Problem Statements

The cracking pattern of the deep beam is an essential topic that researcher wishes to investigate. In these few years, there are some of studies have been carried out on the cracking behaviour of deep beams with the improvement of the reinforcement method. Shahbazpanahi *et al* (2021) proposed the carbon-fibre-reinforced polymer plate strengthening method to deep beam in their research work. Meanwhile, Chinnaraj (2015) held the experiment of deep beam crack analysis with the strengthening effect of fibre-reinforced polymer (FRP) wrapping. These studies provide the reader with the possibility of changing the reinforcing method by analyzing the cracking pattern. However, there are quite less of number for the research work for crack propagation analysis on ordinary deep beam. Other than that, the parameter which affects the cracking behaviour and shear strength is also an essential consideration while performing cracking propagation research. Hassan, Medhlom and Hatem (2018) and Zhang *et al*

(2020) investigated how shear span to depth ratio affect to crack pattern while Mohamed, Farghaly and Benmokrane (2014) and Birrcher *et al.* (2014) investigated the importance of web reinforcement for deep beams against cracking. In these expert studies, different variables are proven to affect deep beam crack development. The crack propagation of an ordinary reinforced deep beam should be investigated in-depth and different variables should be checked for an integrated deep beam cracking propagation study.

Moreover, the finite element method has become popular for deep beam analysis. Some professionals are using software that complies with the finite element method to perform their deep beam analysis. Rai (2021) had performed finite element modelling by using the CDP model available in Abaqus while Ghoraba, El-Zoughiby and El-Metwally (2017) compared the non-linear analysis result with Strut-Tie method which was introduced by many codes like ACI 318-14 code, the Eurocode 2, and the Egyptian code of practice ECP 203. The study about the stimulation for cracking development of deep beam showed its worthy for extra exploration and depth discovery. The reliability of numerical software for deep beam analysis is still a subject of research value and the usefulness of special analyzing procedures performed by numerical software will have a further exploration in this study.

1.4   Aim and Objectives

This report aims to perform a numerical simulation of crack propagation of the deep beam. The study objectives are listed as follow:

i.   To verify the numerical result obtained from the developed model with existing experimental results obtained from the literature.

ii.   To simulate crack propagation in different reinforced concrete deep beam by using numerical method.

iii.   To investigate the parameter that affects the deep beam behaviour including the shear span to depth ratio, longitudinal reinforcement diameter and shear reinforcement position.

1.5   Scope and Limitation of the Study

The scope of this study involves the Finite Element Analysis (FEA) method to study the cracking behaviour of the RC deep beam. An FEA software, namely ABAQUS software is adopted to perform the simulation of RC deep beam by applying monotonic load on top of it. There are three sets of data specimens to be tested and to be explored the behaviour of deep beams under different parameter changes. The first batch will test for the shear span to depth ratio which includes the reference beam, control beam and three tested specimens. The second batch will test for the longitudinal reinforcement which includes the control beam and four tested specimens. The third batch will test for the position of shear stirrups which includes control beam and four tested specimens. The other scope and limitation are summarized as below:

     i.   The concrete type use for this study is C25/60 with cylinder concrete strength of 25.9MPa.

     ii.   All the specimen dimension is set as 350 mm (depth) x 80 mm (width) x 1330 mm (length).

     iii.   The support condition is pinned for the left-hand side support and roller support for the right-hand side support.

     iv.   There are two loading points on the top of specimens and the loading mode is monotonic.

1.6   Contribution of Study

This report had study the reliability of the numerical software for deep beam cracking behaviour study and investigation. Moreover, the three main parameters checking for deep beam strength and cracking behaviour showed some of the useful information helps for deep beam design, which gives ideas to deep beam design enhancement.

Three parameters check performed in this study concluded that shear span to depth ratio plays vital role on deep beam strength capacity and brittle behaviour. Secondly, for the increasing the reinforming bar diameter which is a conventional way for enhancing a flexural beam performance did not show efficiency effect on deep beam performance. Lastly, the position of shear links placed inside deep beam is very sensitive to deep beam shear capacity. By

following these useful conclusions, it can help to save cost for an effective design and also proposed a targeted approach for deep beam design.

Moreover, the proven reliability of numerical simulation way of study enables for the future testing of different parameters or different scenario simulation for deep beam study. It can help to save up huge cost and time for performing conventional experimental study. Therefore, any other innovative architecture design for high-rise buildings or highway bridge can be proposed and its construability can be granted.

1.7   Outline of the Report

Chapter 1 gives some general idea of the deep beam introduction. It mentioned the importance of study and identified out the problem statement which decided the direction of this study report. The aim and objective to be achieved through this report has also been mentioned together with the scope and limitation of this study report.

Chapter 2 contains the detailed review to the literature which provided useful information and guideline to this study. It contained the reviewed study of parameter that affecting the deep beams behaviour and the numerical modelling techniques and discussion written by expert in the past.

Chapter 3 outlines the skeleton for the step of performing the modelling and the detailed parameters to be input into ABAQUS software. It also consisted of the specimen specification for the reference beam, control beam, and test beams.

Chapter 4 discuss the results that captured from the ABAQUS software in term of load-deflection curve, von misses stress contours, PEMAG diagrams, and concrete tension damage contours. The relationship between the result and the factor that affected the result has also been discussed in detail.

Chapter 5 concludes all the findings that extracted from the discussion in the Chapter 4. This chapter also evaluate the objective achievement that led toward the successful completion of study. Some of the recommendations are provided in this chapter for future research purpose.

CHAPTER 2

LITERATURE REVIEW

2.1   Introduction

For a conventional RC beam, the beam is a component that is used to transfer the loading from slab to the column then straight to the earth strata. Thus, the bending behaviour for a beam is more concerned as the upper part of the concrete element is experiencing the compression force while the bottom part of the reinforcement bar is experiencing the tension force. This action behaviour is caused by the distributed loading from the slab. However, it is complexly different from a deep beam which is used as the transfer girder to transfer the huge concentrate load for a tall building. Shear behaviour is to be more concerned over flexural behaviour in deep beam analysis. The shear reaction will create the diagonal tension and compression reaction hence brings the crack (Reddy, Kumar and Monica, 2019). The expert had performed the research work in the aspect of analysing deep beam behaviour. The most common research is about the Strut-Tie model (STM) and Finite Element Analysis (FEA).

The Strut-Tie model is an analysis method that works under the concept of a virtual truss system. As mentioned in Chapter 1, the D - region within the deep beam possesses the behaviour of complex internal stress flowing and it is to be idealized to a simple truss system under the STM (Ismail, Guadagnini and Pilakoutas, 2018). The STM comes with three components which are struts, ties and nodes. The concrete component which handles compressive stress fields acts like struts inside the model, while the reinforcing steel bar which handles tensile stress fields acts as a tie inside the model. The intersection point of strut and tie axes is defined as nodes (Tuchscherer, Birrcher and Bayrak, 2011). The hydrostatic nodal zone is a type of node that all the load is applied perpendicularly to the loaded surface of the node (ACI 318-14, 2014).

The type of hydrostatic nodal zone can be defined into three types which are C-C-C nodal zone, C-C-T nodal zone and C-T-T nodal zone. These types of the nodal zone are categorized by the combination of the stress direction, "C" denotes the compressive stress and "T" denotes the tensile stress. To achieve an equilibrium state, at least three stresses needed to act on one nodal

zone. By checking with the force acting to the nodal zone, the behaviour of the deep beam can be checked. According to Wahlgren and Bailleul (2016), strut-tie model show some characteristic such as:

- concrete tensile strength and minimum reinforcement is neglected
- cracking behaviour cannot be observed
- load for starting of crack cannot be identified.

Hence, the strut-tie model may not be a suitable way for crack propagation analysis. Meanwhile, an alternative way is the FEA software which analyses the model piece by piece able to study the behaviour of an object in a detailed way. The reliability of FEA has been proved in several journals by comparing the result with the experimental result.

Some of the literatures have been reviewed in this chapter to evaluate the knowledge of deep beam behaviour for a better view in researching the crack propagation of deep beams by using numerical methods.

2.2   Crack Propagation of Deep Beam in Different Conditions

Crack propagation of deep beam is an essential study aspect due to the usefulness of deep beam is getting more concern in several years, especially for the urban city which high rise building is the first choice of developer. Expert has investigated the crack propagation of deep beam in different kinds of scenarios including the ordinary deep beam, deep beam with special reinforcement and repaired pre-crack deep beam to explore the crack behaviour of deep beam under a different aspect.

2.2.1   Common Deep Beam

Suresh and Kulkarni (2016) studied the behaviour of reinforced concrete deep beam in terms of its crack pattern, deflection and failure load by experiment and compared the result with non-linear modelling method. Variable parameter for this experiment was the tension reinforcement ratio and the concrete grade. As the result of the crack pattern, the first crack that appeared on the test specimen was a flexural crack that propagated from the bottom of the beam and reached 1/3 depth of beam depth vertically. When the applied load reached 42 % of failure load, a diagonal crack appeared from the support and linked to the

loading point. The crack pattern for specimens with 0.43 percentage of reinforcement and concrete grade with 25MPa are shown in Figure 2.1.

Figure 2.1: Crack Pattern of The Specimen (Suresh and Kulkarni, 2016)

Salamy, Dashlejeh and Arabzadeh (2005) studied the behaviour of deep beams through experiment and analytical methods. The aim of the study included the failure mode, crack patterns and the deflection of the beam. The test specimens possess various dimensions, shear to span ratio, reinforcement ratio and presence of stirrup. As the result, the failure mode of the deep beam was observed and categorized into two main patterns. They were flexural failure and shear failure while the shear failure can further be separated into three versions, which were diagonal tension failure, shear compression failure and shear proper or compressive failure of sturts.

- Tension failure: The diagonal tensile crack led to flexural failure in the compression zone.
- Shear compression failure: Concrete crushing happened in the compression zone which was caused by the main diagonal crack.
- Shear proper or compressive failure of sturts: The deep beam with low shear to span ratio (normally about a/d <1.5) and caused the arch action in deep beam to carry both flexural capacity and shear capacity, sturt axes cannot sustain such load and broke down.

In the aspect of the crack pattern, the experiment result showed the cracking in the direction of longitudinal and was initiated from the support linked toward the loading point diagonally. The experimental crack pattern of specimen beam 14 which with 1.5 spear span to depth ratio is shown in Figure 2.2.
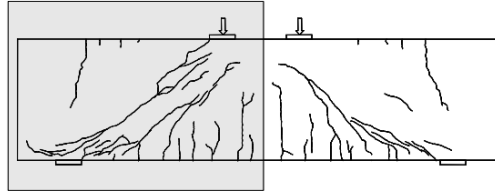
Figure 2.2: Beam 14 With Shear Failure Mode (Salamy, Dashlejeh and

Arabzadeh, 2005)

2.2.2   Deep Beam with Innovative Reinforcement

The deep beam is more critical of shear resistance ability. The special reinforcement method will give a different strength and different crack patterns to the deep beam as the reinforcement changed the behaviour of the deep beam. The shear strength capacity of the deep beam had become an important research target for experts. As technical skills getting more advance, various innovative strengthening methods had been proposed to improve the shear capacity of the deep beam to ensure the sufficient shear strength of the deep beam during its service life.

Chen *et al* (2019) performed research about the shear mechanism and shear strength of a Fibre Reinforced Polymer reinforced concrete deep beam. This study aims to identify the effect on to shear strength of deep beams due to bond behaviour and axial stiffness of FRP and reinforcing bar. A theoretical checking of mechanism was provided as well based on the Cracking Strut and Tie Model (CSTM). The FRP reinforced specimen was chosen for the comparison with steel reinforced deep beam are the G8N8 which with web reinforcement. As the result, it verified that bond behaviour has no or little effect on the beam ultimate carrying capacity. The load-deflection graph of G8N8 with different bond conditions simulate by ATENA is shown in Figure 2.3.
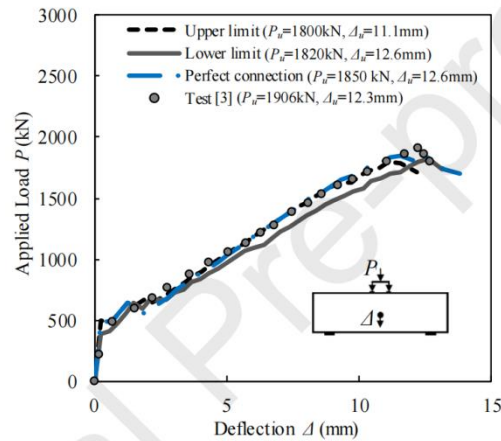
Figure 2.3: Deflection Behaviour For Specimen With Different Bond
Conditions (Chen et al, 2019)

From the graph, it is obvious all the bond conditions give a similar load-deflection pattern. Meanwhile, the stiffness of reinforcement was tested, and it showed a very significant different load-deflection pattern for different stiffness. Two specimens reinforced by steel bar SC1 and SC2 possess different reinforcement ratio stiffness 1.24 % and 0.32 % respectively. This is to show different reinforcement stiffness, steel bar with a modulus of 200GPa made SC2 possess the same stiffness ratio with G8N8 FRP reinforced specimen. These specimens SC1, SC2 and G8N8 were tested under the same bonding condition by using ATENA and their load-deflection graph is shown in Figure 2.4.
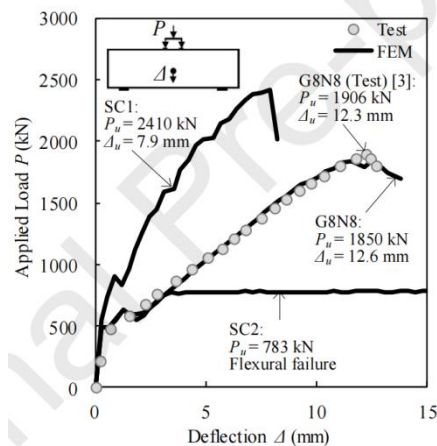
Figure 2.4: Deflection Behaviour For Specimen With Different Reinforcement
(Chen et al, 2019)

For SC1, as the reinforcement stiffness is larger than G8N8, the shear strength is larger than G8N8. While SC2 with the same reinforcement stiffness as G8N8, it has the same load-deflection curve compared to G8N8, but it drops dramatically after flexural failure due to a lower ultimate tensile strength and reinforcement ratio. By observing the crack width of the SC1 specimen in Figure 2.5, SC1 showed a narrower crack width during the failure load of G8N8. The higher axial stiffness and the activation of the interlocking mechanism of aggregate were concluded to be the reason for higher shear resistance and smaller crack width. In conclusion, under the same amount of reinforcement ratio, reinforcement methods with higher stiffness can provide higher shear strength and narrower crack width.
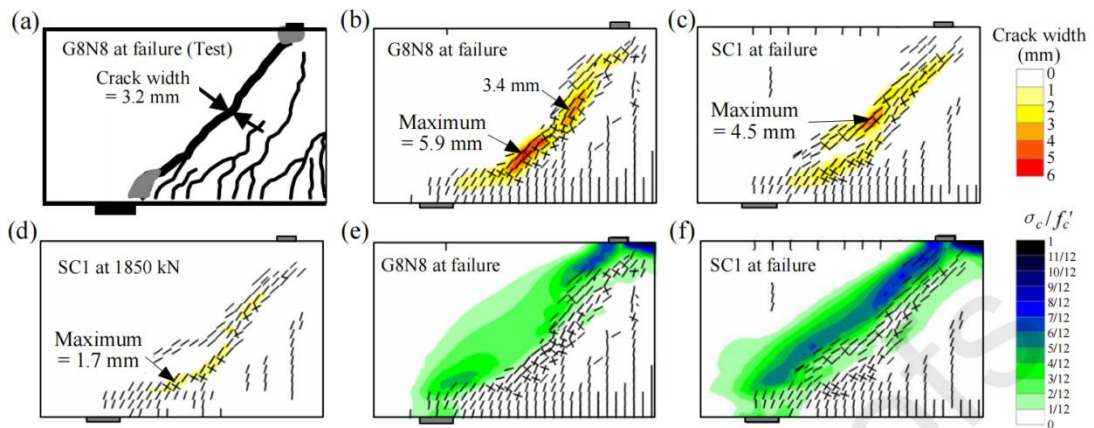
Figure 2.5: Crack Width of G8N8 And SC1 Under Loading 1850kN(Chen et al, 2019)

Abdul-razzaq, Ali and Abdul-kareem (2017) examined the usefulness of the strengthening method to a deep beam with web openings by using steel plates. All the specimens are with an opening on their shear span except for the reference beam. Three parameters to be tested including the shape of the opening, strengthening effect of steel plate and stud connectors. Specimens were tested under a four-point bending system as shown in Figure 2.6.

Figure 2.6: Loading System For The Experimental Test (Abdul-razzaq, Ali
and Abdul-kareem, 2017)

Testing specimen with the opening was proven to have lesser strength compared to references beam without opening the specimen with a horizontal opening that interrupts the inclined strut tends to give the largest losses ultimate strength of 31.7 % compared to other specimens and it showed that inclined compressive strut is the main control factor to the strength of the beam. In addition, the four corners of the opening were experiencing a larger stress effect as cracking and failure are mostly began at that region, cracking paths are shown in Figure 2.7.
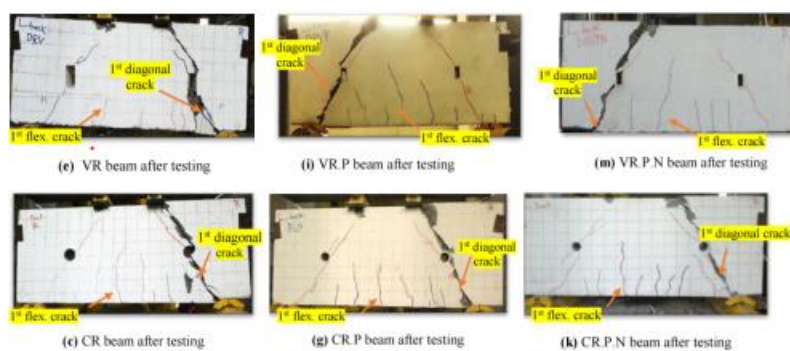
Figure 2.7: Crack Pattern For Different Test Specimens (Abdul-razzaq, Ali
and Abdul-kareem, 2017)

This finding proved that circular openings specimen with no corner had the less ultimate strength loss of 18.3 % compared to other specimens. Specimens strengthen with steel plates possess a higher ultimate shear strength compared to reference specimen by 9 %, 9.3 %, 12 % and 13.2 % for horizontal rectangular, square, vertical rectangular and circular openings respectively. Other than that, the main diagonal crack of the strengthening specimen was not

directly crossing through the opening as a reference specimen while it only propagated around the openings. The combined use of the welding stud connector even gave a higher ultimate shear strength as the stud intercepted to the cracking path of the main diagonal crack. Increment of ultimate shear strength for specimens welded stud connector together with the use of steel plates were 14.3 %, 16.9 %, 17.8 %, 26.9 % for horizontal rectangular, square, circular, and vertical rectangular openings, respectively.

Ibrahim, Wakjira and Ebead (2020) investigated how the Near-Surface Mounted glass Fibre Reinforced Polymer (NSM-FRP) strip helps for shear strengthening of RC deep beam with weak shear strength. The behaviour of the beam affected by the number of FRP strips and steel stirrups reinforced at critical shear span (CSS) were investigated, as well as the configuration of reinforcement interaction at CSS (aligned or unaligned). The study concluded that NSM-FRP were improved the load-carrying capacity greatly ranging from 28.8 % - 55.8 % for strengthening beam which the increased number of strips brought an increment of the ultimate capacity. A specimen without stirrups at CSS possess a better improvement to compare to a specimen with stirrups as stirrups increase the load-carrying capacity hence reduce the relative gain. Moreover, the unaligned configuration of FRP and stirrup gives a better load carrying capacity due to the larger coverage area of unaligned configuration and the area with no reinforcement is lesser. For the cracking aspect, all the specimens were showed a diagonal crack under shear failure. The strengthening specimens gave a smaller crack width compared to the reference beam. For specimens with unaligned configuration possessed a narrower crack width compared to aligned configuration. The crack pattern of the specimens is shown in Figure 2.8 and Figure 2.9. In conclusion, NSM FRP strengthening measure increased ultimate deflection, increased energy absorption and decreased crack width for deep beam.

Figure 2.8: Crack Pattern For Specimens With Only FRP Reinforced (Ibrahim, Wakjira and Ebead, 2020)
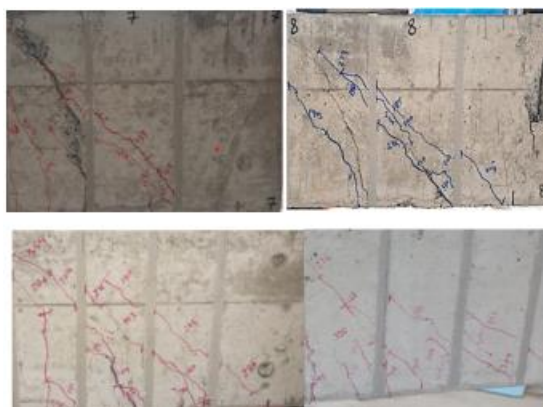
Figure 2.9: Crack Pattern For Both FRP and Stirrup Reinforced (Ibrahim, Wakjira and Ebead, 2020)

2.2.3 Repaired Pre-cracked Deep Beam

Some of the experts also investigated the pre-cracked deep beam behaviour. Innovative repair and rehabilitation techniques were adopted in several to ensure the reliability of the technique in the aspect of crack controlling for deep beam reinforcement. This kind of investigation study has been done experimentally to explore the crack behaviour of a pre-cracked deep beam with an innovative reinforcement design.

Osman *et al* (2017) tested experimentally the behaviour of pre-cracked deep beam with circular opening reinforced with aramid fibre reinforcement polymers (AFRP) and epoxy resin. There were seven specimens (B1-B7) tested under the four-point bending machine including two control beams with and without opening (B1 & B2). The B4 to B7 specimens were loaded initially to simulate the pre-crack situation while the level of preloading ratio to the capacity of control beam B2 for group B4 & B5 and group B6 & B7 were 50 % and 70 % respectively. The result showed that specimen after repairing with AFRP obtained a narrower crack width with a reduction ranging from 25.6 %

to 82.7 % as compared to control specimen B2. Crack width results are shown in Figure 2.10. The crack pattern for repaired specimens also changed to concrete crushing and FRP peeling except B4 specimen with FRP peeling and shear failure. Crack patterns for pre-cracked specimens and control specimens are shown in Figure 2.11. By comparing different pre-crack levels, the larger the pre-crack level, the lower the ultimate load capacity. In conclusion, the application of epoxy resin helps to improve the pre-cracked deep beam behaviour in terms of crack width and load carrying capacity together with changes of failure pattern.
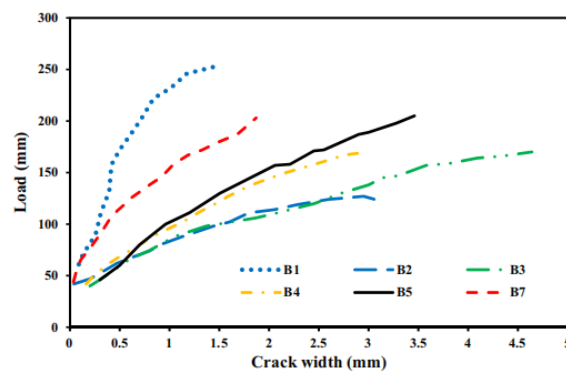
Figure 2.10: Crack Width of Specimens With Different Reinforcement
Conditions Under Different Loading (Osman et al, 2017)
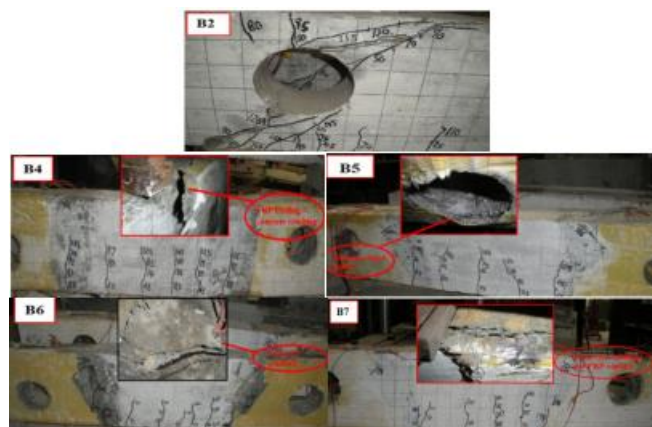
Figure 2.11: Crack Pattern of The Different Deep Beams With Different
Reinforced Methods (Osman et al, 2017)

Ali, Mezher and Raheem (2015) investigated the effectiveness of using Near Surface Mounted (NSM) Carbon Fibre Reinforced Polymer (CFRP) for rehabilitation of pre-cracked deep beam. The pre-cracked specimens were

applied with different FRP reinforcement spacing as RN90-15 & RN45-15 were spaced at 150 mm while RN90-10 & RN45-10 were spaced at 100 mm and inclination of reinforcement configuration where RN90-15 & RN90-10 were inclined at 90 degrees while RN45-15 & RN45-10 were inclined at 45 degrees. As the result, all the reinforced pre-cracked specimens gave a better ultimate load capacity compared to the control beam (C). The specimen RN45-15 had the best load carrying capacity and it showed an increment of 17.1 % compared to the control beam. The result of crack width against load graphs for RN45-15 and control specimens are shown in Figure 2.12. The epoxy resin and FRP reinforcement controlled the shear failure until the occurrence of splitting of concrete bonding as all cracks were happened within epoxy resin area. Meanwhile, the RN90-10 performed worse than control specimen and this claim that 90 degrees of inclination may not be a good, reinforced angle. The closer spacing reduced the ultimate strength of the beam rather than enhance the performance of NSM CFRP as in the result of RN45-10. Both the crack width in different loading stages is shown in Figure 2.13 and Figure 2.14.
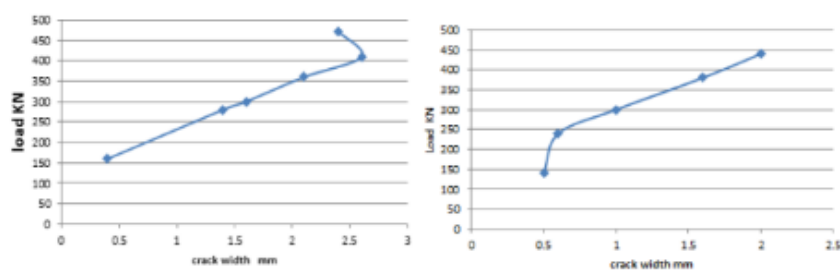
Figure 2.12: Crack Width Against Loading Graph for C Specimen (Left) and RN45-15(Right) (Ali, Mezher and Raheem, 2015))
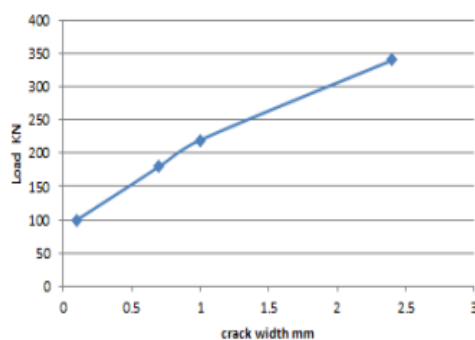
Figure 2.13: Crack Width Against Loading Graph for RN90-10 (Ali, Mezher and Raheem, 2015)
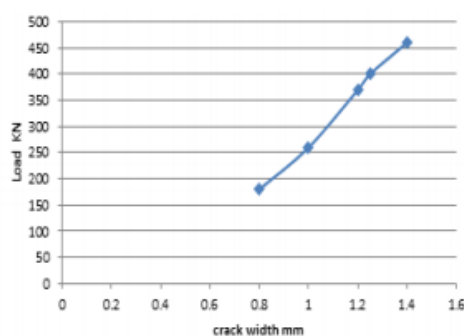
Figure 2.14: Crack Width Against Loading Graph for RN45-10(Ali, Mezher
and Raheem, 2015)

2.3   Parameters Affect the Crack Propagation

The deep beam is always applied to the critical loading condition environment
such as the support of the bridge or the transfer grinder at the base floor of high-
rise buildings and this makes cracking happened in deep beam become a serious
concern to engineers. It is an important task for an engineer to identify the cause
of crack happened in deep beam and the factor affecting the crack propagation
to ensure the safety of the deep beam during its service life.

2.3.1   Shear Span to Depth Ratio

Different values of the span to depth ratio will affect the crack propagation of
the deep beam greatly due to the reason that one of the main determining factors
to define a deep beam is the span to depth ratio. The lesser the span to depth
ratio the beam is known to be "deeper". There are several codes such as IS: 456-
2000 clause-29, ACI-318 clause 10.7.1, BS 8110, set the standard value for span
to depth ratio or the beam height to classify deep beam and normal flexural beam.

Hassan, Medhlom and Hatem (2018) performed research on
identifying the behaviour of deep beams by varying the span to depth ratio of
deep beams. Six deep beams in different values of span to depth ratios varying
from 1.0 to 0.276 were chosen for analysis. Even though the beam dimension
was the same for all specimens, the shear span is varying by adjusting the
position of two points support. As the result, both the first cracking load and the
ultimate load were increased following the decreases of the ratio. Moreover, the
failure mode also changed from flexural failure to diagonal failure when the

span to depth ratio reached 0.552. In Figure 2.15, the crack pattern of six specimen beams is shown. The first three beams (S1 to S3) are with the diagonal crack from the compression zone to toward support but did not reach the support in actual and the flexural crack at the bottom of the beam tension zone are obvious. On the other hand, the other three beams (S4 to S6) are only with the diagonal crack from the inner side of support toward the compression zone and there is no occurrence of flexural crack at the bottom part of the beam.
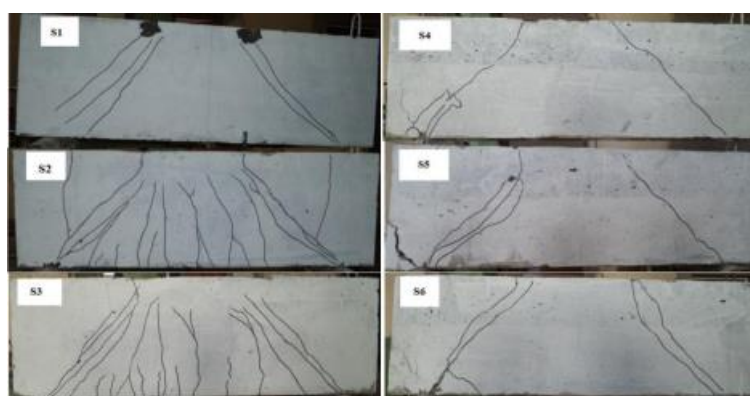
Figure 2.15: Crack Pattern of Specimens (Hassan, Medhlom and Hatem, 2018)

Zhang *et al* (2020) studied the shear capacity performance of high strength reinforced concrete deep beam by varying various parameters and span to depth ratio was one of the parameters. The first three out of eight specimens were designed with different shear span to depth ratios λ of 0.3, 0.6, 0.9 respectively and all other parameters were remained the same. These three specimens are namely MDB1, MDB2, MDB3 and their reinforcement detail are shown in Figure 2.16. For the failure mode result, the cracking load and the ultimate for three specimens were decreasing while the mid-span deflection is increasing with increasing of shear span to depth ratio. All the failure modes for smalls shear span to depth ratio are concluded to be diagonal compression and the failure pattern are shown in Figure 2.17. It is obvious when the shear span to depth ratio increases, the happened of flexural crack increases. This research paper concluded the decreases of cracking load and ultimate load for MDB2 and MDB3 were due to the ineffective of tied-arch action. When the distance between the loading point and the support point is larger (shear span increase

while the beam depth remained constant), the angle of the diagonal concrete strut to the longitudinal axis which for the arch mechanism is smaller. This reduces the effectiveness of arch action that allows the internal stress redistribution.
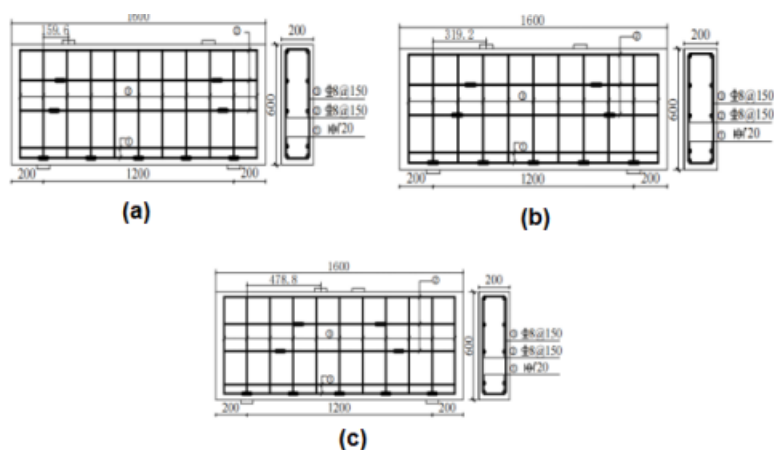
Figure 2.16: Specimens' Detailing: MDB1(a), MDB2(b) and MDB3(c)
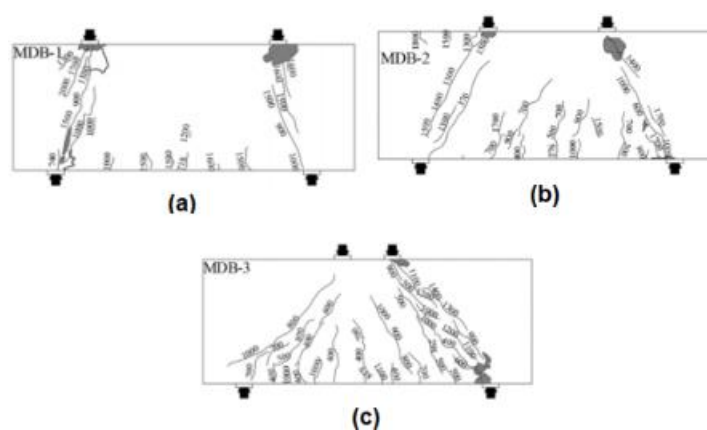
(Zhang et al, 2020)

Figure 2.17: Specimens' Crack Pattern: MDB1(a), MDB2(b) and MDB3(c)

(Zhang et al, 2020)

Kim, Lee and Shin (2011) checked the behaviour of deep beam under bending load and axial load with different shear span to depth ratios. Shear span to depth ratios of 0.5, 1.0, 1.5, were applied to three axial loading conditions which are 0kN, 235kN and 470kN while the bending load of 30kN remained constant to all 9 pieces of specimens. The result showed when two specimens with the same value of 0.5 shear span to depth ratio were subjected to loading,

the specimen with 470kN (5C2) loading encountered a serious crushing compared to the specimen with 235kN (5C2). However, when increasing the shear span to depth ratio (10C1 & 15C2), the failure mode becomes the shear failure instead of crushing of concrete and the crack path was started from the support point to the loading point in a diagonal direction. The failure mode of specimens is shown in Figure 2.18. The authors have concluded that when the deep beam's shear span to depth ratio is small enough, the deep beam will fail in concrete crushing before the shear failure when subjected to a large axial load.

Figure 2.18: Specimens' Failure Mode : 5C1 (Top left), 5C2 (Top right), 10C1 (Bottom left) and 15C2 (Bottom right) (Kim, Lee and Shin , 2011)

2.3.2 Web Reinforcement

Web reinforcement needs to be provided to ensure the sufficient shear strength of the beam. The deep beam is a concrete structure that dealing with a large, concentrated load which makes the shear strength of the deep beam is more important than the flexural support behaviour. The web reinforcement is important for achieving a higher ultimate load capacity and reduce the crack width for deep beams. The vertical web reinforcement increases the ultimate load obviously while horizontal web reinforcement only shows its effect for a beam with web openings (Lafta and Ye, 2016). The effect of web reinforcement on the strength and crack pattern of the deep beam had been studied by experts.

Ibrahim, Wakjira and Ebead (2020) studied the behaviour of Glass Fibre Reinforcement Polymer (GFRP) reinforced deep beam. The presence of web reinforcement is the main concern in this research. Four different web reinforcement configuration tested specimens were without web reinforcement

(G8-8), with vertical web reinforcement only (G8-8V), with horizontal reinforcement only (G8-8H), with both vertical and horizontal reinforcement (G8-8VH). All the specimens were reinforced with 25.4 mm diameter GFRP. The detailing of specimens is shown in Figure 2.19. The result showed that the cracking started for about 20 % -30 % of the ultimate strength for all specimens. The crack patterns were similar among all the specimens which was some vertical flexural crack at the first loading stage and follow with diagonal crack linked among the loading point and the edge of support (within the shear span) during the second loading stage. However, the flexural crack was lesser with a smaller width for specimens G8-8. The crushing of concrete was only happened around the loading point and did not penetrate through specimens for specimens G8-8 while the specimens with web reinforcement (G8-8V, G8-8H, G8-8VH) possess the crushing of concrete all along the strut. The failure pattern of all specimens is shown in Figure 2.20. This shows that web reinforcement contributed a significant distribution of the stress along the strut. Moreover, the specimen G8-8H possessed a smaller diagonal crack width with a larger load capacity compared to G8-8 while G8-8V and G8-8VH possessed the smallest diagonal crack width with a larger load capacity. The load versus crack width graph is shown in Figure 2.21. It concluded that web reinforcement can give a larger load capacity with a smaller diagonal crack width while vertical web reinforcement is more effective compared to horizontal reinforcement.
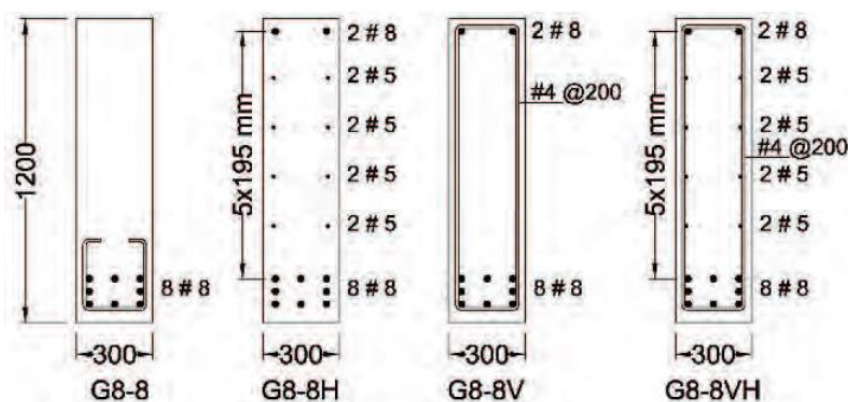
Figure 2.19: Detailing Pattern for GFRP Reinforced Specimens (Ibrahim, Wakjira and Ebead, 2020)
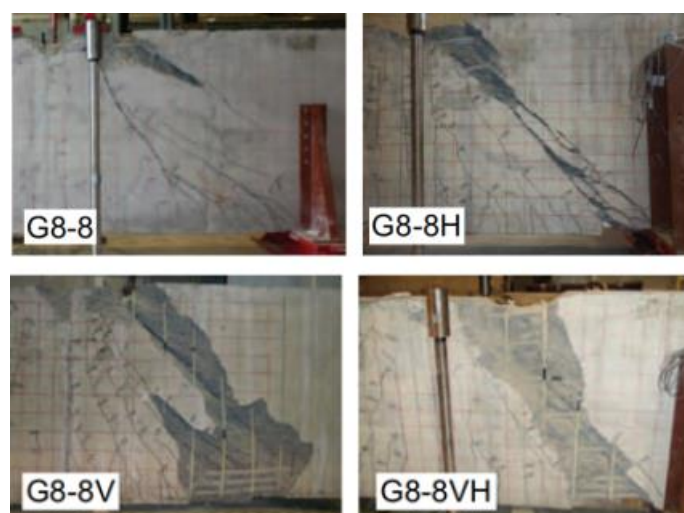
Figure 2.20: Experiment Result for Failure Pattern (Ibrahim, Wakjira and Ebead, 2020)
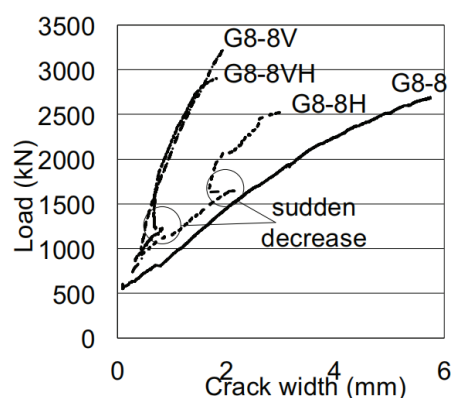
Figure 2.21: Crack Width of Specimen Under Different Loading Magnitude (Ibrahim, Wakjira and Ebead,2020)

Birrcher *et al.* (2014) analysed the minimum web reinforcement for deep beams. The web reinforcement proposed ranges 0 % to 0.3 % for both the vertical and horizontal directions for specimens. For the result, the amount of the web reinforcement was shown that independent of the normalized strength. The specimens with 0 % of web reinforcement showed a diagonal crack due to the transverse tensile stress acting toward the concrete. There was no web reinforcement to distribution this stress and it was carried by the concrete solely thus makes the concrete crush before the specimens reached a larger shear strength. While for the crack width aspect, the higher the ratio of web reinforcement is, the smaller the diagonal crack width is. The specimen with the

larger reinforcement showed the smallest diagonal crack width. The crack width against the ultimate load graph is shown in Figure 2.22. The report concluded the web reinforcements are mainly used for controlling the bottle shape equilibrium of the compressive strut. A reinforcement amount of 0.3 % is the minimum reinforcement to help compressive struts to have an equilibrium mechanism and prevent from splitting due to transverse tensile stress. Other than that, the amount of reinforcement should be determined based on the strut area instead of the gross area of the beam and it should be spaced evenly to have a better diagonal crack width control.
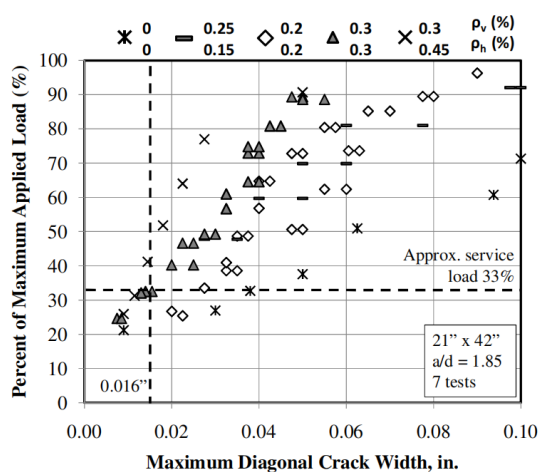
Figure 2.22: Crack Width of Specimens Under Different Loads (Birrcher et al, 2014)

Leon and Appa (2013) tested the behaviour of deep beam with ordinary steel bar reinforcement and replaced version reinforcement with a combination of steel and polypropylene fibre. Seven groups of the specimens were tested under a four-point loading system. These seven groups are categorized as Table 2.1:

Table 2.1: Reinforced Condition for Test Specimens

Series of specimens	Web reinforced condition
1	No web reinforcement
2	0.25 % for vertical, 0.49 % for horizontal
3	0.25 % for vertical, 0.74 % for horizontal
4	0.5 % for vertical, 0.49 % for horizontal
5	1 % steel fibre
6	1.25 % steel fibre
7	1 % steel fibre and 1 % Polypropylene fibre

The physical experiment result showed that series 7 gave the highest ultimate load compared to others. However, series 4 had the least deflection against the ultimate load compared to all other and a phenomenon is observed that specimens with steel fibre experienced larger deflection compared to specimens with original steel bar web reinforcement. For the cracking pattern, the series 1 specimens showed a tiny mid-span crack while it is not observed in series 7. All the specimens crack patterns were the same as the initial crack started at the edge of the support link toward the loading point. Meanwhile, there was a local crushing failure that happened for series 7 at the position near the loading point. The crack pattern is shown in Figure 2.23.

Figure 2.23: Failure Mode for Series 1(Left) and Series 7(Right) (Leon and Appa, 2013)

In Leon and Appa (2013) report, an increased amount of vertical web reinforcement doesn't increase the ultimate strength of the beam which is incompatible with Ibrahim, Wakjira and Ebead, (2020) and Birrcher *et al.* (2014)

research conclusion. The main reason may be the span to depth ratio for this research ranging from 0.7 to 0.9 which is relatively small compared to previous research with a span to depth ratio over 1.0. Thus, the arch mechanism occurs in prior comparison to the effect of web reinforcement and make the increase of vertical web reinforcement do not affect the ultimate strength.

2.3.3   Concrete Strength

Concrete is the element in charge of the compressive strength of the RC beam while steel bars oversee the tensile strength of the RC beam. The higher the concrete strength will usually give the higher the compressive load resist the ability to a beam. In the case of the deep beam, when it is subjected to a large, concentrated load, a compressive strut will then be formed diagonally from the support toward the loading point in as discussed in Section 2.2, so it is an essential concern to figures out the relationship of the concrete strength against the load capacity of the deep beam and how the concrete strength affects the crack pattern of deep beam.

Demir, Caglar and Ozturk (2019) performed research about the parameter that affect the cracking behaviour of deep beams while concrete strength was one of the experimental parameters. Three different concrete strengths of 18.1MPa (C1), 25.3MPa (C2) and 32.0MPa (C3) for the proposed three specimens with the same dimension and shear span to depth ratio. The experimental result showed that the load-carrying capacity increases significantly with the increase of concrete strength. For Strut-Tied Model (STM), it also obtained a result of the directly proportional relationship between concrete strength and ultimate load capacity due to the larger concrete strength gave larger compressive strength of strut. For the crack width aspect, a smaller crack width was observed when the concrete strength increase, and brittle behaviour of specimens were experienced. The relationship of ultimate load carrying capacity against crack width is shown in Figure 2.24.
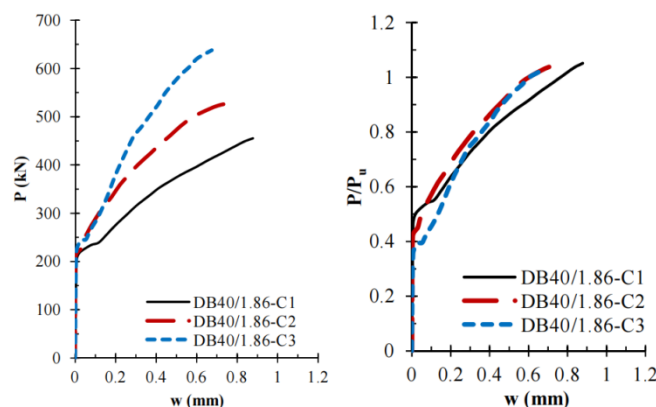
Figure 2.24: Crack Width of Specimen With Different Concrete Strength
Under Different Loads (Demir, Caglar and Ozturk, 2019)

Eun *et al* (2006) performed analysis on the behaviour of deep beam with web opening based on various parameters while concrete strength was one of the parameters for the research. 73MPa ('H' as the first letter of specimen name) and 83MPa ('UH' as the first letter of specimen name) were the concrete strength proposed to test specimens. As the result, the batch of specimens with larger concrete strength possessed a larger ultimate load-carrying capacity compared to specimens with smaller concrete strength. Moreover, the accumulation of strain energy made the specimens with larger concrete strength showed a brittle failure behaviour and their crack width are relatively small. The load against crack width graph for specimens with different concrete strength are shown in Figure 2.25. Meanwhile, the crack mode for both kinds of concrete strength were diagonal splitting mode
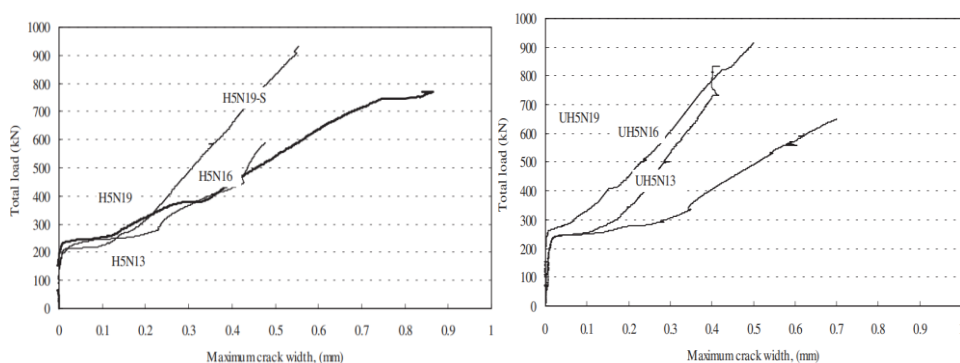
Figure 2.25: Comparison of Crack Width for 73MPa(Left) and 83MPa(Right)
(Eun et al, 2006)

Abdul-razzaq, Jebur and Mohammed (2018) checked the effect of concrete strength on a deep beam with the reinforced strut. There was a total of nine specimens with the different reinforced conditions were tested. Each specimen will be tested for three times different concrete strengths which were increased the concrete strength decreased the concrete strength and normal concrete strength. The result showed when the concrete strength of the deep beam increased, the ultimate carrying capacity load and the deflection of the deep beam will increase. The load versus deflection of different specimens is shown in Figure 2.26. Moreover, the relationship between the loading condition and the concrete strength has also been discovered. For two concentrated loads, increases of concrete strength by 33 % will lead to an increase of load-carrying capacity of 6 -8.5 %; For one concentrated load, increases of concrete strength by 33 % will lead to an increase of load-carrying capacity of 10 - 12.5 %; For uniform distributed load, increases of concrete strength by 33 % will lead to increase of load-carrying capacity of 5 - 8 %. The relationship of the loading pattern against concrete strength is yet to be discussed in this research.
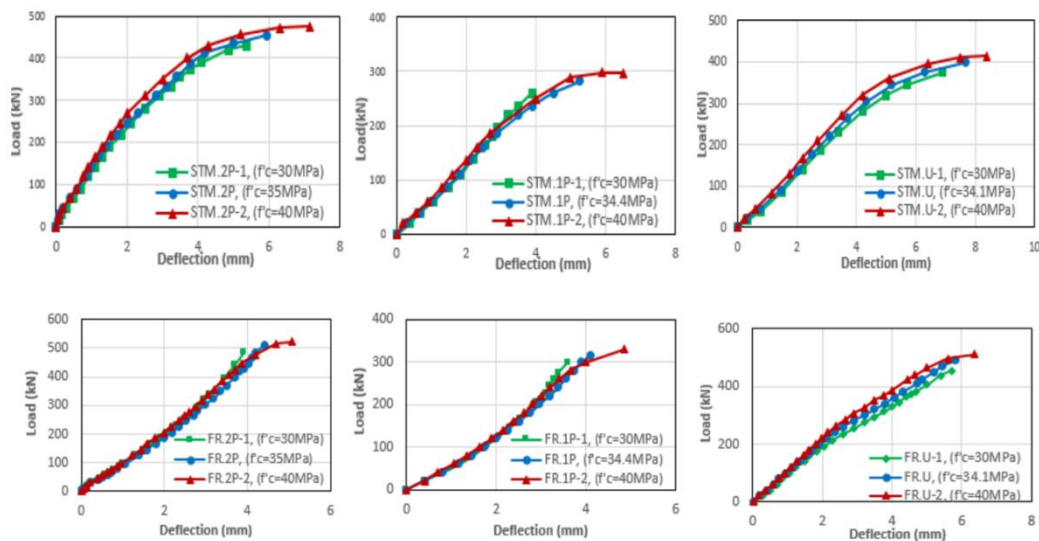
Figure 2.26: Defection At Different Loads for Different Batches of Specimen
(Abdul-razzaq, Jebur and Mohammed,2018))

2.4 Finite Element Method

Finite element analysis is a useful method for analyzing the structure behaviour in deep. This kind of analysis method can perform analysis despite the shape and size of the structure. The analysis mechanism of this method is to covert a complex object into a simpler and smaller element piece for analysis. The analysis process is done piece by piece, the piece's analysis results are then combined for an overview of the target object. The number of the piece for analysis has a great effect on the accuracy of the result as the number element piece more, the modelling result will get closer to realistic result (Shubhangi and Reddy, 2014).

Al-Azzawi, Mahdy and Farhan (2010) studied the geometric behaviour of a deep beam that stings on Winkler foundation, which is also known as a non-linear elastic foundation by using the finite element method. The finite element analysis software used in this research was the ANSYS 11. The three main elements in the model were the concrete, linear spring, and non-linear spring. Model in ANSYS 11 was chosen, isoparametric element (SOLID 65) chosen for concrete, Spring damper model that allowed to perform tension and compression direction in three directions was chosen for linear spring element (COMBIN14), while another spring model with non-linear performance for its load against deflection behaviour was chosen for non-linear spring element (COMBIN39). Two testing conditions were performed for the model which is uniformly distributed load and free end with an end load. The model result concluded that when the mesh size of the model increased, modelling results were getting more accurate. However, the effect of mesh size will get smaller after an optimum value. The graph that signifies the model mesh size effect to the result accuracy is shown in Figure 2.27.

For the effect of subgrade, the result concluded that when the foundation was modelled as a beam under the Winkler foundation, the deflection and the maximum stress will increase due to the Winkler model's ability to simulate the real behaviour of soil and it reduced the modulus subgrade reaction. Meanwhile, the result also concluded that increases in concrete compression strength will show an increment in the ultimate strength of the model. In the comparison of the model result with the present experimental study, both showed a good agreement which shows the reliability and accuracy

of using the finite element method to study the non-linear geometric behaviour of deep beam resting on the Winkler foundation model.
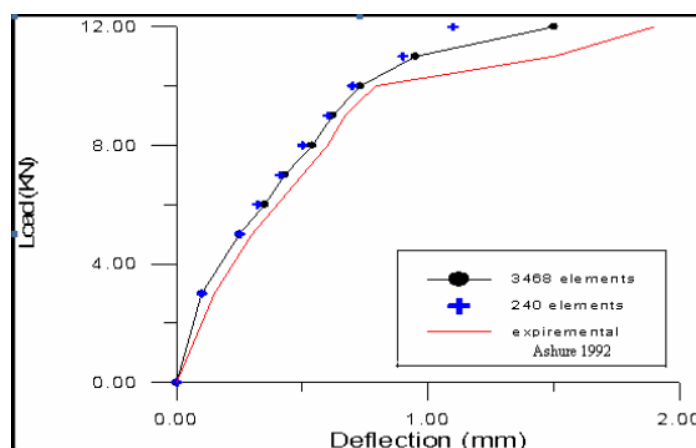
Figure 2.27: Comparison for Load-Deflection Graph for Two Different Mesh Sizes (Al-Azzawi, Mahdy and Farhan, 2010)

Hussain (2018) performed a non-linear study for the behaviour of deep beams with and without opening on their web under direct and indirect loading patterns. The crack propagation and the ultimate load was the study's aim by using a finite element software called ANSYS 12. The modelling result was then compared with the experimental result obtained from the research performed by Yousif (2016). On the aspect for specimen with no opening on web section, the load against deflection graph for both direct and indirect load compared with experiment result are shown in Figure 2.28. From the contour strain of the directly loaded specimen from Figure 2.29, it shows that the stress was travelling from the loading point toward the support point. For the indirect loading pattern, the crack propagation was showed a good agreement with the experiment result as shown in Figure 2.30. While for the specimen with an opening on the web section, the crack propagation and failure were similar as shown in Figure 2.31. The elastic linear behaviour was observed for all beam specimens under shear failure. Both experimental and modelling results agreed that opening on the web will decrease the ultimate carrying capacity of the beam.
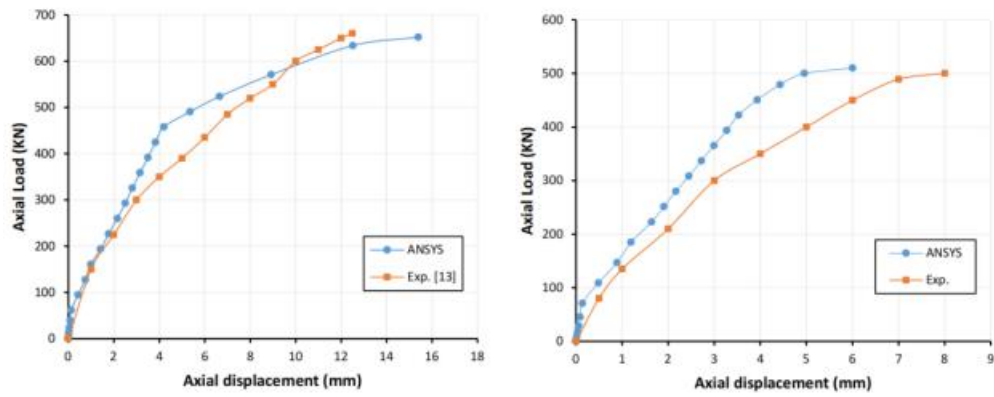
Figure 2.28: Comparison for Modelling and Experiment Result for Direct (Left) and Indirect (Right) Loading Pattern (Hussain, 2018)
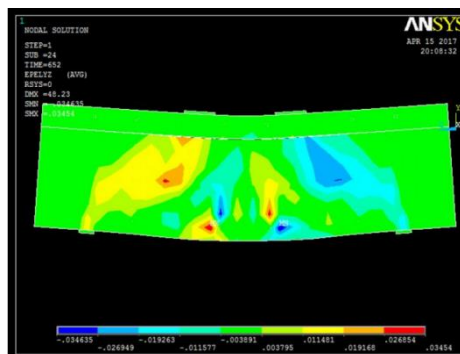
Figure 2.29: Contour Strain Model for Directly Loaded Specimen (Hussain, 2018)

Figure 2.30: Comparison of Crack Propagation for Modelling Result and Experiment Result (Hussain, 2018)
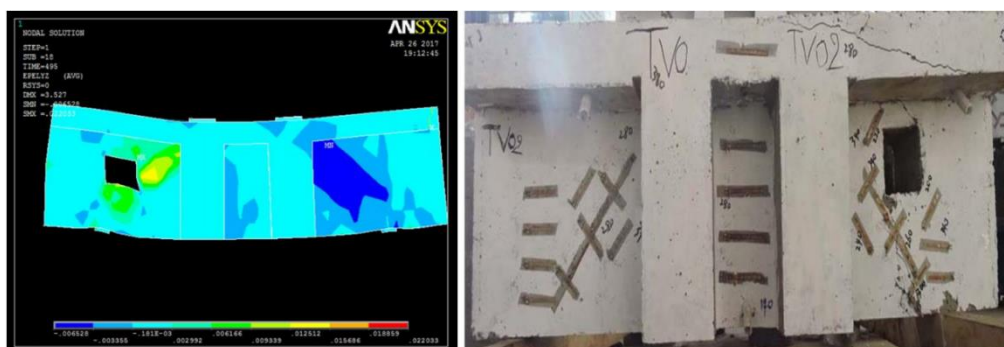
Figure 2.31: Comparison of Crack Propagation for Modelling Result and Experiment Result for Specimen with an Opening (Hussain, 2018)

Alius *et al* (2020) also study the deep beam behaviour with web opening using finite element method with different software which is 3D-NLFEA. The modelling results were then compared with the experimental results that were carried by Yang *et al* (2006). The main study variable for this experiment was the structured and unstructured mesh with the shape element of hexahedral and tetrahedral. As the result, the numerical result had no exactly agreement to the experimental result for the load against displacement result. The numerical result showed a larger displacement for both the hexahedral and tetrahedral element models. The hexahedral element model showed a similar ultimate load-carrying capacity with the experimental result, while the tetrahedral element model gave a lower ultimate load compared with the experimental result. Which are shown in Figure 2.32. For the crack pattern aspect, the model with tetrahedral elements had a result that approached to real flexural crack result due to the unstructured mesh behaviour. On the specimens with hexahedral mesh geometry which is similar to the actual crack result. Comparison crack result are shown in Figure 2.33. The crack width prediction for both models were underestimated which required a larger load to reach the same crack width of actual result that can be reached under a smaller load. The author claimed this might be due to the assumption made between model and test result. The reason causes the incompatibility for both models compared to the experimental result was yet to be discussed in this report.
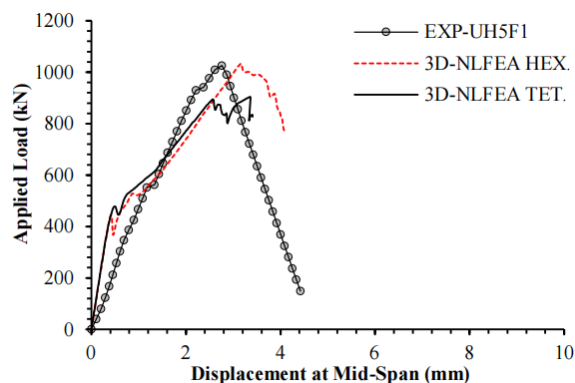
Figure 2.32: Load Against Deflection Graph for Both Simulation and
Experimental Result (Alius et al, 2020)
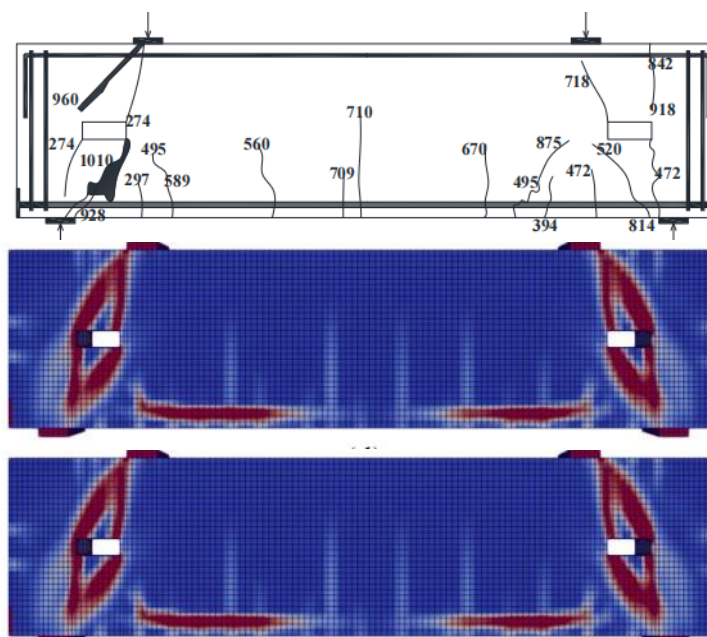
Figure 2.33: Crack Pattern for Experimental Result (Top), Hexahedral
Element Model (Middle) and Tetrahedral Element
Result(Bottom) (Alius et al, 2020)

Rai (2021) investigated the ability of finite analysis software,
ABAQUS to identify the behaviour of deep beams by using the CDP model.
The main goal of this research was to check the reliability of using finite element
analysis to analyse a deep beam behaviour in terms of compression and tensile
stress-strain relationship and the failure mode. A beam specimen that chosen for
modelled was an RC deep beam of an experiment test that carried out by Demir,
Caglar, and Ozturk (2019). The naming for the reference beam was DB60/1.86-

C1/SR and its detailing configuration are shown in Figure 2.34. As the result, both the model result and the experimental result had a great agreement with each other. The crack was initiated by a diagonal crack from the support edge toward the loading point by a failure mode of diagonal shear splitting mode. By observing the maximum principal plastic strain, it shows obviously form as the location of the largest strain was exactly where the diagonal crack happened. The failure pattern of the experimental result and the maximum principal plastic strain are shown in Figure 2.35 and Figure 2.36. Based on the modelling result from ABAQUS, the maximum principal plastic strain was concentrated at the location of diagonal crack failure of the experimental result and the direction was perpendicular to the strain. Meanwhile, the minimum principal plastic strain showed a clear diagonal bottle-shaped strut as in Figure 2.37. It can be concluded that both the maximum and minimum principal strain of finite element analysis had predicted the failure mode of the deep beam successfully during the ultimate loading stage.
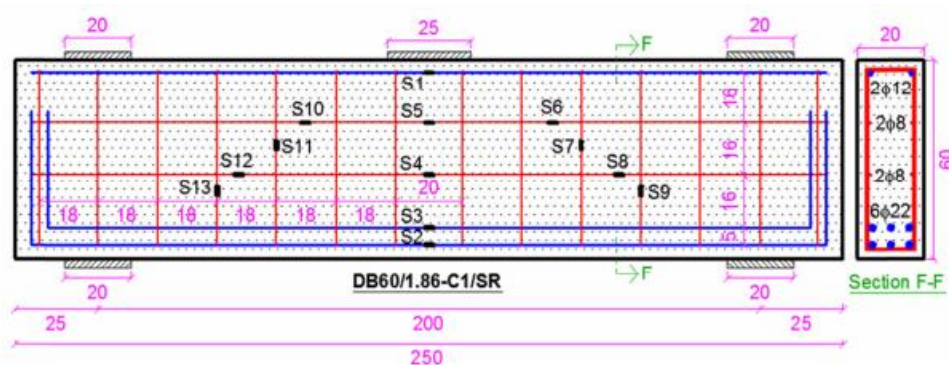
Figure 2.34: Reference Beam Detailing Configuration (Unit In cm Except for Reinforcement Unit In mm) (Rai, 2021)

Figure 2.35: Experimental Crack Pattern for Reference Beam (Rai, 2021)
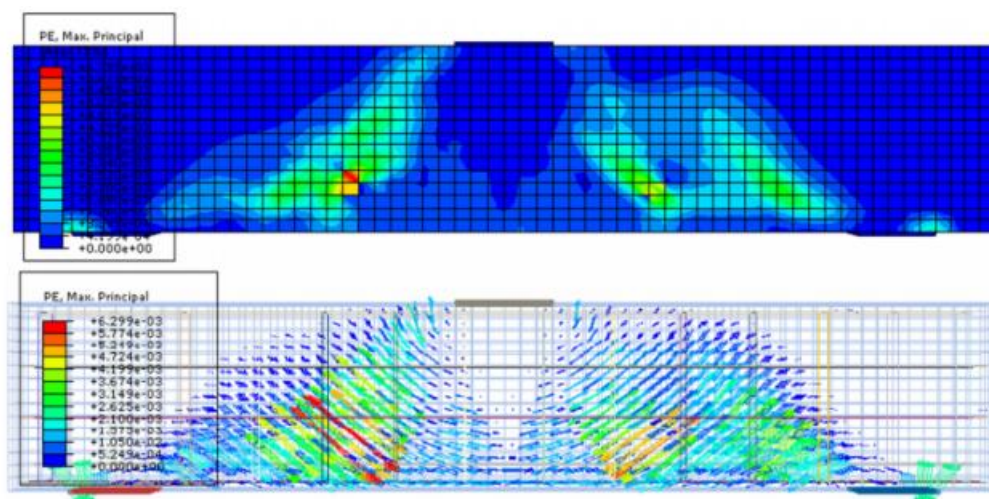
Figure 2.36: ABAQUS Modelling Result for Maximum Plastic Strain
Location (Rai, 2021)
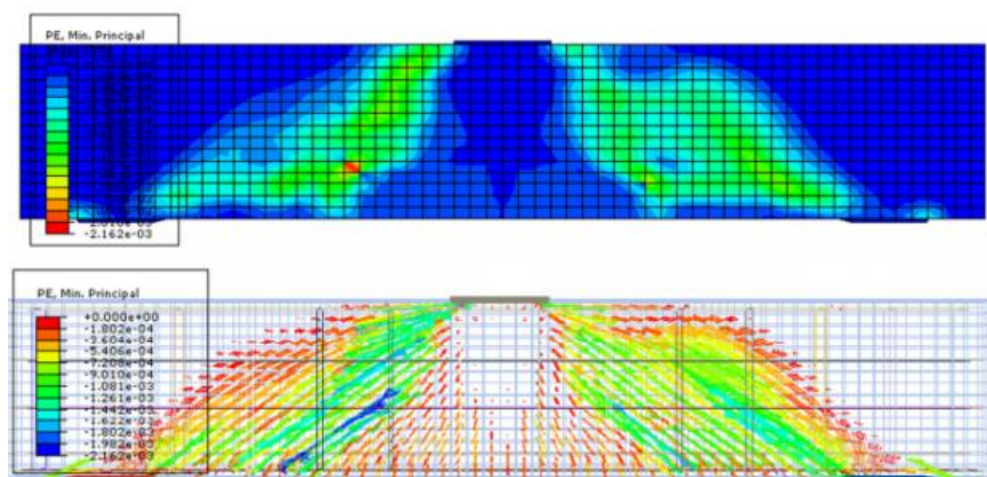
Figure 2.37: ABAQUS Modelling Result for Minimum Plastic Strain
Location (Rai, 2021)

Metwally (2014) performed non-linear finite element analysis to investigate the behaviour of the deep beam reinforced by the Glass Fibre Reinforced Polymer (GFRP). According to the experimental research performed by Andermatt (2013), twelve RC deep beams varying in shear span to depth ratio, effective depth, reinforcement ratio and concrete strength were tested under a four-point loading frame with a load capacity of 6600kN. These twelve specimens were chosen to be modelled by using finite element software ABAQUS. The results showed that both modelling and the experimental result had a high level of similarity in terms of load against deflection, crack pattern,

cracking load and the crack mechanism. For an overview of all twelve specimens, an experimental to numerical result ratio was conducted to identify their relationship. the ratio for ultimate load capacities was 1.01, for mid-span deflection was 0.98, the diagonal cracking load was 0.99 and reserve capacity was 0.98. All the results possessed a standard deviation ranging from 0.05-0.08. Both the experimental result and numerical result indicated a huge reserve capacity was observed and it meant the arch mechanism was initiated after the formation of diagonal crack and redistribution of stress has happened. Moreover, there were four crack patterns observed for all twelve specimens namely, diagonal concrete tension failure, flexural compression failure, shear compression failure and compression strut failure. All these failure patterns were well predicted by the finite element method by showing the strain distribution pattern. All four types of failure patterns are shown in Figure 2.38, Figure 2.39, Figure 2.40 and Figure 2.41.
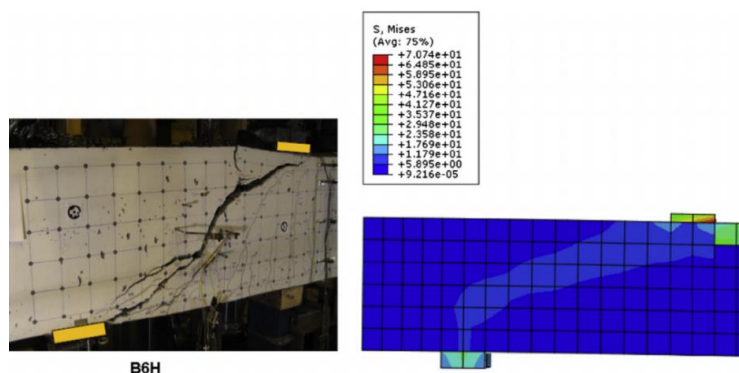
Figure 2.38: Comparison for Experiment Result and Modelling Result for Diagonal Concrete Tension Failure (Metwally, 2014)
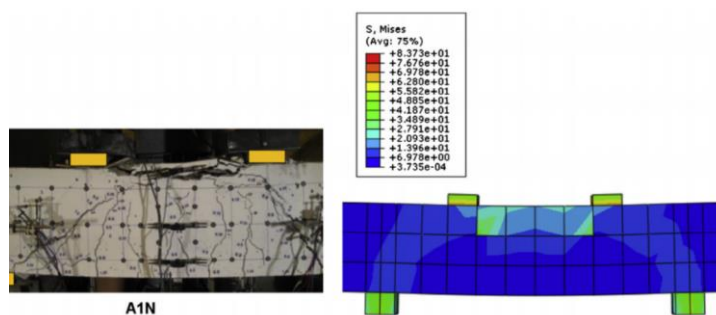
Figure 2.39: Comparison for Experiment Result and Modelling Result for Flexural Compression Zone Between Two Load Point Crushing (Metwally, 2014)
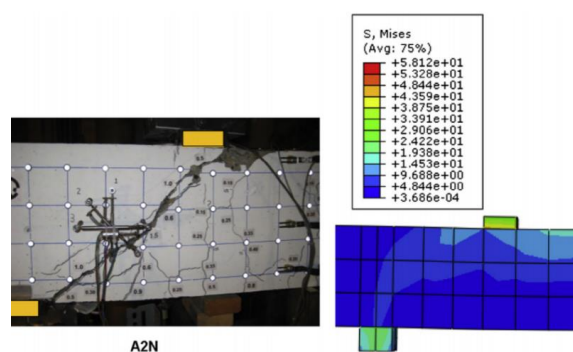
Figure 2.40: Comparison for Experiment Result and Modelling Result for Shear Compression Failure (Metwally, 2014)
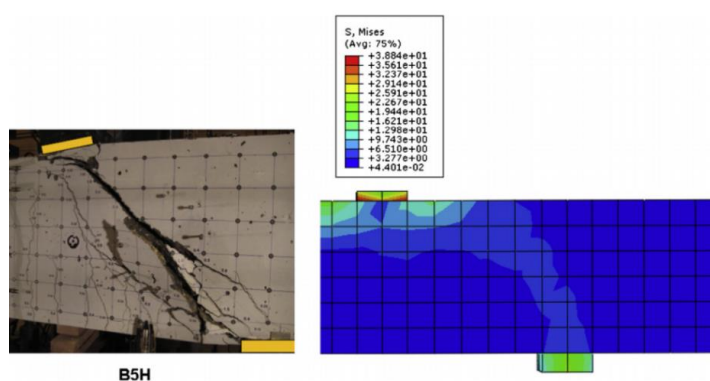
Figure 2.41: Comparison for Experiment Result and Modelling Result for Compression Strut Failure (Metwally, 2014)

These literatures show the deep beam behaviour modelling using finite element analysis method with different kind of the software, including ANSYS, 3D-NLFEA, and ABAQUS. The accuracy of using the numerical software for predicting deep beam behaviour has been proved by comparing the numerical result with the experiment result. Moreover, Alius *et al* (2020) research showed the factor that will affect the numerical result such as mesh size and type of element which is important information for the modelling definition in Chapter 3. However, the deep beam simulation with different parameter change to examine the behaviour of deep beam is yet to be explored and left a research gap.

2.5   Summary

The crack propagation of the deep beam is mainly a diagonal crack that initiates from the inner edge of support linked toward the loading point of the inner edge. Chen *et al* (2020), Abdul-razzaq, Ali and Abdul-kareem (2017) and Ibrahim, Wakjira and Ebead (2020) studies show the deep beams with innovative reinforcement have similar to ordinary deep beams but with a smaller crack width and lesser crack at the same loading compared to original deep beam, this may due to increases of shear strength. Osman et al (2017) experiment showed the failure mode of deep beam covert to concrete crushing instead of diagonal crack due to application of epoxy resin, and the ultimate load become higher with reduction of crack width.

The shear span to depth ratio is one of the main factors that affect the shear strength obviously as the larger the shear span to depth, the smaller the load-carrying capacity and the failure pattern will lead to concrete crushing before the diagonal shear failure. Zhang *et al* (2020) research showed the shorter shear span with the same beam depth will cause the less effective tied-arch action. Web reinforcement plays important role in distributing the stress along the sturt and this makes vertical web reinforcement possess the greatest effect as it can give a larger load carrying capacity and smaller crack width compared to horizontal web reinforcement. Birrcher et al. (2014) claimed that the mechanism for web reinforcement is to maintain the bottle shape equilibrium of the compressive strut and a minimum of 0.3 % are recommended. However, Leon and Appa (2013) research study gave a different result as the effectiveness of vertical web reinforcement will become lesser when the span to depth ratio is small enough. This may be due to the arch mechanism that happened prior to the stress distribution of web reinforcement. For concrete strength that produces compressive strength of a beam, the larger the concrete strength will increase the load-carrying capacity of the compressive strut. The higher concrete strength will make the deep beam behaviour brittle with smaller crack width. Abdul-razzaq, Jebur and Mohammed (2018) identified the effectiveness of concrete strength will be affected by the loading pattern but is yet to be discussed in detail.

The reliability of the numerical method for the behaviour of deep beam has been proven by several experts as the modelling result showed the agreement with the experimental result. This research has covered different

kinds of conditions including ordinary deep beam, deep beam with innovative reinforcement, deep beam with opening etc with various non-linear analysis software including ANSYS, 3D-NLFEA and ABAQUS. Al-Azzawi, Mahdy and Farhan (2010) and Alius et al (2020) also found out that the reliability of the result can be affected by the mesh size and structure of the element model.

CHAPTER 3

METHODOLOGY

3.1   Introduction

This study is aimed to perform crack propagation analysis for ordinary deep beam by using numerical analysis software, namely ABAQUS software. The loaded deep beam was simulated in ABAQUS software, and the crack path was recorded down by observing the change of stress and strain. To prove the reliability of the model, previous work of study was used as a reference to do the validation of the model. Deep beam specimens were tested with the various parameter to identify how the parameter will affect the crack propagation of deep beam.

Before the modelling work, specimen specification and the test setup were determined. The specimen specification includes the dimension of the beam, concrete strength, detailing etc while the test setup included the loading type, loading location, loading magnitude etc. After that was the numerical study. In numerical modelling, there are four major steps to be carried out which are numerical modelling, numerical analysis, result comparison and model optimization.

First and foremost, numerical modelling is carried out by defining material used for modelling, connection condition of each element, model mesh size and type, boundary and loading condition etc. The numerical modelling was the second step performed inside ABAQUS software. This modelling result was compared with the experimental result obtained from the historical work-study. Model re-calibration was carried out when there was inconsistent between modelling result and experimental result, until both results agree with each other. The reason for the model validation is to ensure the reliability of the created model and obtain a model which can simulate real-life condition to model, thus the crack propagation can be observed accurately. When the model was proved to be accurate, numerical analysis for other specimens was carried out. All the results including load-deflection curve, von Mises stress contour, PEMAG

crack distribution, and concrete tension damage contour were recorded and discussed in Chapter 4.

The general workflow for the research methodology is shown in Figure 3.1.
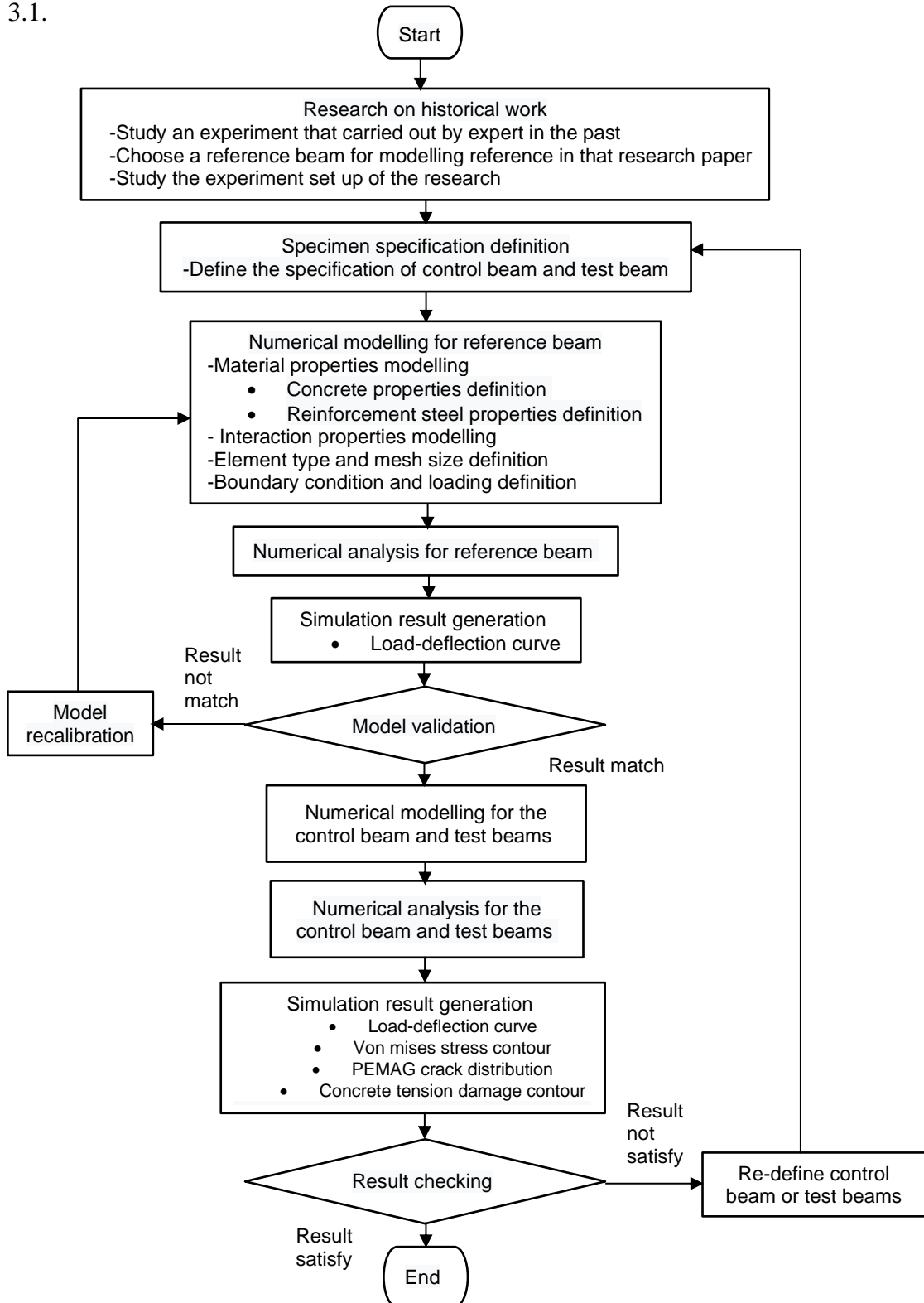
Figure 3.1: Flowchart for Research Methodology

3.2 Historical Work Study

Research work was performed on the experiment study carried by Zhang and Tan (2007) and the result was used as a reference for this numerical study. To validate the modelling result, the load-displacement curve results of both reference beam model result and reference beam experimental result were compared. Model re-calibration was carried out when there was any inconsistency of the result. Specimen properties and conditions kept on tuning to improve the model reliability and increase the accuracy of modelling results.

3.3 Specimen Specification

The specification condition and the number for specimens were decided before the numerical analysis. There were some parameters to vary for exploring out how these parameters affect the cracking behaviour of deep beam. There were total of thirteen specimens modelled in this study, including one reference beam, one control beam and the other eleven test beams with various specifications.

3.3.1 Reference Beam

A reference beam was selected to validate the model created and defined the properties of the material. The reference beam was selected from Zhang and Tan (2007) study. The dimension of the reference beam was 350 mm depth x 80 mm width x 1330 mm length. The shear span to depth ratio for this reference beam was 1.0, which was larger than 0.7 (control beam). The concrete type of C25/30 was adopted as a standard concrete strength for modelling all the specimens including the reference beam. The cylinder compressive strength for the C25/30 concrete strength for the experimental result was tested to be 25.9MPa. The geometry and the specification of the reference beam are shown in Table 3.1. This reference beam was reinforced by four 10 mm diameter steel bar for bottom longitudinal reinforcements. While the 6 mm diameter steel bar was adopted for the top reinforcement and vertical stirrup which with a spacing of 150 mm. The detailing of the reference beam is shown in Figure 3.2

Table 3.1: Reference Beam Geometry and Specification

Parameter	Description
Annotation	R01
Dimension	350 mm (Depth) x 80 mm (Width) x 1330 mm (Length)
Concrete strength	25.9MPa
Shear span to depth ratio	1.0
Flexural reinforcement	2R6 (Top) , 4T10 (Bottom),
Stirrup	R6-150
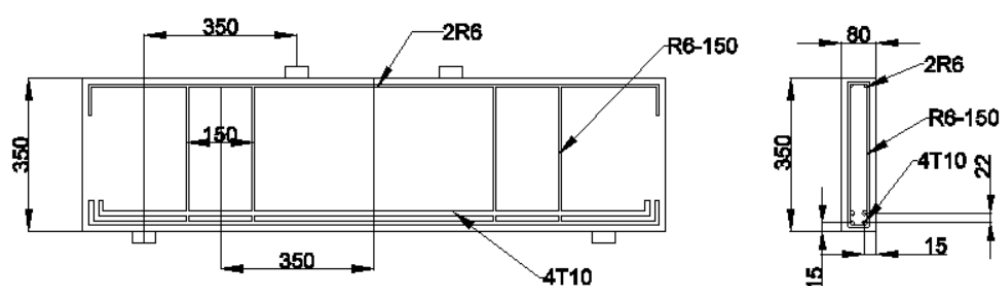
Figure 3.2: Detailing of Reference Beam

The reference beam was loaded until it failed and the result of cracking, critical cracking and the ultimate limit was recorded. The load-deflection curve result was recorded as shown in Figure 3.3. However, the author did combine the result with the other two specimens for comparison. This load-deflection curve was used as reference data for model validation. Other than that, Figure 3.4 shows the sketch of the crack path in a precise manner.
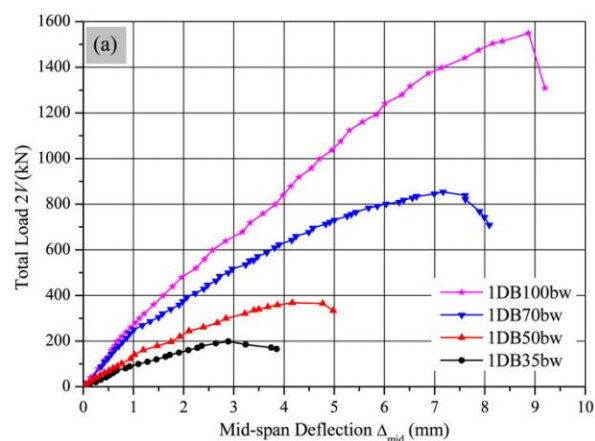
Figure 3.3: Load Deflection Curve Result (1DB35bw Represent the Reference
Beam R01) (Zhang and Tan, 2007)
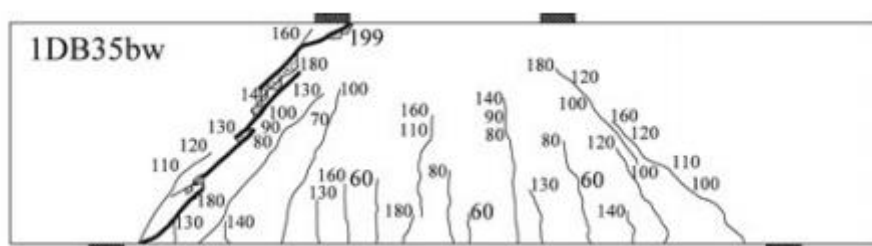
Figure 3.4: Cracking Configuration of the Reference Beam After Loading
(Zhang and Tan, 2007)

3.3.2   Control Beam

The control beam was used to compare with other test specimens that having various shear link position and longitudinal reinforced diameter. This control beam was in the same dimension and concrete strength as the reference beam mentioned in Section 3.3.1. The position of the steel plate for the loading position was moved outward for decrease the shear span length to achieve a shear span to depth ratio of 0.7. This control beam was reinforced with 10 mm diameter steel bars for longitudinal reinforcement while 6 mm diameter steel bars for top reinforcement and vertical stirrups in a spacing of 150 mm. The geometry and the specification of the control beam are shown in Table 3.2 while the detailing of the control beam is shown in Figure 3.5.

Table 3.2: Control Beam Geometry and Specification

Parameter	Description
Annotation	C01
Dimension	350 mm (Depth) x 80 mm (Width) x 1330 mm (Length)
Concrete strength	25.9MPa
Shear span to depth ratio	0.7
Flexural reinforcement	2R6 (Top), 4T10 (Bottom),
Stirrup	R6-150
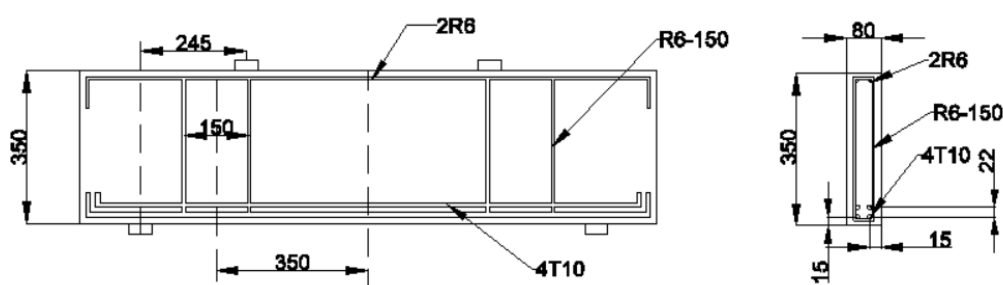
Figure 3.5: Detailing of Control Beam

3.3.3   Test Beam

The test beams were set for investigating the crack propagation behaviour for deep beam with different parameters by comparing the result with each other. All the test specimens were adopting the same concrete strength as the reference beam and control beam which is 25.9MPa cylinder concrete strength. For the first batch of test beam were set for investigating the effect of shear span to depth ratio. There were three test beams with different shear span to depth ratio with the value of 0.85, 0.55 and 0.4 by changing the position of the loading steel plate for decrease the shear span length. Together with the reference beam R01 and control beam C01, there were total of five specimens for compare for analysis of the effect of shear span to depth ratio to cracking behaviour.

For the second batch of test beam were set for investigate the effect of longitudinal reinforcement diameter. There were four test beams with different longitudinal reinforcement diameter with the value of 13 mm, 16 mm and 20 mm, 22 mm while the grade and sizing for the top reinforcement and shear link was maintained. Together with the control beam C01 which with the 10 mm

diameter longitudinal reinforcement, there were total of five specimens for investigate the effect of longitudinal reinforcement diameter to the cracking behaviour of deep beam.

Furthermore, the third batch of test beam were set for investigate the effect of different position of shear link. There were four specimens with the position of shear link distance from the mid span in a value of 375 mm, 400 mm, 425 mm and 450 mm. These specimens were compared with the control beam C01 with a value of 350 mm from the mid span to investigate the cracking behaviour of deep beam with different position of shear link.

Table 3.3: Test Beam Geometry and Specification

Annotation	Description	Remarks
Batch 1: Shear Span to Depth Ratio		
SVD-0.85	2R6 for top reinforcement, 4T10 for bottom reinforcement, shear link placed at 350 mm distance from mid span each side.	Shear span to depth ratio set as 0.85
SVD-0.55		Shear span to depth ratio set as 0.55
SVD-0.4		Shear span to depth ratio set as 0.4
Batch 2: Longitudinal Reinforcement Diameter		
SLR-T13	2R6 for top reinforcement, shear span to depth ratio set as 0.7, shear link placed at 350 mm distance from mid span each side	Longitudinal reinforcement set as 13 mm diameter.
SLR-T16		Longitudinal reinforcement set as 16 mm diameter.
SLR-T20		Longitudinal reinforcement set as 20 mm diameter.
SLR-T22		Longitudinal reinforcement set as 22 mm diameter.

Table 3.3 (Continue): Test Beam Geometry and Specification

Annotation	Description	Remarks
Batch 3: Position of Shear Link		
SVL-375 mm	2R6 for top reinforcement, 4T10 for bottom reinforcement, shear span to depth ratio set as 0.7	Shear link placed 375 mm from mid span.
SVL-400 mm		Shear link placed 400 mm from mid span.
SVL-425 mm		Shear link placed 425 mm from mid span.
SVL-450 mm		Shear link placed 450 mm from mid span.

All the detail description of the test beam is stated in Table 3.3. For the annotation of Batch 1, "S" represented "Specimen", "VD" represented "Shear span to depth ratio", "0.85" represented the shear span to depth value for that beam; For the annotation of Batch 2, "S" represented "Specimen", "LR" represented "Longitudinal reinforcement", "T13" represented the longitudinal reinforcement sizing for that beam; For the annotation of Batch 3, "S" represented "Specimen", "VL" represented "Position of Shear Lin", "375 mm" represented distance from the mid span to the position of shear link position for that beam. Meanwhile, all the detailing of the test beams are shown in Figure 3.6 to Figure 3.8.

48

(a)

(b)

(c)
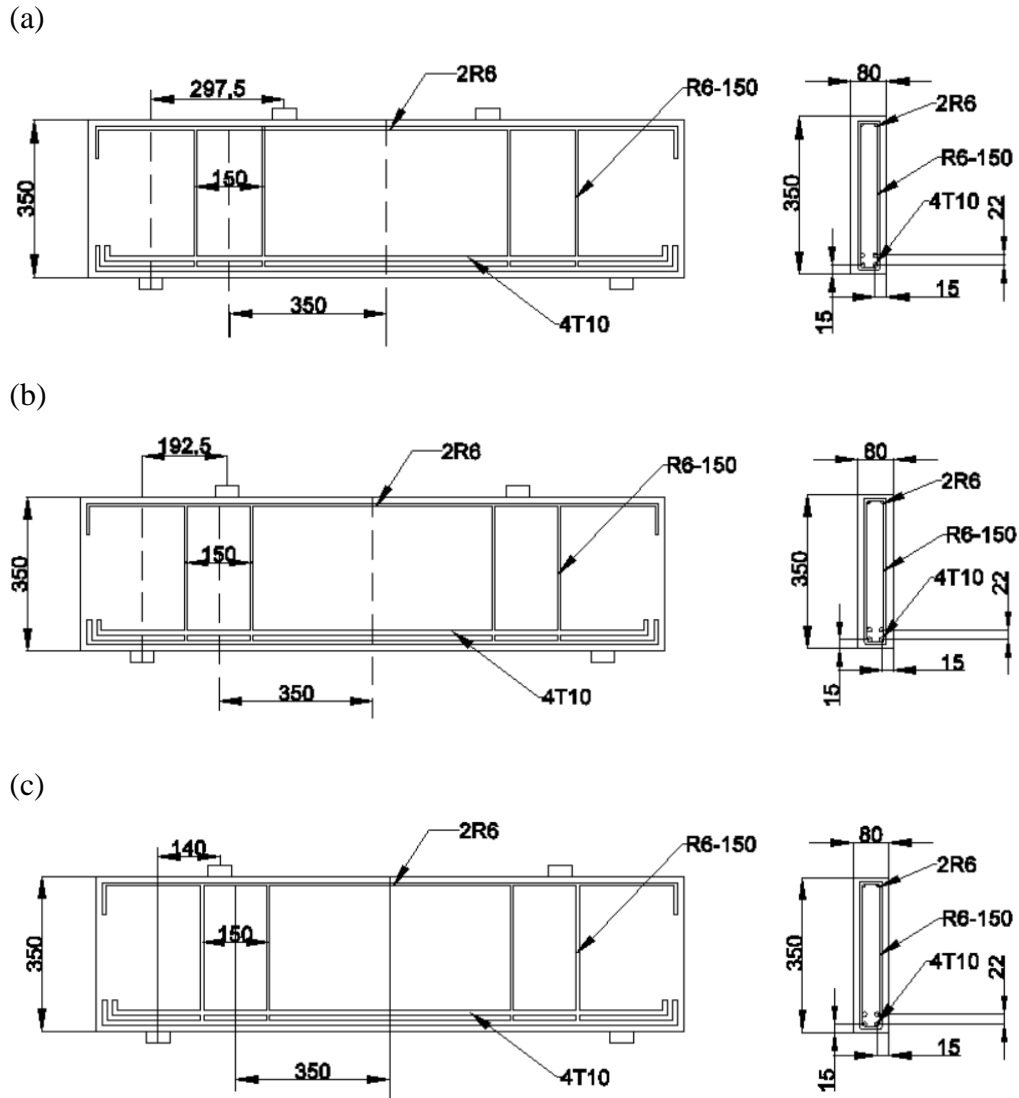
Figure 3.6: Detailing for Test Beams for Batch 1: Shear Span to Depth Ratio
(a: SVD-0.85; b: SVD-0.55; c: SVD-0.4)

(a)

(b)

(c)

(d)
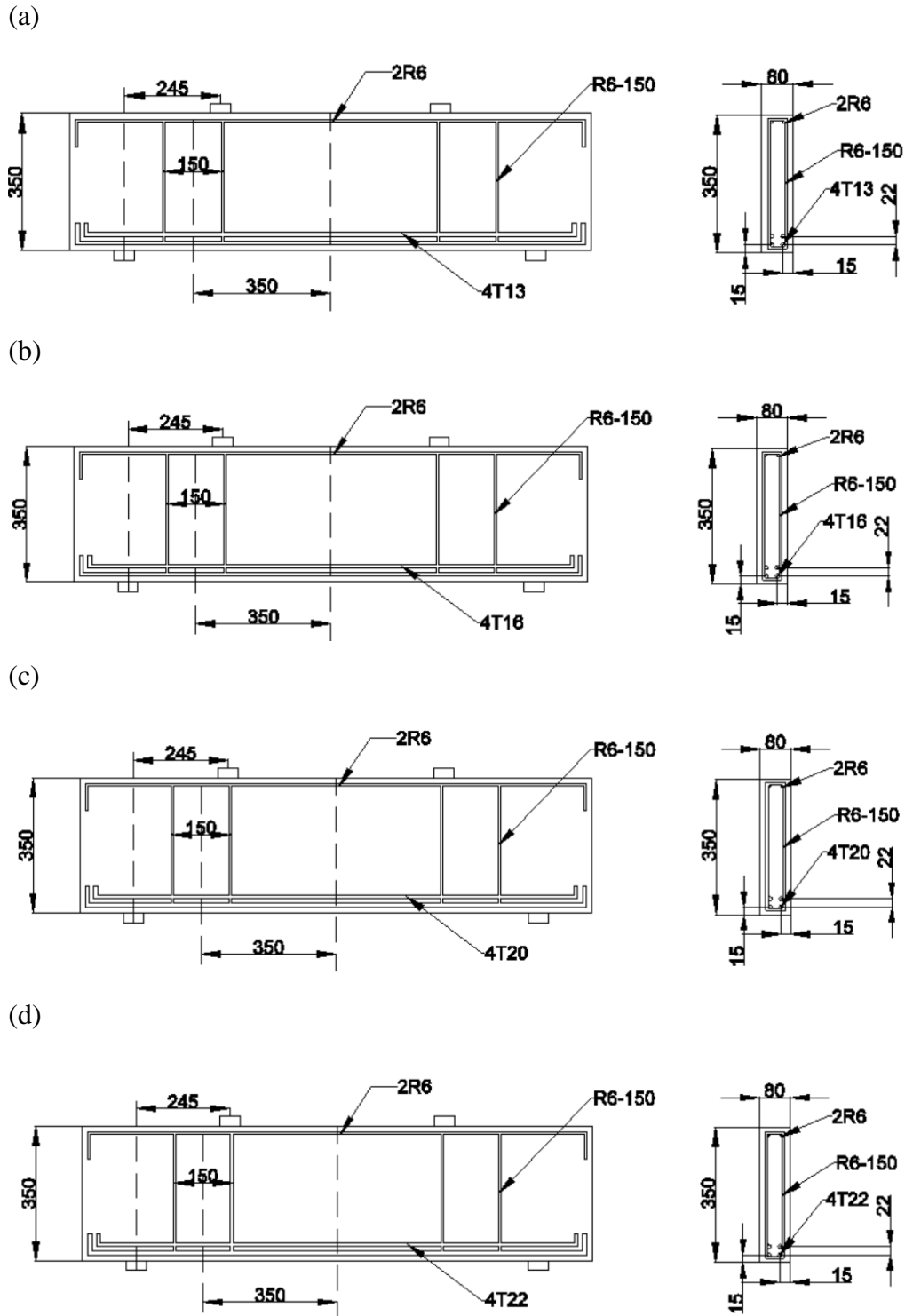
Figure 3.7: Detailing for Test Beams for Batch 2: Longitudinal Reinforcement Diameter (a: SLR-T13; b: SLR-T16; c: SLR-T20; d: SLR-T22)

(a)

(b)

(c)

(d)
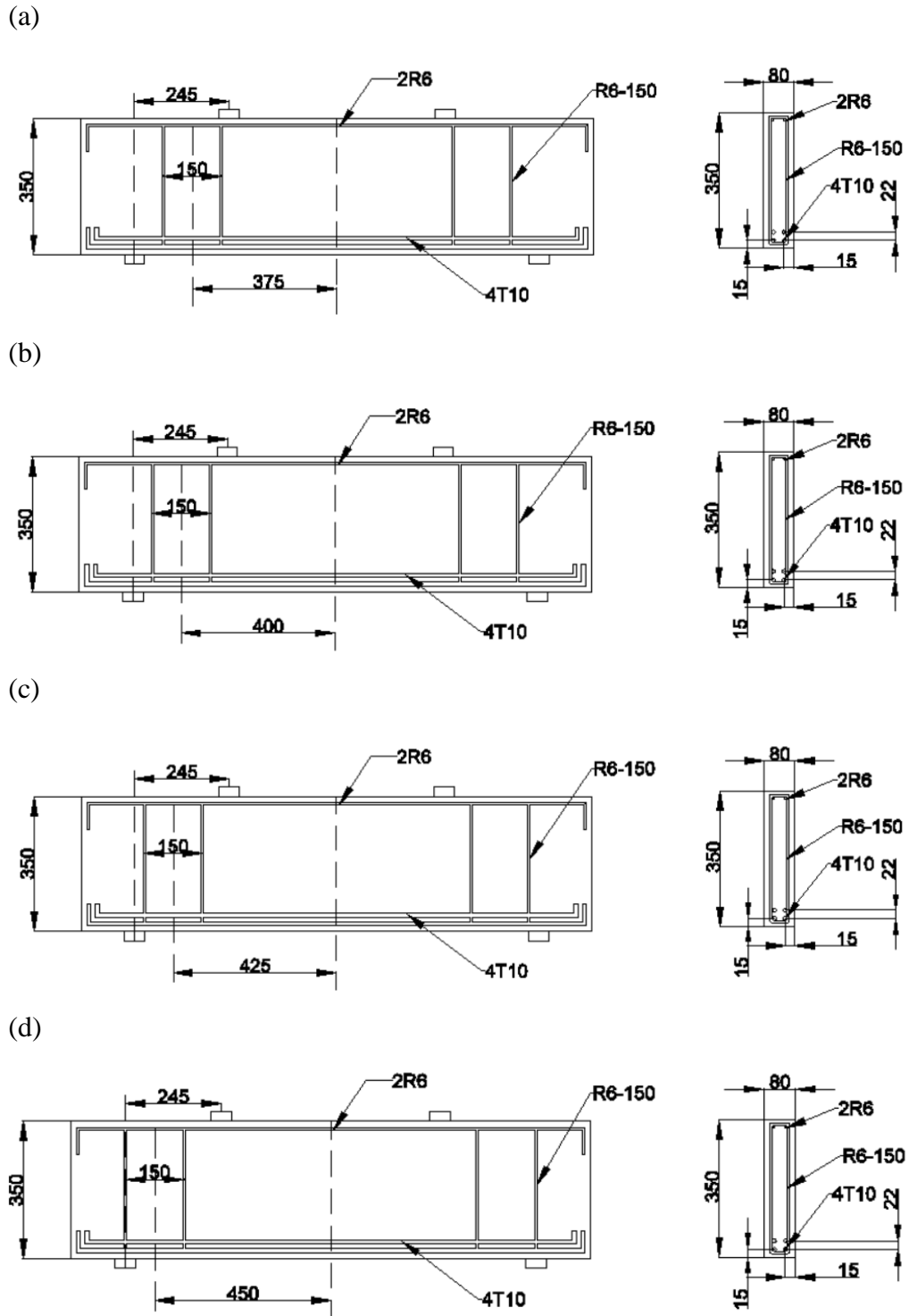
Figure 3.8: Detailing for Test Beams for Batch 3: Position of Shear Link (a: SVD-375 mm; b: SVD-400 mm; c: SVD-425 mm; d: SVD-450 mm)

3.4   Numerical Modelling

The numerical model was developed by using ABAQUS software under the Finite Element Analysis concept. The model was examined under a monotonic load to observed the crack propagation and compared it with the historical experiment result obtained by Zhang and Tan (2007). The two main techniques adopted by ABAQUS software to simulate concrete behaviour were smeared crack model and the Concrete Damaged Plasticity model (CDP Model).

The CDP model was chosen to be used for this study analysis. According to the ABAQUS user manual, this CDP model can be used for concrete and quasi-brittle material in all types of structure including beams which is this study object. This model analysis can undergo with the presence of re-bar inside the analysis object. Other than that, the CDP model also possesses the capability to analyse the rate of straining which is useful for crack propagation analysis. This CDP model was designed to be used for concrete objects loaded under the monotonic, cyclic and dynamic loading while this study was carried under a monotonic loading situation.

There were four stages for the numerical process including, material modelling, loading definition, element type and mesh size scheme, and material bonding & boundary condition. Firstly, material modelling needs to be carried to define all the element material properties such the concrete cover, longitudinal bar, horizontal bar, vertical stirrups, steel plate etc. For the element type and size, the element for concrete and steel bar element type needs to be decided based on the available element given in ABAQUS software and the optimum element size need to be defined for an accurate result. Lastly, the bonding condition for the steel re-bar against the concrete and concrete against the steel plate need to be defined while translation degrees of freedom for the support condition need to be defined in boundary condition definition.

3.4.1   Material Modelling

Material modelling is to define the properties of each of the elements that can be found in a deep beam model. The properties mean the strength, elastic of modulus, Poisson ratio etc. The three main elements that exist inside the deep beam are the concrete, steel for reinforcement and the steel plate.

3.4.1.1 Concrete

Firstly, the concrete modelling required several parameters including the density, characteristic of the strength of concrete, young modulus of concrete, dilation angle, eccentricity, ratio of the second stress invariant to the tensile Meridian, ratio of initial equi-biaxial compressive strength to initial uniaxial compressive strength, viscosity parameter.

The details of concrete properties are referring to EN 1992-1-1:2004 (European Commission, 2004). The density of concrete is 2500kg/m^3 and the concrete cylinder compressive strength for the C25/30 concrete which were used in the experiment of Zhang and Tan (2007) is 25.9MPa. The Poisson ratio is 0.2 for uncracked concrete. There is an equation been explored for the computation of modulus of elasticity which is Equation 3.1 by Pauw (1960) and the calculation result was 30725.89MPa.

$$E_c = 0.0736\omega^{1.51}(f'_c)^{0.30} \tag{3.1}$$

where:

ω = concrete density, kg/m^3

f'_c = concrete compressive cylinder strength, MPa

For CDP model definition in Abaqus requested different kind of the parameter input for the plasticity zone of concrete behaviour. As referring to Rai (2021), the dilation angle which is the internal angle of friction was set to be 33˚. The value falls in the recommended value of 20˚ to 40˚ for concrete. For eccentricity which referring the distance from the loading point to the neutral axis of the beam is set as 0.1. The ratio of initial equibiaxial compressive strength to initial uniaxial compressive strength was taken as 1.16. The ratio of the second stress invariant to the tensile Meridian must be set within a safety range of $0.5 < K_c < 1.0$, was chosen to be 0.667 which is the default value in ABAQUS. The viscosity parameter used for computing the viscoplastic regularization in the concrete constitutive equation was set to be 0.02. These value were set in initial and the fine tuning of the parameter was done during the modelling to make the modelling result converge to experimental result obtained from Zhang and Tan (2007).

Table 3.4: Parameter Definition for Concrete Properties

Parameter	Symbol	Value
Dilation angles	φ	33°
Eccentricity	e	0.1
Ratio of initial equi-biaxial compressive strength to initial uniaxial compressive strength	f_{bo}/f_{co}	1.16
Ratio of the second stress invariant to the tensile Meridian	K or K_c	0.667
Viscosity parameter	μ	0.02

The stress-strain relationship of the concrete is essential to identify either the stress or strain in the situation of one of them is remained unknown. There is a useful formula to identify the stress-strain relationship of plain concrete in compression, which are the equations proposed by Carreira and Chu (1985). The equation for the stress-strain relationship is shown in Equation 3.2 and the constant, β is the material parameter which can be obtained by using Equation 3.3, Equation 3.4, and Equation 3.5. The computed value for β value was 2.061. The β value was the concrete characteristic constant used for computing out the stress-strain relationship curve by using Equation 3.2 and the result are shown in Figure 3.9.

$$\frac{f_c}{f'_c} = \frac{\beta(\varepsilon/\varepsilon\prime)}{\beta-1+(\varepsilon/\varepsilon\prime)^\beta} \tag{3.2}$$

where:

ε = strain, mm/mm

ε' = ultimate strain, mm/mm

$$\beta = \frac{1}{1-(\frac{f'_c}{\varepsilon'_c E_{it}})} \tag{3.3}$$

$$E_{it} = \frac{f'_c}{\varepsilon'_c}(\frac{24.82}{f'_c} + 0.92) \tag{3.4}$$

$$\varepsilon'_c = (1680 + 7.1f'_c) * 10^{-6} \tag{3.5}$$

where:

f'_c= concrete compressive stress, N/mm^2
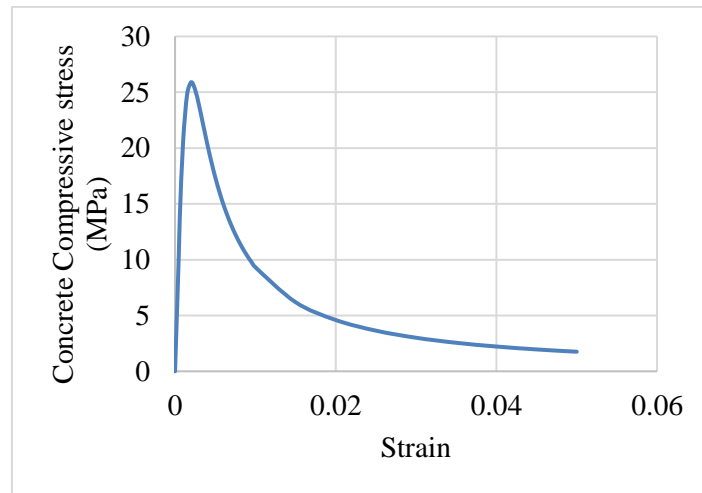
Figure 3.9: Stress-Strain Relationship Curve in Compression

For the stress-strain relationship in tension, the equation proposed by Wahalathantri *et al* (2011) was adopted to identify the stress-strain relationship. Wahalathantri *et al* (2011) modified the Nayal and Rasheed (2006) to avoid the possibility of run time error occur in ABAQUS. The declination of critical tensile strain at the maximum tensile stress from σ_{t0} to 0.8 σ_{t0} were then moved forward to create a slanted portion at the value of 1.25ε_{cr} and the tensile stress are then become 0.77 σ_{t0}. The modified model is shown in Figure 3.10, while the result obtained by using the modified model is shown in Figure 3.11.
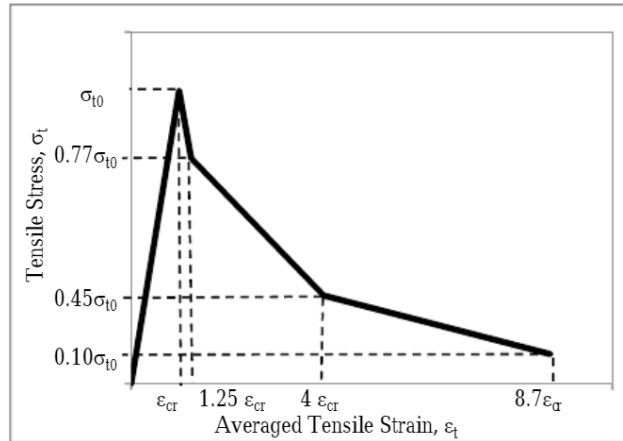
Figure 3.10: Modified Stress-Strain Relationship in Tension Model
(Wahalathantri, et al, 2011)
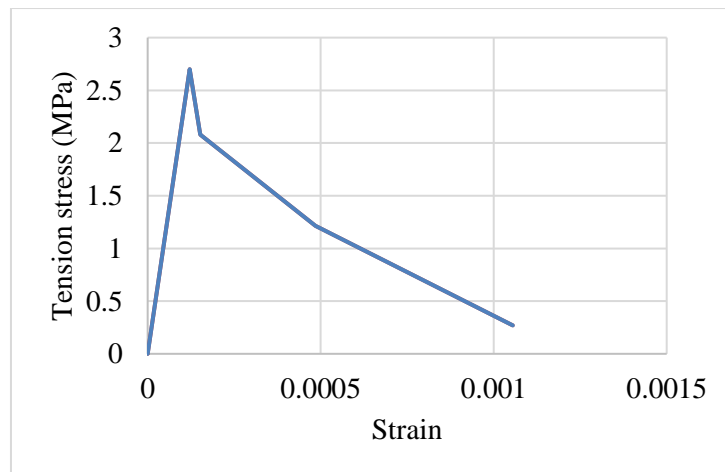
Figure 3.11: Stress-Strain Relationship Curve in Tension

For the concrete damage behaviour, the formula derived in the report of Lima *et al* (2016) was adopted for the computation of the damage parameter. There was an assumption made which is the concrete will not be damaged until the concrete reached its concrete compressive strength and concrete tensile strength. Thus, the damage of concrete will increase uniformly when the concrete strength starts decreasing after the peak of its strength. Equation 3.7 shows the computation of the compression damage parameter while Equation 3.8 shows the computation of the tensile damage parameter. The computation result for the damage factor of compression and tension are shown in Figure 3.12 and Figure 3.13, respectively.

$$d_c = 1 - \frac{f_c}{f'_c} \tag{3.7}$$

where:

f_c = compressive stress on descending limb, N/mm^2

f'_c = peak compressive stress, N/mm^2

$$d_t = 1 - \frac{\sigma}{\sigma_{t0}} \tag{3.8}$$

where:

σ = tensile stress on the descending limb, N/mm^2

σ_{t0} = peak tensile stress, N/mm^2
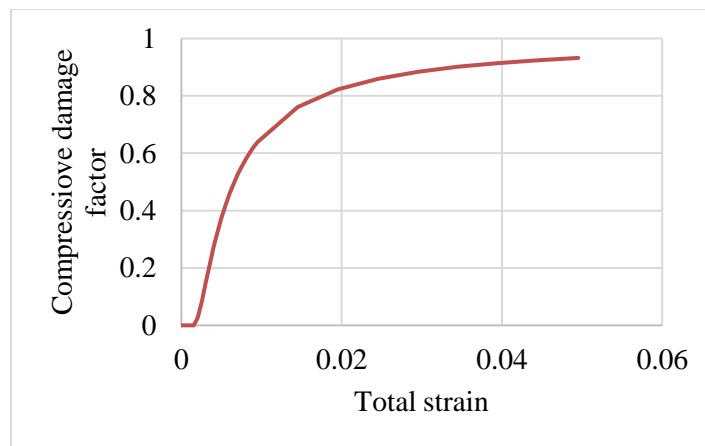
Figure 3.12: Concrete Damage Curve in Compression
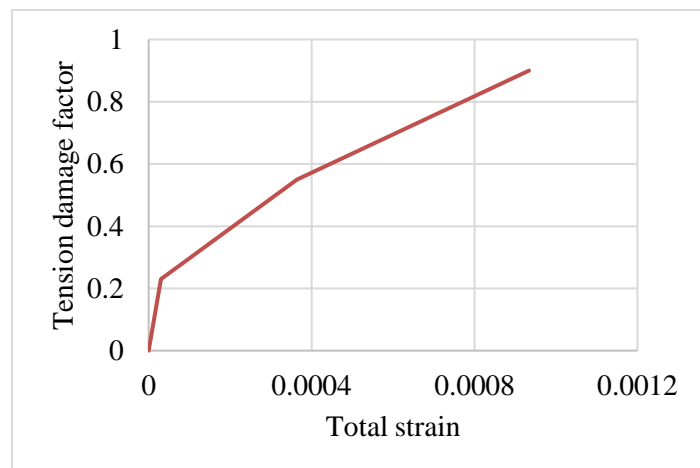
Figure 3.13: Concrete Damage Curve in Tension

3.4.1.2 Steel Properties for Reinforcement Bar

The wire type element in ABAQUS software was the element that uses for model steel reinforcement bar modelling. Like concrete element, there were some of the properties were inserted to the software for material modelling such as the density, modulus of elasticity (*E*), Poisson ratio (*v*), yield strength and plastic strain.

The details of steel properties were referring to EN 1993-1-1:2005 (European Commission, 2005). The density of steel is 7850kg/m^3, the Poisson ratio for steel inelastic range is 0.3 and the young modulus value is around 210000MPa. According to Zhang and Tan (2007), the yield stress for each of the steel bars used is showed as below:

Table 3.5: Type of Steel Used

Annotation	Remarks
R6	6 mm diameter
T10	10 mm diameter
T13	13 mm diameter
T16	16 mm diameter
T20	20 mm diameter
T22	22 mm diameter

By using the young modulus given in the report, the yield strain was calculated out by using Equation 3.9:

$$E = \frac{yield\ stress\ (\sigma)}{yield\ strain\ (\varepsilon)} \qquad (3.9)$$

The modelling method for the steel properties was the bi linear curve of stress-strain relationship and the parameter required includes the yield stress, yield strain, ultimate stress, and ultimate strain. The ultimate strain for steel is set for 0.02 while all other the computed result is shown in Table 3.6.

Table 3.6: Parameters Definition for Steel Properties

Type	Parameter definition			
	Young Modulus (GPa), E	Yield Stress (MPa), σ	Yield Strain(mm/mm), ε	Ultimate Stress (MPa), f_u
R6	195	426	2.1846×10^{-3}	488
T10	198	469	2.3687×10^{-3}	622
T13	190	520	2.7368×10^{-3}	611
T16	194	499	2.5722×10^{-3}	648
T20	193	522	2.7047×10^{-3}	592
T22	197	520	2.6396×10^{-3}	614

3.4.2   Interaction Properties

The interaction properties between each of the elements were defined for ABAQUS analysis. Two main types of interaction properties, the interaction condition between reinforcement bars to concrete and the interaction condition concrete to steel plates were defined in this modelling project

The steel reinforcements are embedded inside the concrete block to form a reinforced concrete deep beam and it is not allowed to have any movement inside the concrete beam. The interaction properties were chosen to be modelled as an embedded element. The concrete which is also a solid continuum element was defined as the host element while the steel reinforcement was the embedded elements that lie within the concrete and the node of steel reinforcement will be the embedded node constrained by the node of concrete. The translational degrees of freedom and initial pore pressure degree of freedom at the node of steel reinforcement was eliminated and this node was constrained by the interpolation value of the concrete's node (host element). Meanwhile, the rotational degree of freedom for the steel reinforcement's node was reserved and this rotational degree was not restricted by the embedded condition.

The steel plates that transferring load to the beam specimen will not have any movement among each other. Therefore, the tie constraint condition was adopted for the interaction properties between steel plates and concrete. The

concrete which is in the constrained condition was defined as the slave surface while the steel place was the master surface. The contract between these two surfaces were under the surface-to-surface contact condition. Only the tangential behaviour and the normal behaviour were selected for the mechanical properties. The tangential behaviour friction formulation was set as rough as the slipping is not desired. While the normal behaviour was selected as hard contact for pressure over closure.

3.4.3   Element Type and Mesh Size

The concrete part for the beam was modelled as a solid continuum element ('C') of a three dimensional ('3D') eight-node ('8') with linear reduce integration ('R'), which is denoted as C3D8R. However, the linear reduce integration have a numerical problem of mesh distortion called hourglassing which is caused by the stiffness reduction. Therefore, the linear reduce integration will be performed under the hourglass control. The steel plates which are also a solid continuum element were assigned the same element type as the concrete which was C3D8R.

The steel reinforcement was modeled as a truss element ('T') in three dimensional ('3D') with 2 nodes ('2'), which is denoted as T3D2. The truss element is used for the slender structure like wire. This element supports the loading along the central axis only and no force or moment acting perpendicularly or angled to the element will be supported while the 2 nodes properties make the element interpolate the displacement and the position of the structure linearly and produce constant stress for the whole element.

According to the research result of Al-Azzawi, Mahdy and Farhan (2010), smaller mesh size can give an accurate result compared to larger mesh size. However, when mesh size is too small will take a longer time for analysis. This study was adopting a mesh size of 25 mm as the coarse aggregate size was in between 20 mm to 25 mm.

3.4.4   Boundary Condition and Load Definition

The support condition for the specimen was set as pinned-roller support. For the pinned support on the left-hand side of the beam, the boundary condition was

defined as pinned by restricting the translation (U) in the x, y, and z-axis while only the rotation (UR) for the z-axis was set as released, rotation (UR) for x and y-axis was as constraint condition as well due to unnecessary. Meanwhile, the boundary condition for the right-hand side support was defined as roller support which allows the movement along the x-axis by restricting the translation (U) in the y and z-axis while rotation (UR) for the x and y-axis was set as a constraint condition. This boundary condition was applied at the middle centre line which was set by using partition function at the support so the support was acting as line support to the steel plate as what the experiment setup showed in Zhang and Tan (2007) research paper.

Two steel plate loading points was assigned a monotonic load of 250kN magnitude (P/2). A reference point was created on the top of the steel plate as a loading point with a concentrated load. The loading was transferred to the steel plate by a roller in the experiment. Therefore, multi-point constraint interaction was adopted to simulate this condition by converting the load from the reference point into line load that acting toward the centre line of the steel plate evenly. The concentrated load was assigned at the CF2 with a magnitude of -250kN while the negative sign indicates the downward direction.

3.5   Result Verification

The model reference beam was verified with the experimental results obtained from the experimental study of Zhang and Tan (2007) to examine the reliability and the accuracy of the model. The parameter adopted as a standard for verification was the load-deflection curve. Other than that, the concrete tension damage contour was compared with the crack pattern of the reference beam's experiment result. This result verification aims to check whether the numerical model complies with the actual reference specimen's behavior and to avoid inaccuracies caused by the numerical problem. If the model shows any noncompliance with the actual experiment result, the re-calibration of the model is necessary to carry out. The model re-calibration includes the mesh size adjustment, stress-strain relationship of the concrete, dilation angles of concrete etc.

3.6 Manual Calculation for Shear Capacity

To justify the trend of the finding from the parameter checking, manual calculation for estimating the shear capacity of the specimen is required. There were a lot of formula provided for calculating the shear capacity of the deep beam. Chetchotisak *et al* (2014) provided guideline for the manual calculation formula. The proposed Strut and Tie Model inside this journal was utilized for the shear capacity computation. The proposed formula for STM is showed in Equation 3.10.

$$V_n = v f'_c sin\theta_s b_w w_s + A_h f_{yh} tan\theta_s + A_v f_{yv} \qquad (3.10)$$

where:
v = concrete efficiency factor
f'_c = concrete compressive strength, N/mm^2
f_{yh} = yield strength of horizontal reinforcement, N/mm^2
f_{yv} = yield strength of vertical reinforcement, N/mm^2
b_w = width of deep beam, mm
A_h = areas of horizontal web reinforcement, mm^2
A_v = areas of vertical web reinforcement, mm^2
θ_s = angle between the concrete compression strut, °
w_s = width of prismatic strut, mm

For the formula to identify the v, concrete efficiency factor, this journal paper suggested a formula introduced by Zwicky and Vogel (2006). The formula is showed in Equation 3.11.

$$v = (1.8 - 38\varepsilon_1)(f'_c)^{-1/3} \qquad (3.11)$$

where:
ε_1 = tensile strain in the concrete in the direction of tension tie

Chetchotisak *et al* (2014) also suggested the value of tensile strain in the concrete in the direction of tension tie should be approximated as strain at

cracking of concrete which is 0.00008. Since the true geometry for the concrete strut is hard to determine, struts are assumed to have a uniform geometry along the cross section, which also addressed as prismatic strut. Two of the suggested formula from Chetchotisak *et al* (2014) was adopted in determining the width of prismatic struts which are showed in Equation 3.12 and Equation 3.13.

$$w_s = \sqrt{(kd)^2 + (w_b)^2} \tag{3.12}$$

$$w_s = kd \tag{3.13}$$

where:

d = effective depth of deep beam, mm

The value of k is a constant obtained from a classical bending theory for a single reinforced beam as below Equation 3.14.

$$j = 1 - \frac{k}{3} \tag{3.14}$$

While j is the constant for obtaining the angle between the concrete compression strut, which showed in Equation 3.15.

$$tan\theta_s = \frac{jd}{a} \tag{3.15}$$

where:

d = effective depth of deep beam, mm

a = shear span, mm

According to Dhahir and Nadir (2020), the formula for obtaining the angle between the concrete compression strut are showed in Equation 3.16.

$$\theta_s = tan^{-1}(\frac{0.9d}{a}) \tag{3.16}$$

Therefore, by comparing Equation 3.16, Equation 3.15 and Equation 3.14, the value of k was concluded as 0.3 and it was adopted for the further shear

capacity of deep beam for each of specimen. Since the proposed STM formula are only deal with the layout of the deep beam, concrete strength and shear link yield strength, the checking for specimen was only be provided to the parameter checking of Batch 1: Shear span to depth ratio while for specimen shear strength capacity for the parameter checking for Batch 2: Longitudinal reinforcement ratio and Batch 3: Position of shear link were not applicable to be checked by this formula but the strength can still be estimated as they were just a modified specimen based on Control Specimen C01.

3.7   Summary

In this chapter, there are two main parts for the methodology which are the planning stage and the numerical modelling. For the planning stage, the historical work which performed by Zhang and Tan (2007) was studied and a reference was chosen from it for model verification purpose. Other than that, the specimen specification and the experiment setup were also decided and refer to this history of work. For the numerical modelling, there is another four-step involved which are material properties modelling, interaction properties modelling, element type and mesh size definition, and boundary condition and load definition. All the steps for numerical modelling are aimed to obtain a modal that can represent the realistic condition of a specimen. These steps will keep on tuning until achieving the desired result when compared to the experiment carried by Zhang and Tan (2007) for the reference beam. The indicator for comparison was the load defection curve produced by ABAQUS software. When the desired model was obtained, the other test specimens with various parameter changes and the control beam were modelled to simulate the loading condition for crack propagation observation, thus the study objective achieved.

CHAPTER 4

RESULTS AND DISCUSSION

4.1   Introduction

This chapter discussed the results output from the numerical analysis form the ABAQUS finite element software. The results of the reference beam, control beam, and other eleven test beam are discussed in this chapter in term of load-displacement curve, von Mises stress contour, plastic strain magnitude (PEMAG), and concrete tension damage.

The discussion of the result is started with the data validation of the references beam, R01 and experimental beam result obtained from Zhang and Tan (2007). This is to validate the modelling technique and the parameter chosen for data input to the software which can obtained a model that can simulate the real-life condition. The result is discussed in three batch in depth for exploring the effect of shear span to depth ratio, longitudinal reinforcement ratio and the position of shear link to the cracking behaviour of ordinary deep beam. Each of the testing parameter is evaluated by comparing among the five specimens for a precise conclusion.

4.2   Data Validation of Reference Beam

The numerical analysis begin with its result validation of the reference beam with the experimental result that obtained from Zhang and Tan (2007). The reference beam R01 was modelled out in accordance with the dimension of the experimental beam which with 350 mm in depth, 80 mm in width and 1330 mm in length. The top reinforcement was modelled as two R6 diameter steel bar while the bottom reinforcement was four T10 diameter steel bar, and the shear link was R6 diameter which placed 350 mm from the mid span.

The result validation is to obtain the model that can reflect the real time behaviour of the deep beam. However, the CDP model requested different kind of the concrete properties in plastic zone, therefore trial and error for the dilation angle and the viscosity was performed to obtain the real result that is most approach to the real-life scenario, the final decision for the dilation angle and

the viscosity were 33° and 0.02 respectively. Moreover, the interaction properties and the boundary condition were checked for the ensure the modelling program can be run for analysis without any numerical error. The index for modelling result validation was the load displacement curve, both load displacement curve result was compared as shown in Figure 4.1, and the validation result was tabulate in Table 4.1
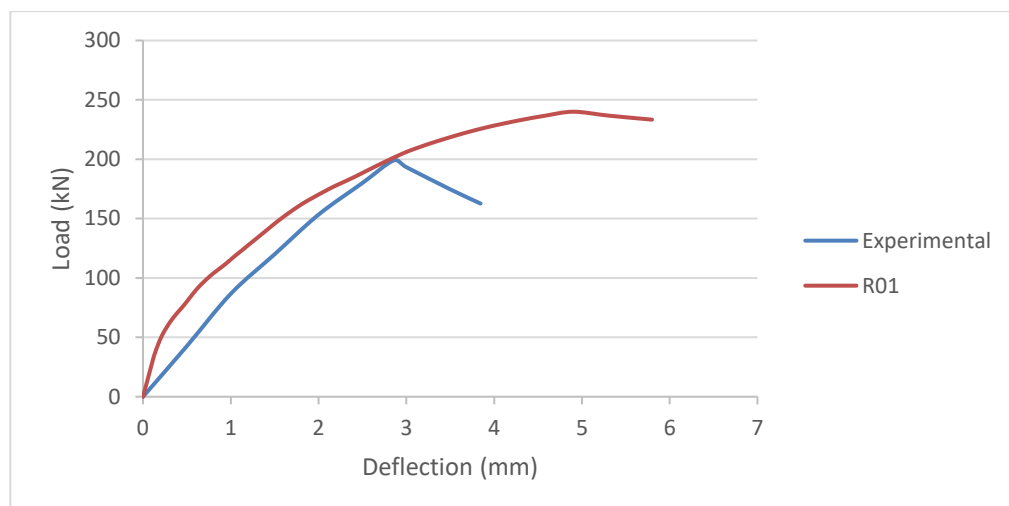
Figure 4.1: Load Deflection Curve Comparison for Experimental Result and
Numerical Result

Table 4.1: Comparison for Experimental Result and Numerical Result

Specimen	Initial cracking load (kN)	Percentage for difference (%)	Failure load (kN)	Percentage for difference (%)
Experimental	60	-	199	
R01	33.33	44.45	240	20.60

From the load-deflection curve result showed in Figure 4.1, the first crack for R01 was happened when the load reached 33.33kN and the deflection was 0.12134 mm while according to the experimental result obtained from Zhang and Tan (2007) the initial crack was happened when the load reached 60kN which is 44.45 % higher than the R01. While for the failure load, R01 was failed at the load magnitude of 240 kN while the failure load for the

experimental result was 199kN which is 20.60 % lower than the R01. It is obvious that the modelled reference beam R01 was quite stiff at the initial loading stage, and it was hard for it to deflect as compared to the experimental data. However, the gap between the R01 and experimental result was getting smaller when the loading goes on. There are two reasons may cause this distorted result, first, the assumption made for performing the finite element analysis was the uniform, isotropic for each element which is not reflect the actual condition of concrete. Concrete consists of aggregate and cement while we cannot ensure the distribution of the aggregate was consistent. Secondly, the interaction properties between reinforcement bar and concrete was defined under fully embedded which already ignore the friction and the condition of bonding when the load is increased, especially the possibility of slipping of reinforcement bar (Deng, Qie and Wang, 2015).

Other than the load deflection curve, the cracking behaviour of the beam has also been compared. The index for checking the cracking for the reference beam R01 was the concrete tension damage as it shows how the concrete splitting. Figure 4.2 shows the experimental cracking result for the beam which obtained from Zhang and Tan (2007). Figure 4.3 shows the numerical cracking result of the reference beam R01. Each result shows the diagonal crack path precisely at the diagonal concrete strut which originated from the inner support to the loading plate. Not only that, but the vertical crack also which developed at the bottom of the mid span and propagated upward vertically was showed out obviously for both cracking results. In short, despite the horizontal crack happened at the two side of the edge, the main cracking behaviour from the numerical result of R01 was in accordance to the experimental result from Zhang and Tan (2007), thereby the reliability of numerical modelling for cracking behaviour was then proven.
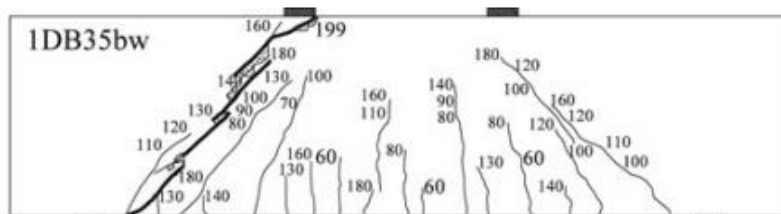
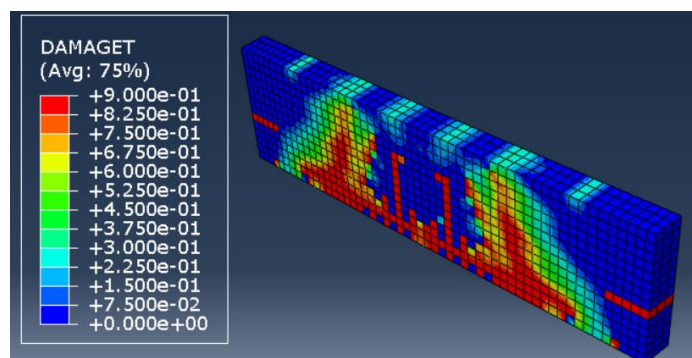Figure 4.2: Experimental Result for Crack Pattern

Figure 4.3: Numerical Result for Concrete Tension Damage of R01

In conclusion, the specimen R01 showed a stiffer behaviour in the initial stage as compared to experimental specimen. However, the load deflection behaviour of R01 reassembles well to the experimental result in term of trend. Both specimens are showing the result in a similar trend which are allowed to provide a converging result. As for the cracking behaviour, the main crack path showed a good agreement to the experimental result. Therefore, the data input for various of parameter and the modelling technique showed a satisfactory result and the reliability of model are proved, thus the study objective is archived.

4.3   Control Beam with Smaller Shear Span to Depth Ratio

The verified modelling input data was adopted to perform the modelling of control beam, C01 which with a smaller shear span to depth ratio of 0.7. The dimension of control beam was exactly same with the reference beam, R01 which in a dimension of 350 mm depth x 80 mm width x 1330 mm length. The reinforcement layout of C01 was also refer to R01 as 2R6 for the top reinforcement and 4T10 for bottom reinforcement, while shear link R6 provided at 350 mm distance from the mid span each side, in a spacing of 150 mm for

two number of shear links. Load deflection curve of C01 was generated out for obtaining the cracking load and the failure load.

Figure 4.4 reveals the load deflection curve of C01. From Figure 4.4, the curve showed a constant gradient in the initial stage until the specimen experiencing the loading of 50kN with the deflection of 0.1432 mm. This point is defined as the first cracking load. Beyond that point, the curve continues its path until a dropping of the experience load during the loading magnitude of 290kN with a deflection of 6.715 mm. As the dropping of the experience load, this point is defined as the failure load of the C01 specimen.

The result of load deflection curve for control beam, C01 displayed as similar trend as reference beam, R01. However, this specimen C01 showed stronger beam behaviour due to the reason of smaller shear span to depth ratio, which is in a good agreement to finding of literature study in Chapter 2.
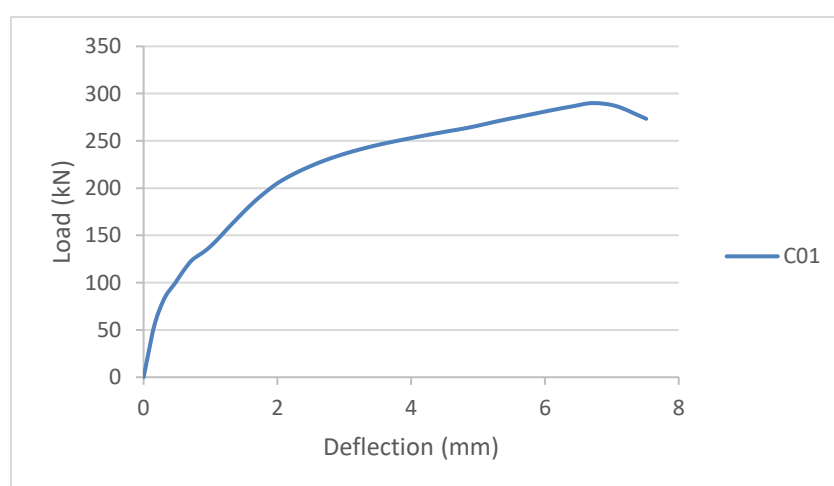

Figure 4.4: Load-Deflection Curve for Specimen C01

4.4 Effect of Shear Span to Depth Ratio

The effect of different shear span to depth ratios to deep beam cracking behaviour was the first element to study. There are three of the test specimens which are SVD-0.85, SVD-0.55 and SVD-0.4 are modelled for a comparative study in this sub chapter. These three test specimens were compared together with reference beam, R01 and control beam, C01 for investigation the relationship between them.

4.4.1 Load-Deflection Curve

The load-deflection curve was one of the indices to study the beam strength when the shear span to depth ratio change. The cracking load and the failure load for the beam specimen can be identified from the load-deflection curve, and the level of deflection under each stage of the load can be studied. Based on the loading level and the deflection level, strength of the beam can be told. Figure 4.5 shows the load-deflection curve for all the specimen for the comparative study. Figure 4.6 and Figure 4.7 show the enlarged view of the cracking load and the failure load for all the specimens respectively, to gain a more precise and aesthetic view of the result. All the result for the cracking load, failure load, maximum deflection, and the percentage for increment are tabulated in Table 4.2.
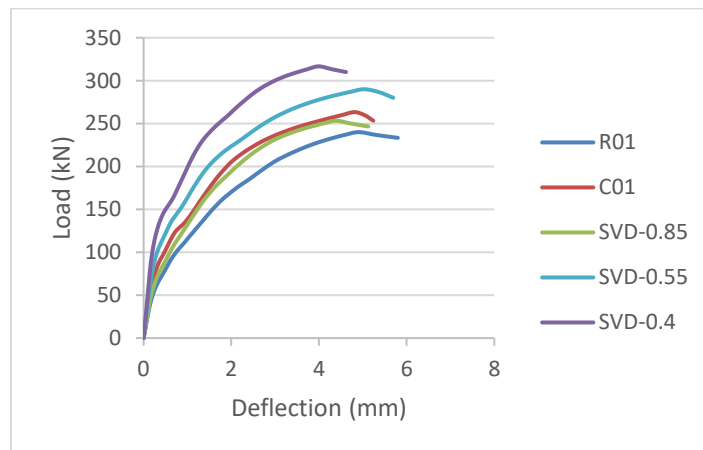

Figure 4.5: Load-Deflection Curve for Comparison for Batch 1 Test Beams
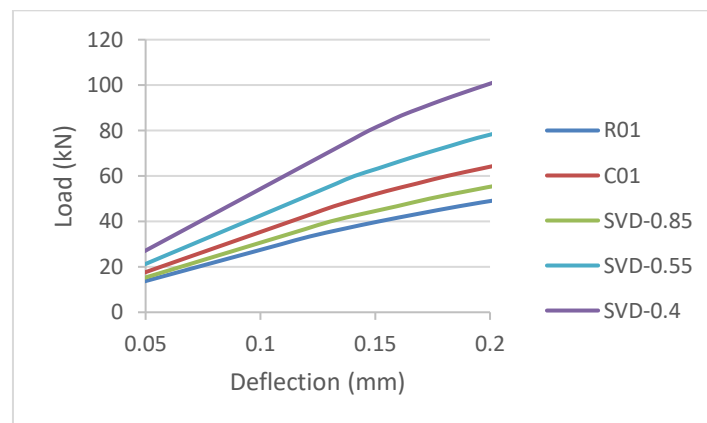

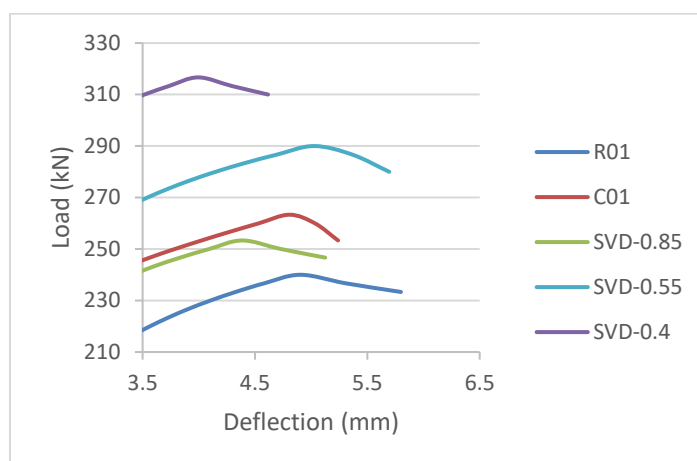Figure 4.6: Enlarged View for Yield Point for Batch 1 Test Beams

Figure 4.7: Enlarged View for Failure Point for Batch 1 Test Beams

Table 4.2: Result Comparison for Initial Cracking Load and Failure Load for
Batch 1 Test Beams

Specimen	Shear span to depth ratio	Initial cracking load (kN)	Percentage for increment (%)	Failure load (kN)	Percentage for increment (%)
R01	1.0	33.33	-	240.00	-
SVD-0.85	0.85	40	20.01	253.33	5.55
C01	0.7	50	25	263.33	3.95
SVD-0.55	0.55	60	20	290.00	10.13
SVD-0.4	0.4	80	33.33	316.67	9.19

Based on the result summarized in Table 4.2, there is an obvious improvement of the specimen strength as the shear span to depth ratio decrease for RC deep beam. Each of the improvement for the initial cracking load was ranging around 20 % to 34 %. In the aspect for failure load, there is a smaller improvement for the which ranging from 3.95 % and up to a maximum value 10.13 %. The relatively small increment for the failure load may be due to the reason for same concrete strength and the reinforcement steel bar provided. Since all the material are remain consistent, the improvement of the failure load will not be large as there is a constraint for the strength. The shear strength

capacity for each of the specimen was calculated out by using the Strut and Tie model which mentioned in Chapter 3. As there were two ways to obtain the prismatic strut width which can give two different results, the result obtained by using Equation 3.12 will denote as Formula 1 while result obtained by using Equation 3.13 will denote as Formula 2. The result for the manual calculation is concluded in Table 4.3.

Table 4.3: Result Comparison for Maximum Shear Capacity for Batch 1 Test Beams with Proposed STM Model

Specimen	Numerical Result (kN)	STM model result by Formula 1 (kN)	Percentage for difference (%)	STM model result by Formula 2 (kN)	Percentage for difference (%)
R01	240.00	262.42	9.34	240.75	0.31
SVD-0.85	253.33	278.70	10.01	254.89	0.62
C01	263.33	296.77	12.70	270.61	2.53
SVD-0.55	290.00	316.05	8.98	287.37	0.91
SVD-0.4	316.67	335.11	5.82	303.94	4.02

From the summarized result in Table 4.3, it is obviously found that the STM model result obtained from Formula 1 is overestimated the load for approximately 20 % to 25 %. While STM model result obtained from Formula 2 shows a satisfactory agreement to the numerical result which had the difference within 5 %. The differences for both results can be explained as the formula derived under the concept of "prismatic strut" which assuming the strut have a uniform cross section along their length., which may not be true in actual condition. Although there still have great differences for the result among the numerical result and the STM model result by using Formula 1, all the results show a same trend which is a increasing of failure load when the shear span to depth ratio decrease which proven the correctness and the reliability of the result.

Theoretically, it was expected the deep beam with the smaller shear span to depth ratio possess a larger strength. In the aspect of cracking load and

the failure load the result was matched to this expectation greatly. However, the maximum deflection of the specimen was not in a consistent trend. The result of the deflection curve is tabulated in Table 4.4.

Table 4.4:   Maximum Deflection for Each Test Specimen Under Batch 1
                    Before Failure

Specimen	Shear span to depth ratio	Maximum deflection at the mid span (mm)
R01	1.0	4.90
SVD-0.85	0.85	4.39
C01	0.7	4.81
SVD-0.55	0.55	5.02
SVD-0.4	0.4	3.99

The deflection of the deep beam should be lesser as the shear span to depth ratio decreasing. However, the deflection result for C01 and SVD-0.55 are not in accordance with the theoretically expectation. The possible reasons for the incorrectness of the result can claim to the misinterpretation of the failure load point. The failure load point for the result is determined when there is a sudden increment for deflection. Due to the reason that numerical analysis software will not terminate the program even the model is considered failed, the failure point needs to be interpreted by oneself. Therefore, the possibility of human error must be considered.

In short, the smaller the shear span to depth ratio, the stronger the deep beam is in term of both yielding strength and ultimate strength. However, the improvement of the ultimate strength may still constraint to material properties.

4.4.2   Von Mises Stress Contour

Von Mises stress contour is one of the ways to study the cracking behaviour of the concrete for deep beam. The von Mises stress contour show the stress distribution pathway of the beam during loaded. Therefore, the stress contour captured during the beam failure, also known as the ultimate load, indicate the fracture location of the beam. The stress distribution path may also be

considered as the possible cracking path. The von Mises stress contour for all the specimens in this subtopic are shown in Figure 4.8.
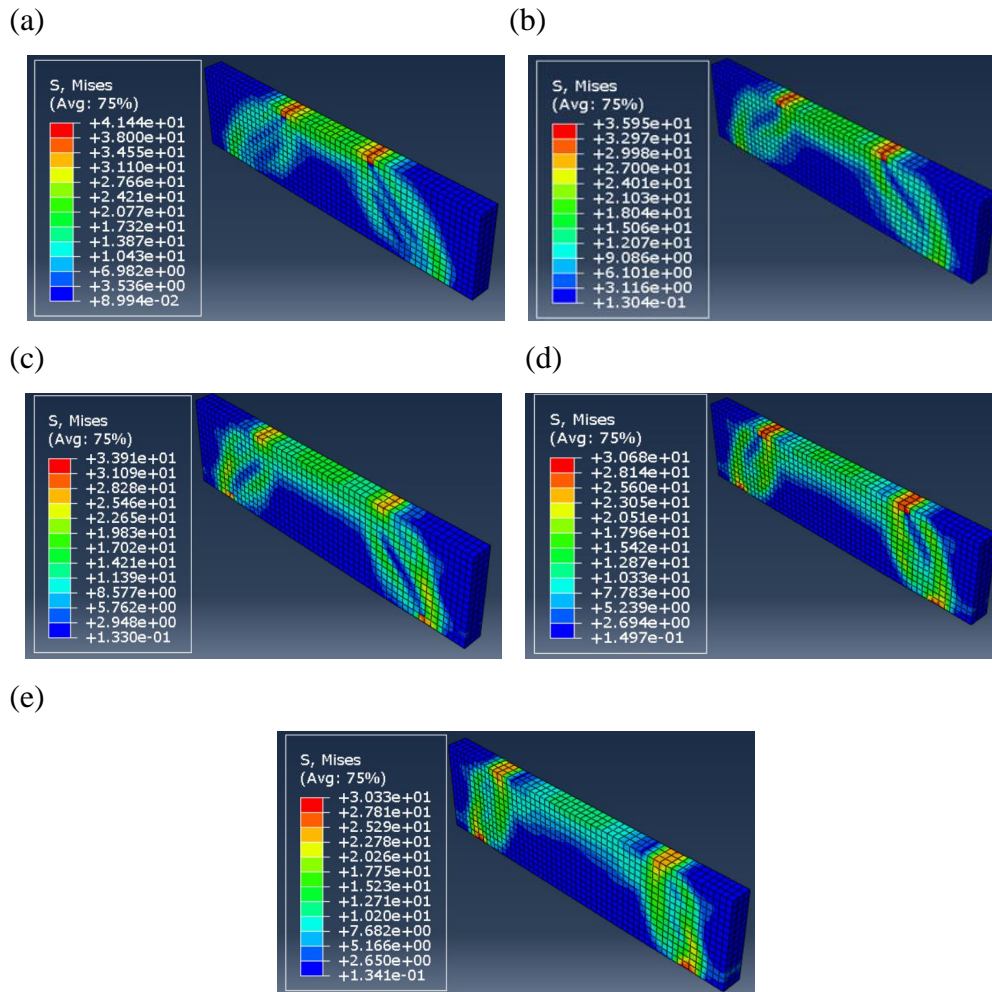
(a) (b)

(c) (d)

(e)

Figure 4.8: Von Mises Stress Contour for Specimens Under Batch 1(a: R01; b: SVD-0.85; c: C01; d: SVD-0.55; e : SVD-0.4)

Based on the overall von Mises contours, the stress distribution of the specimen from the steel plate location and linked with each other. The stress experience from the loading steel plate will be higher as compared to the support steel plate. From the failure condition of the stress distribution contour, it is known that the stress is travelling from the loading steel plate to the support steel plate through the concrete compressive strut. Other than that, the bottle shape of the stress distribution is obvious for all the specimen, thus it may conclude that these beams are fail in the diagonal shear splitting mode and it is a compression shear failure.

The effect of the shear span to depth ratio lowers the area of stress distribution. From Figure 4.8 (a), it was obvious that the area spread for stress distribution become lesser compared to the R01 with 1.0 shear span to depth ratio. Other than that, by comparing the Figure 4.8 (b) to (e), the cracking path also become less inclined when the shear span to depth ratio. This can be concluded that the stress distribution path is in accordance with the concrete compressive strut. In addition, the shear span to depth ratio also helps in reducing the stress gain by deep beam when the angle become larger. However, the effect of reducing become lesser as the shear span to depth ratio decrease. This can be concluded θ_s is effective in reducing the maximum stress cater by the deep beam but this effect will become less significant when the $\theta_s >$ 55.22∘.The result of maximum stress for each of the specimen is tabulated in Table 4.5.

Table 4.5: Results of Angle Between Compressive Strut and Maximum Stress for Each Specimen Under Batch 1

Specimen	Shear span to depth ratio	θ_s , angle between the concrete compression strut	Maximum stress, N/mm^2
R01	1.0	38.38∘	41.44
SVD-0.85	0.85	42.98∘	35.95
C01	0.7	48.53∘	33.91
SVD-0.55	0.55	55.22∘	30.68
SVD-0.4	0.4	63.20∘	30.33

4.4.3 Plastic Strain Magnitude (PEMAG) Diagram

Plastic Strain Magnitude Diagram recorded the concrete plastic strain distribution. This data also useful for identifying the cracking behaviour of the deep beam. The plastic strain captured during the beam failure, also known as the ultimate load, for identify the greatest strain location of the beam. The plastic strain magnitude for all the specimen in this subtopic are shown in Figure 4.9.
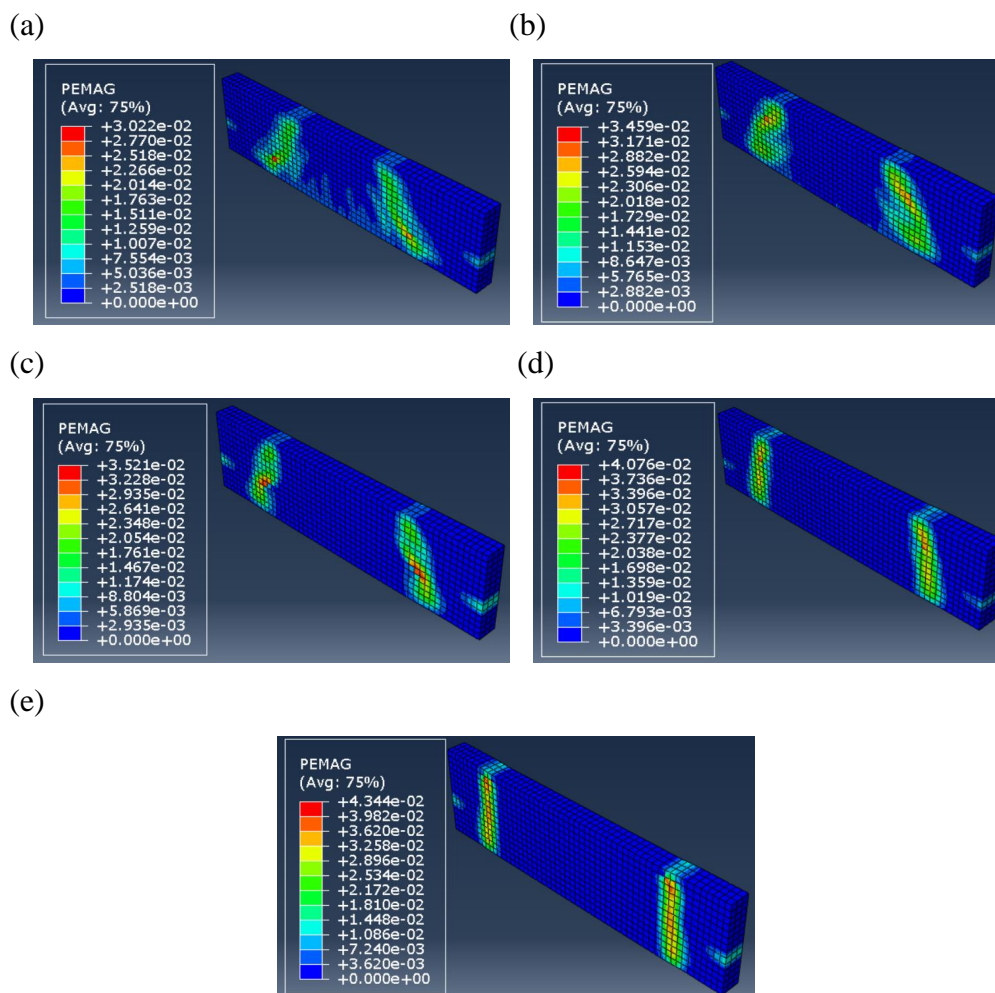
(a)
(b)

(c)
(d)

(e)

Figure 4.9: Plastic Strain Magnitude Diagram for Specimens Under Batch 1(a: R01; b: SVD-0.85; c: C01; d: SVD-0.55; e : SVD-0.4)

Like von Mises stress diagram, the plastic strain was connecting the loading steel plate with the supporting steel plate for all the specimen data. These phenomena justify that the cracking path of the deep beam are in accordance with the concrete compressive strut and the presence of the plastic strain in the compression region signifies the happened of the concrete crushing between the loading and supporting steel plate. Furthermore, the micro strain for the mid span located at mid span of R01 are not showed up in the remaining specimen and the plastic strain for deep beam also become more concentrated as the shear span to depth ratio decreased. This represents that the smaller shear span to depth ratio is effective in limiting the crack distribution.

In addition, the shear span to depth ratio will increase the plastic strain value for specimen at ultimate load. This can attribute as the shorter shear span

increase the stiffness of beam and become brittle, thus explained why the deflection of specimens become lesser when shear span to depth ratio decrease. The result for strain in compressive strut for each of the specimen is tabulated in Table 4.6.

Table 4.6:   Results of Angle Between Compressive Strut and Strain in Compressive Strut for Each Specimen Under Batch 1

Specimen	Shear span to depth ratio	θ_s , angle between the concrete compression strut	Strain in compressive strut, mm/mm
R01	1.0	38.38°	0.03022
SVD-0.85	0.85	42.98°	0.03459
C01	0.7	48.53°	0.03521
SVD-0.55	0.55	55.22°	0.04076
SVD-0.4	0.4	63.20°	0.04344

4.4.4   Concrete Tension Damage Contour

Concrete tension damage contour is an illustration of concrete crack in term of post concrete cracking damage due to tensile stress. This data is reliable for identifying the crack pattern of the deep beam. The concrete tension damage recorded at the failure load for each specimen the beam failure, shows the post concrete crack location of the beam. The concrete tension damage for all the specimens in this subtopic are shown in Figure 4.10.

(a)   (b)

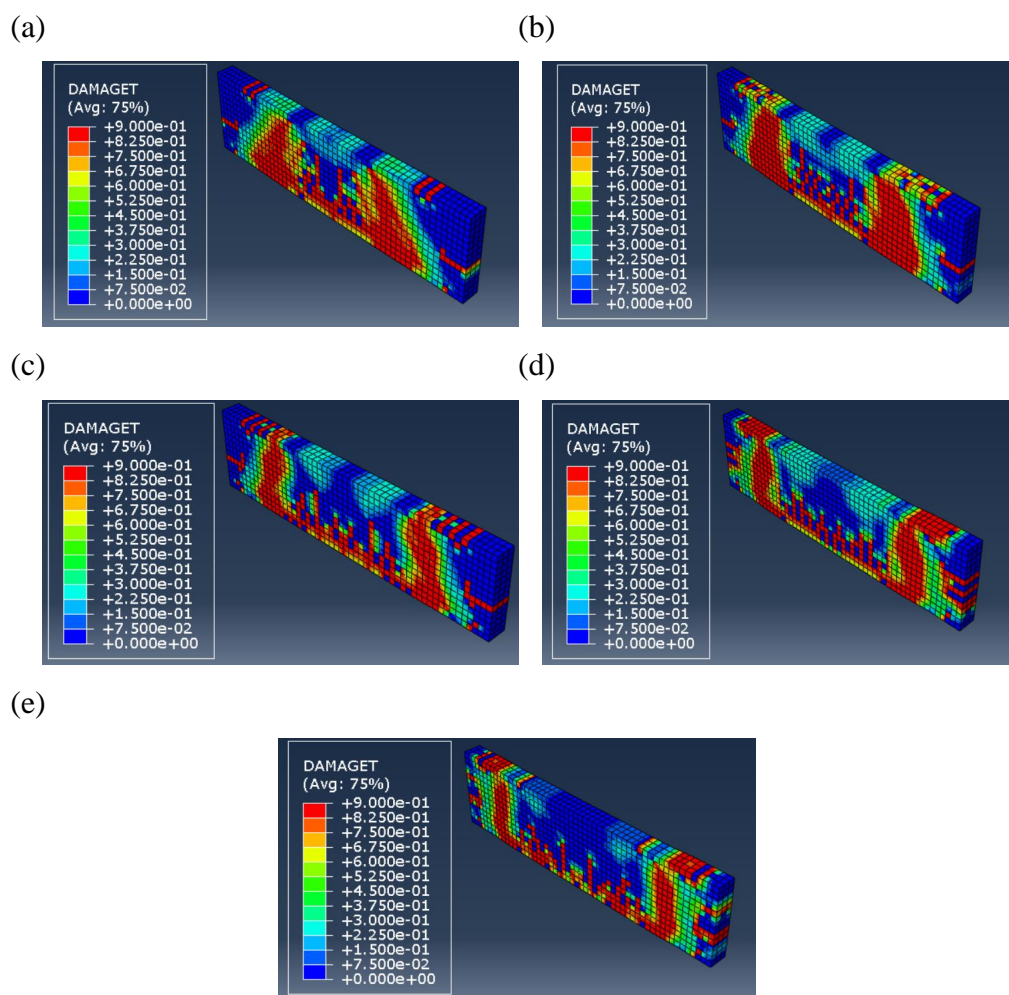(c)   (d)

(e)

Figure 4.10: Concrete Tension Damage for Specimens Under Batch 1 (a: R01;
b: SVD-0.85; c: C01; d: SVD-0.55; e : SVD-0.4)

All the concrete tension damage contour shows a similar appearance. There are some vertical upward cracks develop at the mid span for all the specimen which can be considered as the flexural crack. Furthermore, there is a large, covered area for the concrete tension damage in the path of the plastic strain location which discuss in previous sub chapter, thus the main diagonal crack in the direction of concrete compressive strut can be grantee. There is an arch shape concrete tension damage contour been observed for all the specimen, which represent the arch action of concrete compressive strut and it connected to the tensile tie at bottom region of beam. The top severe part of the concrete damage result recorded can be claimed as the concrete tension damage contour are sensitive and showed out all the damaged part, therefore the severe part of the part can be claimed as crushing of concrete.

Moreover, the concrete tension damage matched with the PEMAG result greatly. The effect of the shear span to depth ratio which help to control the crack are proven by comparing the contour result with the PEMAG, for example, the concrete damage section of SVD-0.4 are more lesser and concentrated as compared to SVD-0.85.

4.5   Effect of Longitudinal Reinforcement

The effect to the deep beam cracking behaviour while different longitudinal reinforcement ratio provided to the deep beam was interested to study in this sub chapter. There are four of the test specimens which are SLR-T13, SLR-T16, SLR-T20 and SLR-T22 are modelled for a comparative study in this sub chapter. These four test specimens were compared together with control beam, C01 which reinforced with 2T10 for longitudinal reinforcement.

4.5.1   Load-Deflection Curve

Similarly, the load-deflection result is adopted to be used as an indicator to tell the strength of the specimen. Figure 4.11 shows the load-deflection curve for all the specimen for the comparative study. Figure 4.12 and Figure 4.13 show the enlarged view of the cracking load and the failure load for all the specimens respectively, to gain a more precise and aesthetic view of the result. All the result for the cracking load, failure load, maximum deflection, and the percentage for increment is tabulated in Table 4.7.
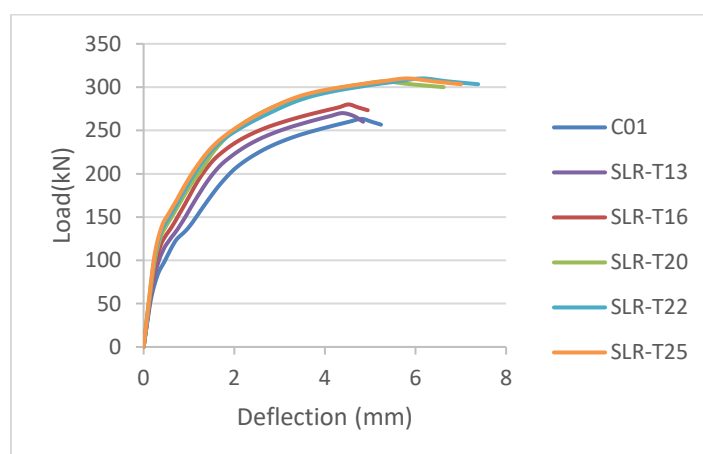

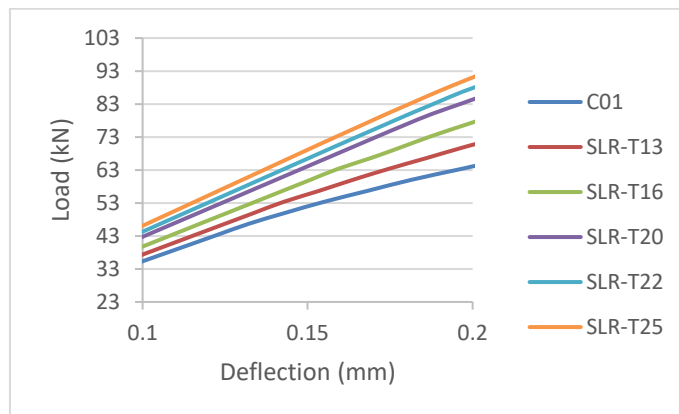Figure 4.11: Load-Deflection Curve for Comparison for Batch 2 Test Beams

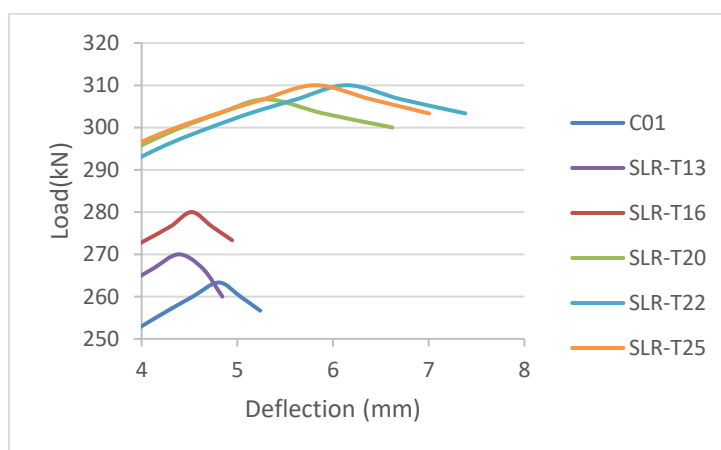Figure 4.12: Enlarged View for Yield Point for Batch 1 Test Beams

Figure 4.13: Enlarged View for Failure Point for Batch 1 Test Beams

Table 4.7: Result Comparison for Initial Cracking Load and Failure Load for Batch 2 Test Beams

Specimen	Longitudinal Reinforcement diameter (mm)	Initial cracking load (kN)	Percentage for increment (%)	Failure load (kN)	Percentage for increment (%)
C01	10	50	-	263.33	-
SLR-T13	13	53.33	6.66	270.00	2.53
SLR-T16	16	63.33	18.75	280.00	3.70
SLR-T20	20	70	10.53	306.67	9.53
SLR-T22	22	70	0	310.00	1.09
SLR-T25	25	70	0	310.00	0

Based on the result summarized in Table 4.7, the increased diameter of longitudinal reinforcement bar enhances the strength of the beam in term of cracking load and failure load. However, the increment range was limited, and it show an incline initially and a decline afterward for both cracking load and failure load. There is an extra specimen, SLR-T25 which equipped with 25 mm diameter longitudinal reinforcement modelled to check the condition of SLR-T20 and SLR-T22 as the enhancement effect terminated at the transition from SLR-T20 to SLR-T22. From the table result, it is proven that the enhancement effect by increasing diameter of longitudinal reinforcement did stop when beyond certain value, as it is 22 mm diameter T22 bar for this study. This enhancement also only helps the specimen reached a maximum ultimate strength for 310.00 kN, this value falls between the range of maximum shear capacity for spear span to depth ratio 0.7 deep beam which is 327kN to 270kN as calculated in previous chapter.

Moreover, the von Mises stress contour for reinforcement cage for C01, SLR-T20, SLR-T22, and SLR-T25 are compared for identification of the stress distribution condition for longitudinal reinforcement bar when it fail. The von Mises stress contour for reinforcement cage of specimens are shown in Figure 4.14. It is obvious that the stress gain by longitudinal reinforcement for specimen C01 is large during failure load which is 426.9 N/mm^2, while for specimen SLR-T20 to SLR-T25 are low which is in a range of 36.21 N/mm^2 to 214.9 N/mm^2. These phenomena represent that the deep beam specimen for SLR-T20, SLR-T22, and SLR-T25 fail before the longitudinal reinforcement experience the maximum stress it can be sustained. In other word, the longitudinal reinforcement is not playing the main role in catering the failure load.

(a)   (b)

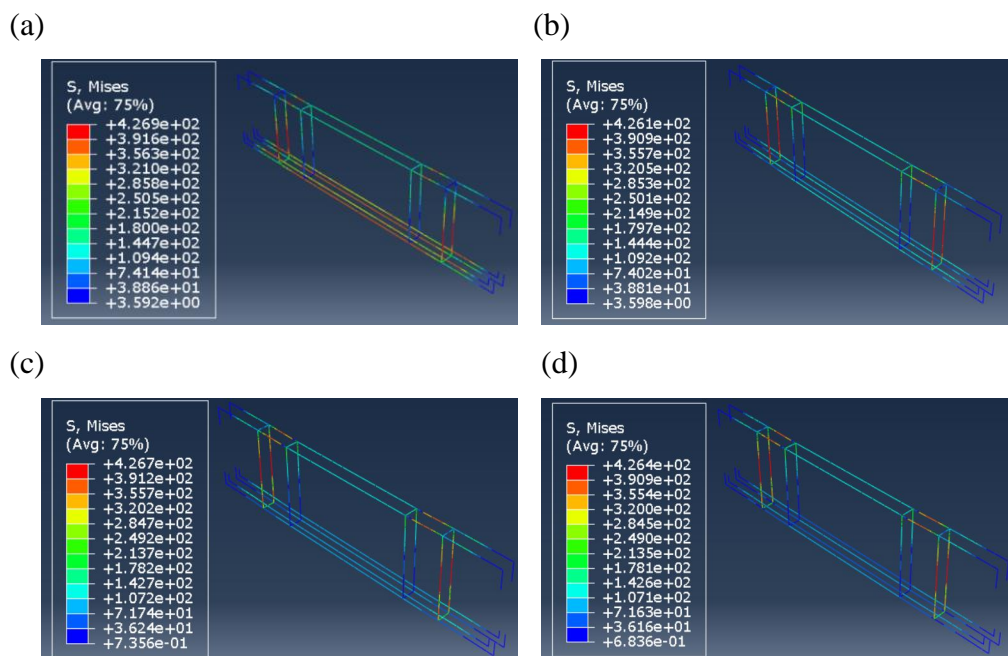(c)   (d)

Figure 4.14: Von Mises Stress for Reinforcement Cage Under Batch 2 (a: C01;
b: SLR-T20; c: SLR-T22; d: SLR-T25)

According to Zhang *et al* (2020), the effect of longitudinal reinforcement ratio is significant as it mainly control the stiffness of beam for shallow beam. While for the deep beam, the stiffness of deep beam is controlled and limited, which cannot be enhanced when beyond certain limit. Furthermore, the shear failure is main failure mode rather than flexural failure, the longitudinal reinforcement ratio shows a very little and limited influence on the deep beam. Hence, the longitudinal reinforcement has less impact to deep beam while compared to shear span to depth ratio.

Theoretically, it was expected the deep beam with larger longitudinal reinforcement diameter possess a larger strength and have a lesser deflection value. However, the maximum deflection of the specimen was not in a consistent trend. The result of the deflection curve is tabulated in Table 4.8.

Table 4.8: Result for Maximum Deflection Before Failure and Deflection
Under the Failure Load of C01 for Batch 2 Test Beams

Specimen	Longitudinal reinforcement diameter (mm)	Maximum deflection at the mid span (mm)	Deflection under the failure load of C01, 263.33kN (mm)
C01	10	4.81	4.81
SLR-T13	13	4.38	3.88
SLR-T16	16	4.52	3.30
SLR-T20	20	5.30	2.35
SLR-T22	22	6.15	2.51
SLR-T25	25	5.82	2.35

Like previous subtopic, the maximum deflection at the mid span did not show a consistency result. Therefore, the deflection of each specimen based on the weakest failure load specimen, C01 was tabulate out and it shows the desired relationship. Under the same loading, the deflection of each specimen decreasing as the longitudinal reinforcement diameter increasing. For the inconsistency of the maximum deflection result is attribute to the misinterpretation of the failure load point as mentioned in precious topic.

In short, the influence of the longitudinal reinforcement is small and limited. The larger the diameter of the longitudinal reinforcement enhance the strength of deep in term of both yielding strength and ultimate strength up to a specific limit. For this study, 22 mm diameter reinforcement bar is the pivot point of the enhancement effect. Beyond this pivot point, the specimen fails before the longitudinal reinforcement bar experienced it ultimate stress capacity.

4.5.2 Von Mises Stress Contour

For the cracking behaviour aspect, von Mises stress contour is captured to identify and predict the possible crack path. The stress contour captured during the beam failure, also known as the ultimate load, indicate the possible fracture location of the beam as that region experienced the greater stress. The von Mises stress contour for all the specimen in this subtopic is shown in Figure 4.15.
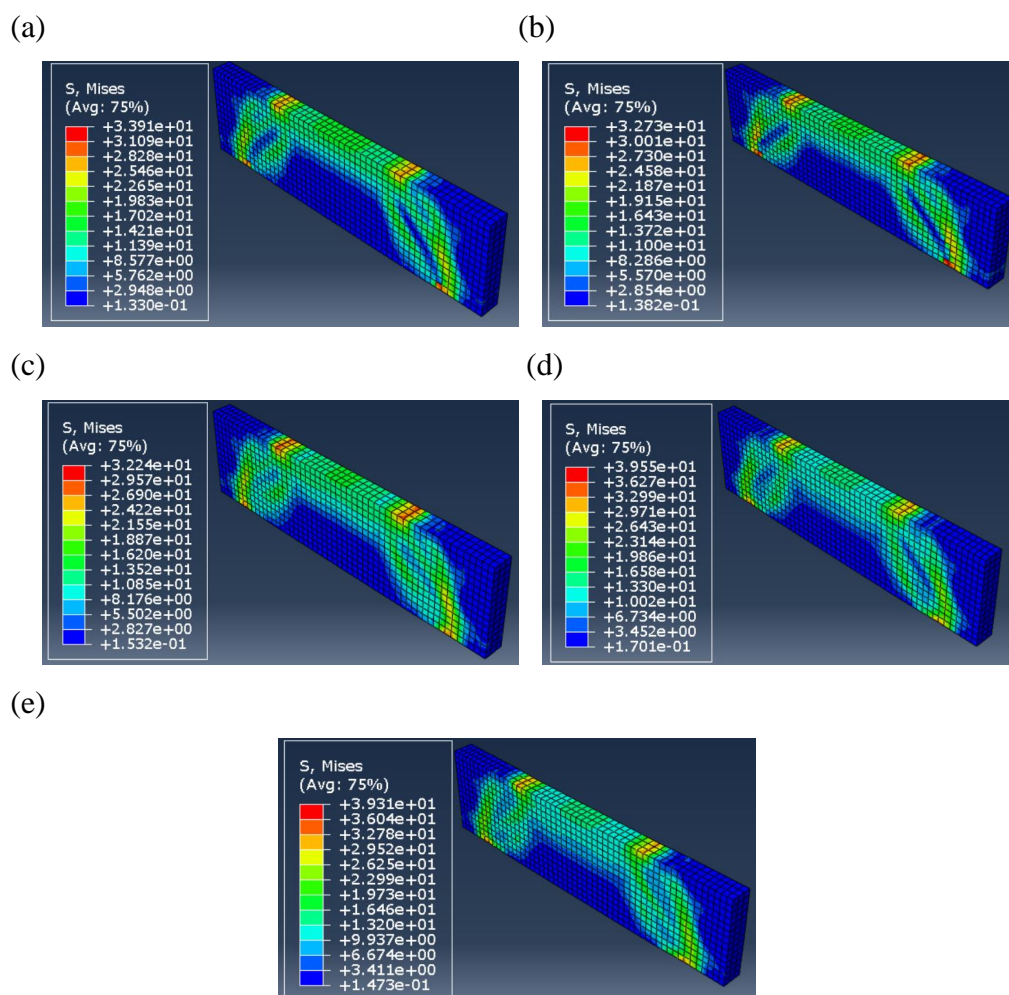
(a) (b)

(c) (d)

(e)

Figure 4.15: Von Mises Stress Contour for Specimens Under Batch 1 (a: C01;
b: SLR-T13; c: SLR-T16; d: SLR-T20 e : SLR-T22)

All the specimen showed a similar contour, stress distribution path linking from the loading steel plate to the support steel plate and the stress experienced at the loading steel plate is larger than supporting steel plate. This show the same conclusion as mentioned in previous chapter as the stress are distributing through the concrete compressive strut and the specimen beams are fail in the diagonal shear splitting mode and it is a compression shear failure.

While for the effect of longitudinal reinforcement to the stress distribution was not obvious. For the specimen SLR-T20 and SLR-T22 showed a larger stress distribution area in a bottle shape at their failure load. This may attribute to the reason that under the failure load, longitudinal reinforcement is yet to gain the stresses before the beam failure, but specimen is experiencing a larger load due to larger longitudinal reinforcement enhances the strength of

specimen in term of failure load, there is a 10.13 % from SLR-T16 to SLR-T20. Thus, it can be concluded that the longitudinal reinforcement has little or no effect the to stress distribution in concrete.

4.5.3   Plastic Strain Magnitude (PEMAG) Diagram

Plastic Strain Magnitude Diagram has also been generated for identify the greatest strain happened in beam for predicting the possible location of crack path. The plastic strain magnitude for all the specimen in this subtopic are shown in Figure 4.16.

(a)   (b)

(c)   (d)

(e)   (f)
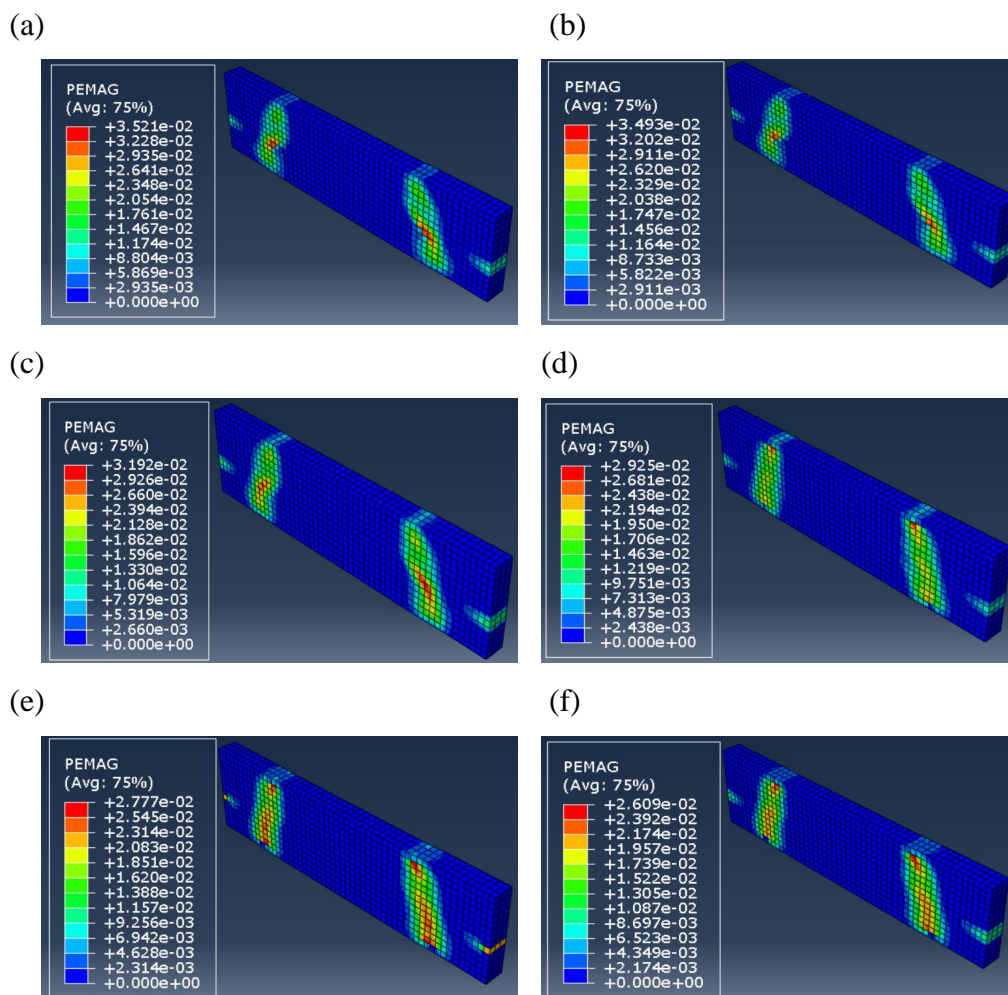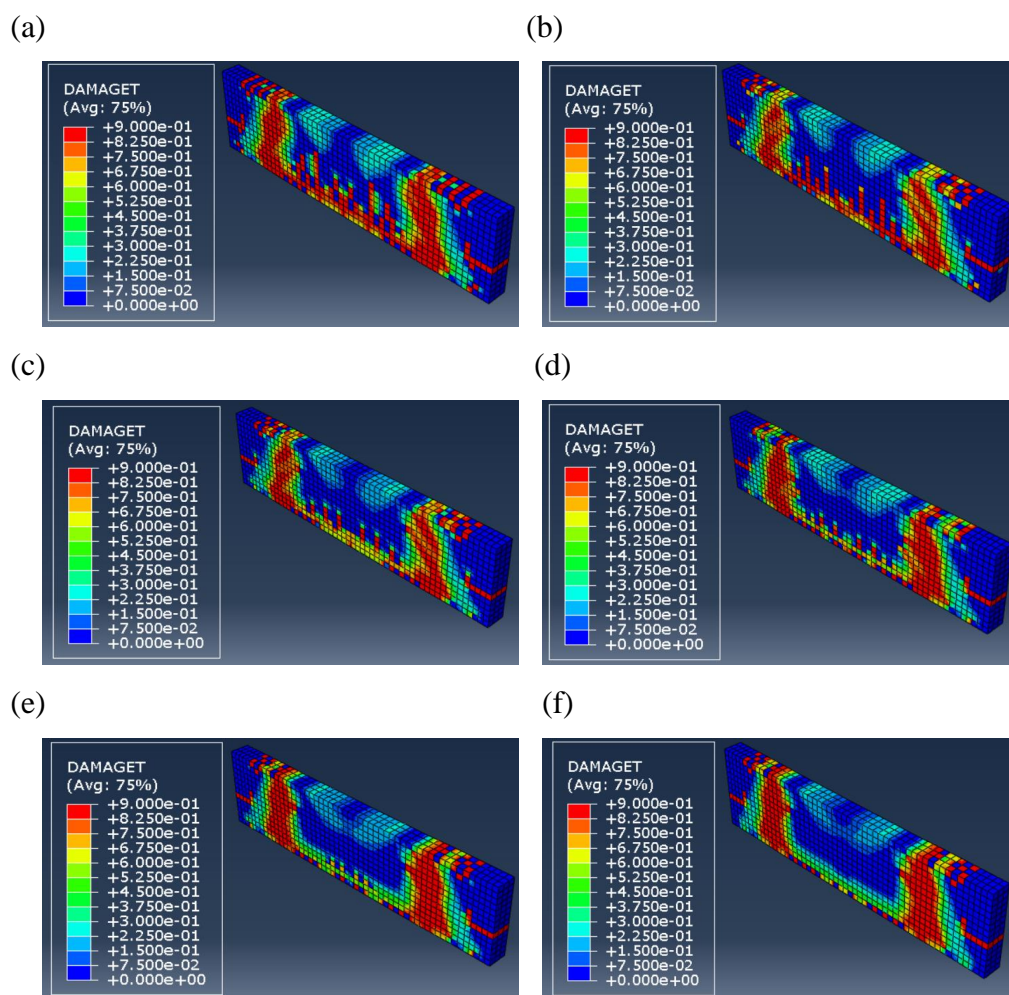

Figure 4.16: Plastic Strain Magnitude Diagram for Specimens Under Batch 2
              (a: C01; b: SLR-T13; c: SLR-T16; d: SLR-T20 e : SLR-T22; f:
              SLR-T25)

From the plastic strain contour, it shows the location of plastic strain was connecting the loading steel plate with the supporting steel plate for all the specimen data. For the specimen of SLR-T20, SLR-T22, and SLR-T25, the area that shows up the plastic strain become wider and less incline while for the specimen of SLR-T13, SLR-T16, and C01 are showed a relative narrower area that happened of plastic strain. The wider plastic strain effective area may claim to a larger load applied to the specimen, thus the area affected is larger. In the aspect of plastic strain magnitude, increase of longitudinal reinforcement help to decrease the plastic strain, but the favourable effect stops at a limit. As for this case, specimen SLR-T20, SLR-T22, SLR-T25 show a similar strain value with a difference not more than 3 %. The result for strain in compressive strut for each of the specimen is tabulated in Table 4.9.

Table 4.9:   Result for Strain in Compressive Strut for Batch 2 Test Beams

Specimen	Longitudinal reinforcement diameter (mm)	Strain in compressive strut (mm/mm)	Percentage of difference, (%)
C01	10	0.03521	-
SLR-T13	13	0.03493	0.8
SLR-T16	16	0.03192	8.62
SLR-T20	20	0.02925	8.36
SLR-T22	22	0.02777	5.06
SLR-T25	25	0.02609	6.05

4.5.4   Concrete Tension Damage Contour

Concrete tension damage contour has then been captured for identifying the crack pattern of the specimen with different longitudinal reinforcement diameter. The post concrete crack location is then be compared to investigate the effect of different diameter of longitudinal reinforcement. The concrete tension damage for all the specimens in this subtopic is shown in Figure 4.17

(a) (b)

(c) (d)

(e) (f)

Figure 4.17: Concrete Tension Damage for Specimens Under Batch 2 (a: C01;
b: SLR-T13; c: SLR-T16; d: SLR-T20 e : SLR-T22; f: SLR-T25)

Based on the concrete tension damage contour result, the concrete tension damage still covered the path of the plastic strain location which discuss in previous sub chapter, thus the main diagonal crack in the direction of concrete compressive strut is remain and the longitudinal reinforcement did not affect the cracking along the compressive strut. However, the flexural crack at the mid span showed an obvious decrease in term of length and number as the diameter of longitudinal reinforcement increase. For instance, the mid span vertical flexural crack for SLR-T25 is quite small and did not well develop upward while the C01 having a large affect area for the mid span vertical flexural crack with a length of 1/3 to 2/3 of the beam depth. This justify the function of longitudinal reinforcement is mainly for controlling the flexural behaviour of rather than the

shear behaviour of deep beam, which deep beam is mean to cater the huge shear force.

4.6   Effect of Position of Shear Link

The effect to the deep beam cracking behaviour with different position of shear link placement was interested to study in this sub chapter. There are four of the test specimens which are SVL-375 mm, SVL-400 mm, SVL-425 mm and SVL-450 mm are modelled for a comparative study in this sub chapter. These four test specimens were compared together with control beam, C01 which with a 350 mm distance from the mid span placing of shear link.

4.6.1   Load-deflection curve

The load-deflection result is also playing a role of indicator to show the effect of different position of shear link to the beam strength. Figure 4.18 shows the load-deflection curve for all the specimen for the comparative study. Figure 4.19 and Figure 4.20 show the enlarged view of the cracking load and the failure load for all the specimens respectively, to gain a more precise and aesthetic view of the result. All the result for the cracking load, failure load, maximum deflection, and the percentage for increment are tabulated in Table 4.10.
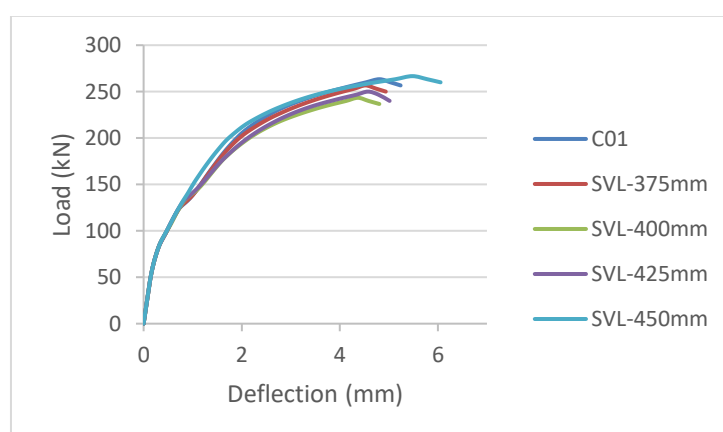
Figure 4.18: Load-Deflection Curve for Comparison for Batch 3 Test Beams
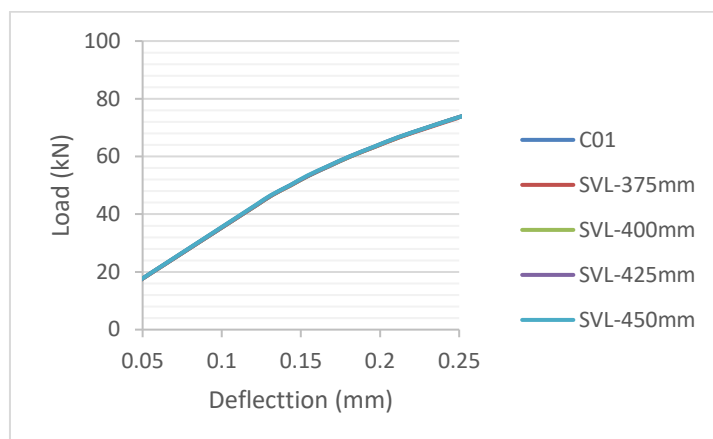
Figure 4.19: Enlarged View for Yield Point for Batch 3 Test Beams
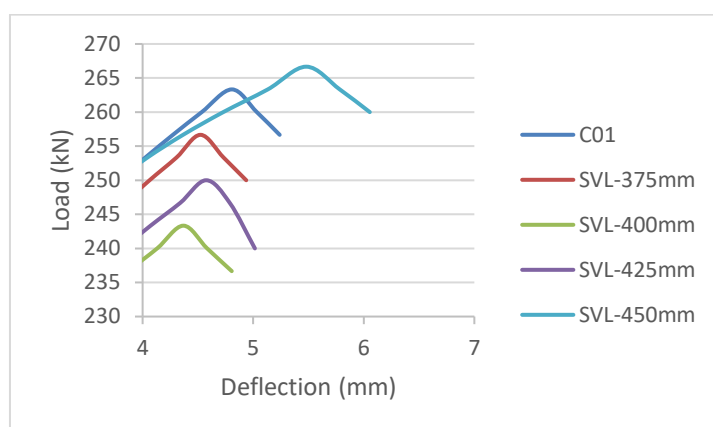
Figure 4.20: Enlarged View for Failure Point for Batch 3 Test Beams

Table 4.10: Result Comparison for Initial Cracking Load and Failure Load for Batch 3 Test Beams

Specimen	Shear link position measured from mid span (mm)	Initial cracking load (kN)	Percentage for increment (%)	Failure load (kN)	Percentage for increment (%)
C01	350	50		263.33	
SVL-375 mm	375	46.67	6.66	256.67	-2.53
SVL-400 mm	400	46.67	0	243.33	-5.2
SVL-425 mm	425	46.67	0	249.99	2.74
SVL-450 mm	450	46.67	0	266.67	6.67

Based on the result summarized in Table 4.10, by increasing the length for placement of shear link which measure from the mid span did not increase the strength of the specimen in term of failure load and initial cracking load. The failure shows a decreasing initially and turn the trend into increasing afterward. By comparing the specimen C01 and SVL-450 mm, the failure load differences between them are small, which is 3.33kN in magnitude and 1.26 % in percentage. This implies that when the shear link keeps on moving to reach a specific position the strength will be gain back. In other word, the changing position of shear link makes the strength become symmetric, as it is lowest strength for SVL-400 mm and strongest For C01 and SVL-450. One of the similarities of C01 and SVL-450 for explaining this result is under the position of these two specimens, one of the shear links will locate under the steel plate which used for loading and supporting. Therefore, the shear link may directly sustain the loading from top or the supporting load from bottom and shows a stronger behaviour. Moreover, changing position of shear link only create little or no effect to the load for initial crack.

The von Mises stress contour for reinforcement cage of specimen C01, SVL-400 mm, and SVL-450 mm are shown in Figure 4.21. From the figure, the stress gain by shear link for SVL-400 mm is low during its failure load which is 243.9 N/mm^2, while for the specimen C01 and SVL-450 mm are high and critical which are 426.9 N/mm^2 and 455.2 N/mm^2. This implies that the shear link for the SVL-400 mm cater very little amount of stress, and the stress flow through the concrete directly while the C01 and SVL-450 mm did cater a larger amount of stress. This explained why the C01 and SVL-450 mm is stranger than SVL-400 mm. Moreover, the vertical shear link did not provide the significant effect to deep beam shear capacity because the shear is mostly transferred by strut and tie action (Zhang *et al*, 2020). Therefore, the when the position of shear link did not cover the path of strut-tie action, that section is considered as no shear reinforcement.

(a) (b)

(c)
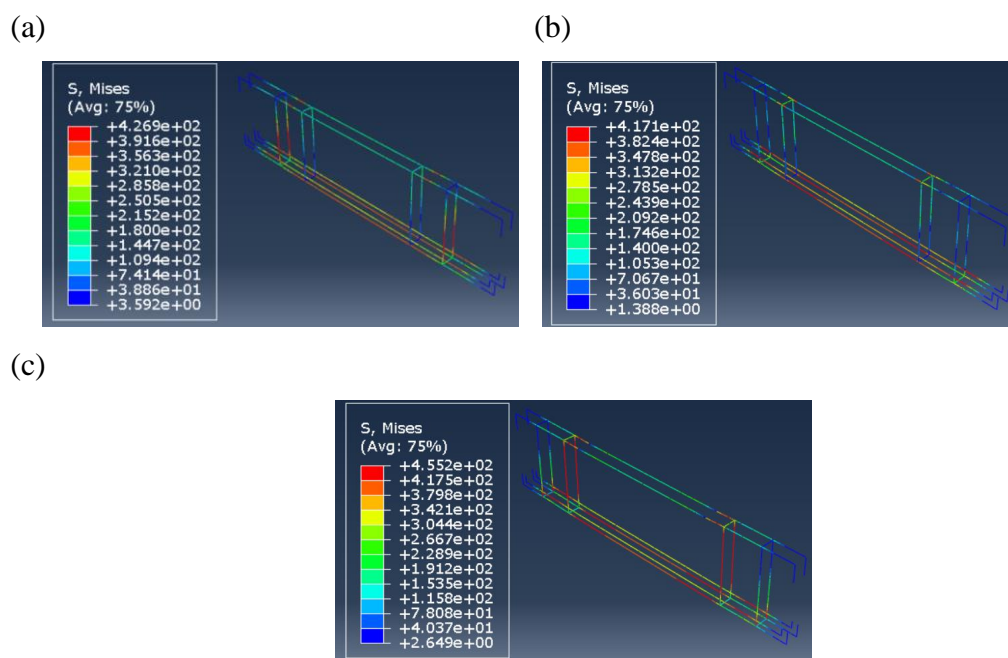
Figure 4.21:   Von Mises Stress for Reinforcement Cage Under Batch 3 (a: C01;
                b: SVL-400 mm; c: SVL-450 mm)

In the aspect of deflection, the specimen did not show a consistent increasing result but show a similar relationship as the failure load. The result of the deflection curve is tabulated in Table 4.11.

Table 4.11: Result for Maximum Deflection Before Failure for Batch 3 Test Beams

Specimen	Shear link position measured from mid span (mm)	Maximum deflection at the mid span (mm)
C01	350	4.81
SVL-375 mm	375	4.52
SVL-400 mm	400	4.37
SVL-425 mm	425	4.57
SVL-450 mm	450	5.49

This result of maximum deflection at the mid span agrees with the relationship of the failure load of specimen. The deflection for SVL-400 mm is the lowest which is 4.37 mm while SVL-450 mm gives a larger deflection of 5.49 mm. This implies that the SVL-400 mm fails before it deflects while SVL-

450 mm deflected more before it fails. It can attribute to the shear link that helps to cater the stress. In short, the influence of the shear link is sensitive to its position. Not only that, but the position of the shear link must also approach to the strut and tie effective section as near as possible to get the greatest enhancement of beam strength.

4.6.2   Von Mises Stress Contour

In the same way, the von Mises stress contour is collected in order to detect and forecast the fracture route. The ultimate load, or stress contour, captured during beam failure indicates the likely fracture site of the beam since that region sustained the most stress. The von Mises stress contour for all the specimen in this subtopic is shown in Figure 4.22.

(a)   (b)

(c)   (d)

(e)
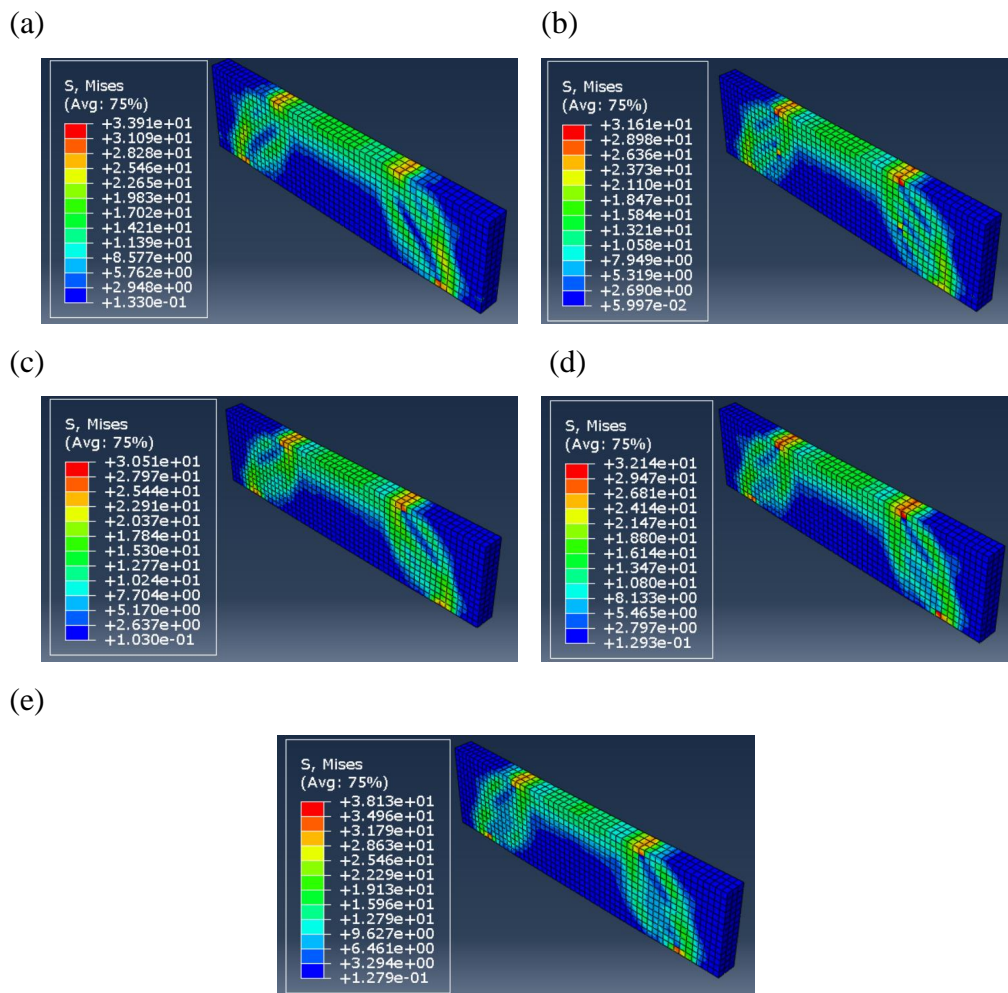
Figure 4.22: Von Mises Stress Contour for Specimens Under Batch 3 (a: C01; b: SVL-375mm; c: SVL-400mm; d: SVL-425mm; e: SVL-450mm)

Same as previous discussion, all specimen showed a similar contour, stress distribution path linking from the loading steel plate to the support steel plate and the stress experienced at the loading steel plate is larger than supporting steel plate. While for the effect of position of shear link was not obvious. For the specimen C01 and SVL-450 mm less concentrate stress path but with a larger magnitude compared to other specimens, which are 33.91 N/mm^2 and 38.13 N/mm^2 respectively. Specimen SVL-400 mm show the lowest stress distribution magnitude, which are 30.51 N/mm^2. This may attribute to the reason that under the failure load, the low effectiveness of stress distribution causes the beam to fail as the shear link is not place at the suitable position for SVL-400 mm while the stress distribution for C01 and SVL-450 mm are effective, hence the stress during the failure load is larger. In short, it can be concluded that the position of shear link has little or no effect the to stress distribution in concrete.

4.6.3   Plastic Strain Magnitude (PEMAG) Diagram

Plastic Strain Magnitude Diagram was captured to determine the largest strain that occurred in the beam to anticipate the location of a fracture route. The plastic strain magnitude for all the specimen in this subtopic was showed in Figure 4.23.

(a)   (b)

(c)   (d)

(e)
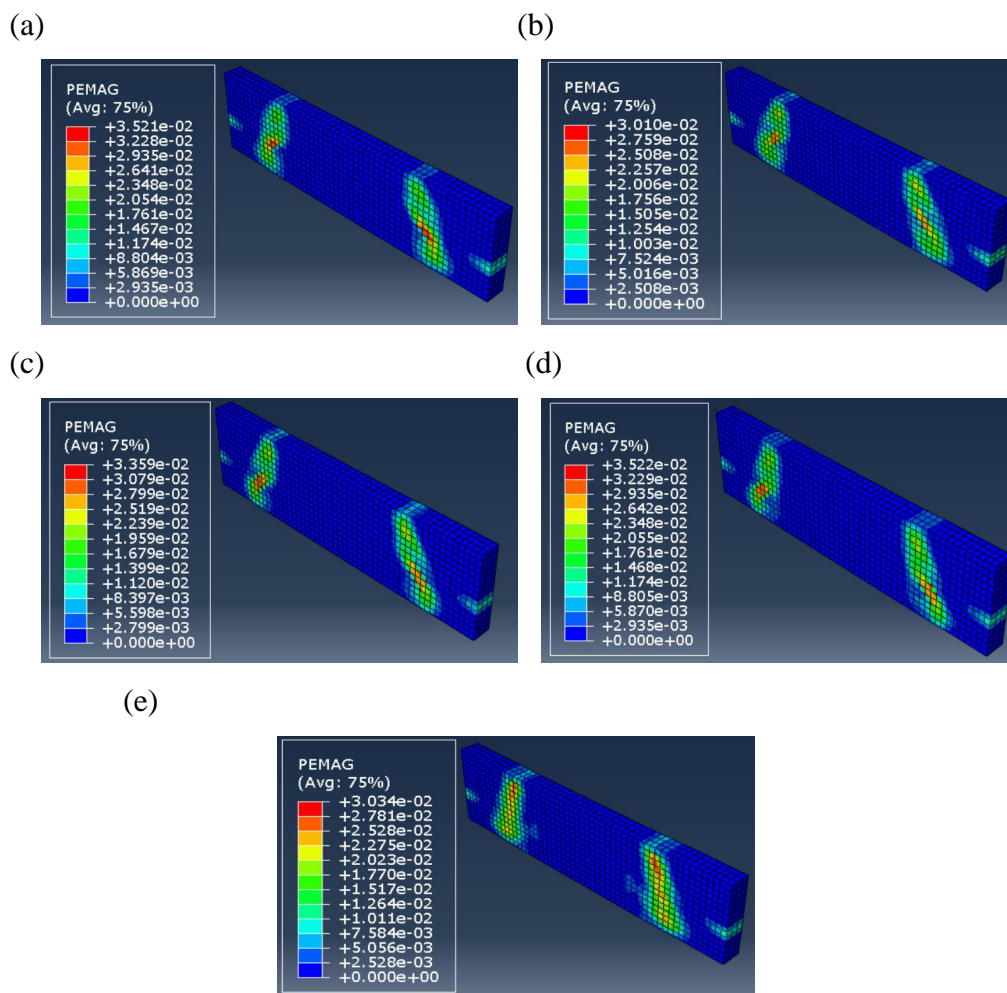
Figure 4.23: Plastic Strain Magnitude Diagram for Specimens Under Batch 3
(a: C01; b: SVL-375 mm; c: SVL-400 mm; d: SVL-425 mm; e:
SVL-450 mm)

The position of plastic strain was linking the loading steel plate with the supporting steel plate for all specimen data, as shown by the plastic strain contour. However, the magnitude for the plastic strain during the failure load did not show a converging result. The specimen C01 and SVL-425 mm showed a larger plastic strain about 0.03521 and 0.03522 respectively, while the SVL-375 mm and SVL-450 mm show a smaller plastic strain as 0.03010 and 0.03034 respectively. The specimen SVL-400 mm which mentioned above as the weakest specimen show a moderate plastic strain value for 0.03359 which is smaller than C01 and SVL-425 mm. By comparing the specimen behaviour with the specimen C01, the SVL-400 mm and SVL-425 mm is a specimen with a larger plastic strain magnitude under a smaller failure load, which means the

sustainability of this specimen is weak. While the specimen and SVL-375 mm and SVL-450 mm is a specimen with a small plastic strain under a larger loading, which implies that the beam is stronger. Therefore, a conclusion can be made from this finding, which are the shear link position that place at 400 mm to 425 mm from the mid span is undesired as it gives a lower sustaining low with a larger crack width. The result for strain in compressive strut for each of the specimen is tabulated in Table 4.12.

Table 4.12: Result for Strain in Compressive Strut for Batch 3 Test Beams

Specimen	Shear link position measured from mid span (mm)	Strain in compressive strut (mm/mm)	Failure load (kN)
C01	350	0.03521	263.33
SVL-375 mm	375	0.03010	256.67
SVL-400 mm	400	0.03359	243.33
SVL-425 mm	425	0.03522	249.99
SVL-450 mm	450	0.03034	266.67

4.6.4   Concrete Tension Damage Contour

Concrete tension damage contour had been captured to explore the relationship of different position of shear link and the crack pattern. The effect of different shear link position to the post concrete crack is to be investigate in this sub chapter. The concrete tension damage for all the specimens in this subtopic are shown in Figure 4.24.

(a)

(b)

(c)

(d)

(e)
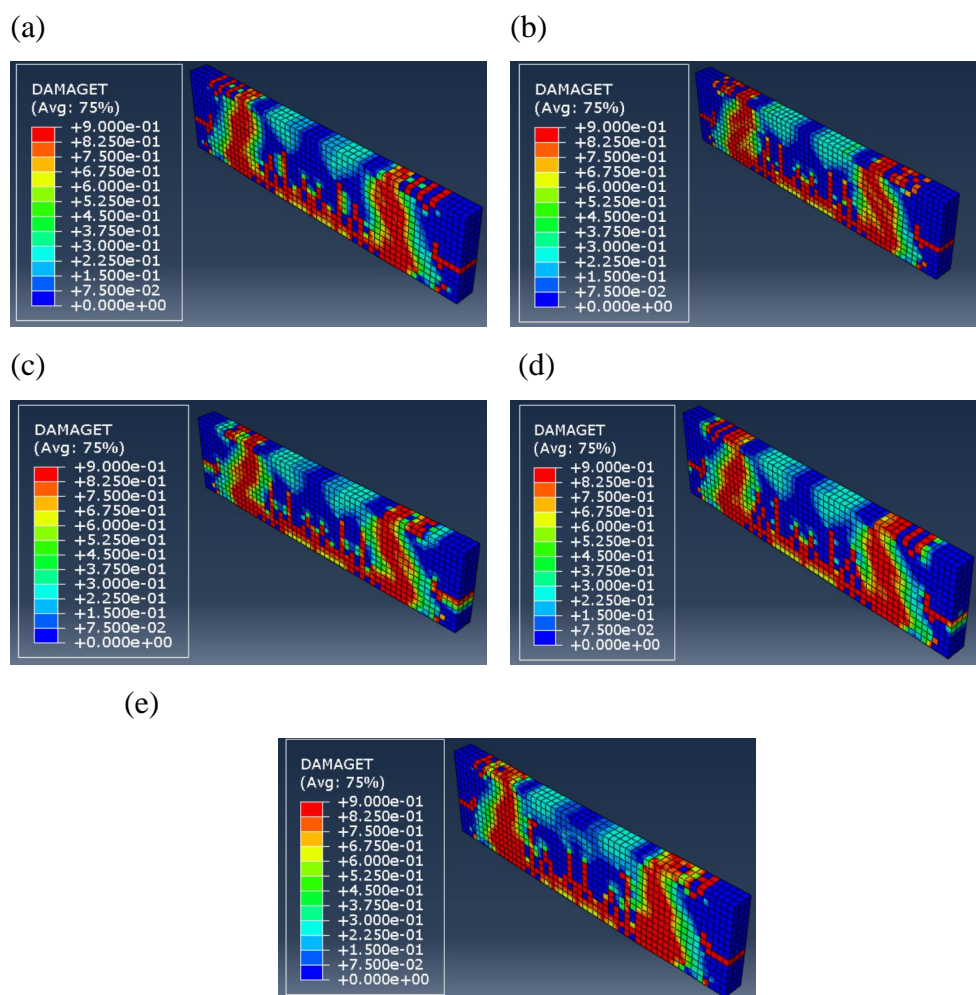
Figure 4.24: Concrete Tension Damage for Specimens Under Batch 3 (a: C01; b: SVL-375 mm; c: SVL-400 mm; d: SVL-425 mm; e: SVL-450 mm)

Like the previous two sub chapter, the main concrete tension damage is still in accordance with the plastic strain while with a lot of vertical flexural crack at the mid span, thus the main diagonal crack in the direction of concrete compressive strut is remain. However, different position of the shear link do affect the concrete tension damage contour. For example, the specimen SVL-400 mm which discuss as the bad placement of shear link position in the previous discussion show an obvious cracking path of the at the compressive strut with a less spreading area. While the specimen SVL-450 mm which discussed as the best location of the shear link placement possess the wide spreading area for the concrete tension damage contour. Not only that, but the vertical concrete tension damage also locate at the mid span of the SVL-450mm

is longer than other specimen and reached 2/3 of beam depth. Therefore, this justify that the suitable placing of shear link helps the specimen SVL-450 mm to cater more load and the diagonal crack path become wider and the flexural cracking effect is more obvious as the shear cracking effect did aid by the shear link when the stress pass through the shear link.

4.7   Summary

In a nutshell, the smaller the shear span to depth ratio, the larger the strength of the deep beam in term of yield strength and fracture strength. By reducing the shear span to depth ratio even helps for control the cracking region of deep beam and increase the stiffness of the beam. However, since the stiffness of the beam been increased, the behaviour of beam become more brittle and showed a low deflection before failure. This outcome had connected to the study result that mentioned in Section 2.3.1 completely.

The failure of deep beam consists of flexural failure and shear failure. By increasing the longitudinal reinforcement, it helps to reduce the effect of flexural failure only. When the flexural failure is fully eliminated, increasing of diameter of longitudinal reinforcement will not help to enhance the strength of deep beam. In cracking behaviour aspect, increasing of the longitudinal reinforcement will reflect lesser number of mid span vertical flexural crack with shorter length. The plastic strain in the concrete compressive strut also helps to reduce but with a limit when the flexural effect gets the maximum enhancement the plastic strain reduction will also been terminated.

The position of shear link is very sensitive to deep beam behaviour in term of strength and cracking. The suitable location for shear link which connected coincide with the compressive strut do enhance the beam strength and delay the failure, fully utilized the strength of deep beam before its failure by distributing the stress to the shear link. For cracking behaviour, the flexural crack at the mid span is obvious due to a reason that the shear crack is delayed by the shear link and the development of the flexural crack are proceeding.

CHAPTER 5

CONCLUSION AND RECOMMENDATIONS

5.1   Conclusion

In a nutshell, this research has successfully performed the numerical analysis by using ABAQUS software. Three set of specimens including one reference beam, one control beam and thirteen test specimens are developed and compared for identify the effect of different parameter to the deep beam behaviour in term of strength and cracking behaviour. The study objectives were achieved through the completion of this study.

The first objective is to verify the numerical result obtained from the developed model with existing experimental results obtained from the literature. The numerical result showed stiffer behaviour than the experimental result as percentage different in yield strength was 20.6 %. However, the load-deflection behaviour of reference beam resembles well to the experimental result in term of trend. The ability of provide a converging result are proved and the main cracking path for both results had a good agreement as well. The modelling technique and data were proven reliable to carry on the modelling of the control beam and test beam for further study.

The second objective is to simulate crack propagation in different reinforced concrete deep beam by using numerical method. The crack propagation for all the deep beams were similar. The vertical upward crack was developed in the mid span and is considered as the flexural crack. While for the main cracking path was in the direction of the concrete compressive strut. The diagonal crack was developed symmetrically and showed an arch shape which connected to the tensile tie at the bottom. The top part of some specimens showed a severe concrete crushing. By changing the different parameter will only change the flexural crack length at the mid span, diagonal crack angle, and the crack affected area, while the crack propagation pattern remained same.

The third objective is to investigate the parameter that affects the deep beam behaviour including the shear span to depth ratio, longitudinal reinforcement diameter and shear reinforcement position. The smaller shear

span to depth ratio provided enhancement ranging from 3.95 % to 10.13 % for deep beam shear capacity. For cracking aspect, decreasing the shear span to depth ratio caused the crack affected area become smaller, and brittle effect are shown. The enhancement effect brought by larger longitudinal reinforcement was only within 10 % for shear strength and it showed only 1.09 % of enhancement effect when bar diameter goes beyond 20 mm. For the crack behaviour, the flexural crack at mid span decreased to below 1/3 of beam depth when the bar diameter increased until 16 mm and above. For the effect of the shear link position, it is a crucial and sensitive item to be considered for deep beam development. Only the shear link that were placed at the position that coincide with the compressive strut shows 1.27 % of enhancement effect in shear capacity and it shows 7.6 % of reduction when shear link placed beyond that region. While for the cracking aspect, the flexural crack at the mid span were long for the shear link positioned in the suitable area as it delayed the shear failure while the flexural failure continues.

All the study objectives had accomplished and obtained the achievement in the study's aim to perform the numerical analysis to the crack propagation of deep beam.

In short, this study had proved the reliability of performing the behaviour analysis of deep beam by using FEA method. To create a strong deep beam and with lesser crack, the shear span to depth ratio must be as small as possible and the position of shear link must be placed wisely. Moreover, increase the longitudinal reinforcement diameter which is a conventional way to enhance the performance of flexural beam should not be the first choice of enhancing the deep beam strength, unless the aim is to eliminate the flexural crack at the mid span of deep beam, as it is not effective to strength and crack behaviour.

5.2 Recommendations

The reliability of the numerical study on deep beam behaviour by using ABAQUS software is proven. However, there still have some space for future improvement on this study. Here are some of the recommendations proposed for the future study.

First recommendation is refining the modelling technique that adopted in this study. The result that obtained from numerical modelling is in stiff behaviour in the initial stage and it only get close to experimental result as the loading condition continue. A revised modelling technique should be used to get the result. The interaction properties between the reinforcement bar and the concrete should be revised as if adopting the fully embedded condition it will ignore the slipping possibility for the reinforcement bar.

The second recommendation is adding one more section for the parameter checking of position of shear link which is the layout of shear link placement. As the result obtained, the behaviour of shear link will become effective when it placed within the concrete compressive strut region. Based on the von Mises stress contour, the concrete compressive strut is in diagonal with angle. By combining these two observations, it should be checked the effect of shear link placed directly intersect with the concrete compressive strut.

The third recommendation is verifying the numerical model with the experimental result. Under the influence of Covid-19 pandemic, the numerical model was verified with the experimental result that obtained from Zhang and Tan (2007), which is not enough and comprehensive. Other than that, the result obtained from the hand-on experiment also can be used for performing the three ways cross checking for the shear capacity of deep beam with different shear span to depth ratio, instead of checking with mathematical formula solely. Therefore, laboratory test should be conducted for a comprehensive and persuasive conclusion.

REFERENCES

Abdul-razzaq, K. S., Ali, H. I. and Abdul-kareem, M. M., 2018. A New Strengthening Technique for Deep Beam Openings Using Steel Plates. *International Journal of Applied Engineering Research*, 12, pp. 15935-15947 .

Abdul-razzaq, K. S., Jebur, S. F. and Mohammed, A. H., 2018. Concrete and Steel Strengths Effect on Deep Beams with Reinforced Struts. *International Journal of Applied Engineering Research*, 13, pp. 66-73.

Adinkrah-Appiah, K., Adom-Asamoah, M., Afrifa, R. O, and Abeka, H., 2014. Evaluation of Shear strength of reinforced concrete deep beams.*ACI Structural Journal*, 111(3), pp. 718–720.

Andermatt, M. and Lubell, A., 2013. Behavior of Concrete Deep Beams Reinforced with Internal Fiber-Reinforced Polymer—Experimental Study. ACI Str. J., 110, pp. 585-594.

Andermatt, M. and Lubell, A., 2013B. Strength Modeling of Concrete Deep Beams Reinforced with Internal Fiber-Reinforced Polymer. ACI Str. J., 110, pp. 595-605.

ACI 318-14, 2014. *ACI 318-14. Building Code Requirements for Structural Concrete.American Concrete Institute*.

Ali, A. A. M., Mezher, T. M. and Raheem D., 2015. Rehabilitation of RC Deep Beams for Shear after Pre-crack by Near Surface Mounted CFRP Rods. *International Journal of Engineering Research and Technology (IJERT)*, 4(9), pp. 350–353.

Alius, F. *et al.*, 2020. Non-linear finite element analysis of reinforced concrete deep beam with web opening. *Journal of Civil Engineering*, 35(1), p. 3.

Al-Azzawi,A.A., Mahdy,A.H. and Farhan O. Sh., 2010. Finite element analysis of curved beams on elastic foundations. *Journal of the Serbian Society for Computational Mechanics*, 4, pp. 13-42.

Birrcher, D. B. *et al.*, 2014. Minimum web reinforcement in deep beams. *ACI Structural Journal*, 111(1), pp. 224–225.

Carreira, D.J. and Chu, K.H., 1985. Stress-strain relationship for plain concrete in compression. ACI Jorunal, Proceedings, 82(6), pp.797-804.

Chetchotisak, P. *et al.*, 2014. New strut-and-tie-models for shear strength prediction and design of RC deep beams.*Computers and Concrete*, 14(1), pp. 19–40.

Chinnaraj, C., Prasannan, S., Balavignesh, U. and Bastina, A.S., 2015. Study of crack development on deep beams with and without FRP. *International Journal of Applied Engineering Research*, 10(19), pp. 14350–14355.

Chen, H. *et al.*, 2020. Modeling of shear mechanisms and strength of concrete deep beams reinforced with FRP bars. *Composite Structures*, 234, p. 111715.

Chin, S. C. and Ing, D. S., 2015. Behaviour of reinforced concrete deep beams with openings in the shear zones. *Journal of Engineering and Technology*, 6(1), pp. 60–71.

Deng, S., Qie, Z. and Wang, L., 2015. Nonlinear Analysis of Reinforced Concrete Beam Bending Failure Experimentation Based on ABAQUS.*Proceedings of the First International Conference on Information Sciences, Machinery, Materials and Energy*, 126(Icismme), pp. 440–444.

Demir, A., Caglar, N. and Ozturk, H., 2019. Parameters affecting diagonal cracking behavior of reinforced concrete deep beams. *Engineering Structures*, 184, pp. 217–231.

European Commision, 2004. BS EN 1992-1-1:2004 Eurocode 2: Design of concrete structures – Part 1-1: General rules and rules for buildings.

Eun, H. C. *et al.*, 2006. On the shear strength of reinforced concrete deep beam with web opening. *Structural Design of Tall and Special Buildings*, 15(4), pp. 445–466.

Harsha, G. S. and Raju, P. P., 2019. Shear Strength of Deep Beams : A State of Art. *International journal of recent technology and engineering*, 7(6C2), pp. 532–535.

Ghoraba, A. K., El-Zoughiby, M. E. and El-Metwally, S. E., 2017. Strut-and-Tie Model Versus Nonlinear Finite Element Analysis of Rc Continuous Deep Beams With and Without Openings. *Engineering Research Journal*, 155, pp. 47–67.

Hassan, H., Medhlom, M. and Hatem, M., 2018. Behavior of self-compact reinforced concrete deep beams with small shear span to depth ratio. *MATEC Web of Conferences*, 162, pp. 1–8.

Hussain, H., 2018. Finite Element Analysis of Deep Beam Under Direct and Indirect Load. *Kufa Journal of Engineering*, 09(02), pp. 152–167.

Ibrahim, M., Wakjira, T. and Ebead, U., 2020. Shear strengthening of reinforced concrete deep beams using near-surface mounted hybrid carbon/glass fibre reinforced polymer strips. *Engineering Structures*, 210, p. 110412.

Kim, H. S., Lee, M. S. and Shin, Y. S., 2011. Structural behaviors of deep RC beams under combined axial and bending force. *Procedia Engineering*, 14, pp. 2212–2218.

Lafta, Y. J., 2016. Specification of deep beams affect the shear strength capacity. *Civil and Environmental Research*, 8(2), pp. 56–68.

Lima, M.M., Doh, J.H., Hadi, M.N. and Miller, D., 2016. The effects of CFRP orientation on the strengthening of reinforced concrete structures. The Structural Design of Tall and Special Buildings, [e-journal] 25(15), pp.759-784.

Leon, R. J. and Appa Rao, G., 2013. Performance of RC deep beams with different combinations of web reinforcement. *Applied Mechanics and Materials*, 343, pp. 21–26.

Metwally, I. M., 2014. Nonlinear analysis of concrete deep beam reinforced with GFRP bars using finite element method. *Malaysian Journal of Civil Engineering*, 26(2), pp. 224–250.

Mohamed, A. R., Shoukry, M. S. and Saeed, J. M., 2014. Prediction of the behavior of reinforced concrete deep beams with web openings using the finite element method. *Alexandria Engineering Journal*, 53(2), pp. 329–339.

Mohamed, K., Farghaly, A. S. and Benmokrane, B., 2014. Effect of web reinforcement in FRP-reinforced deep beams. *Proceedings of the 7th International Conference on FRP Composites in Civil Engineering, CICE 2014*.

Nayal, R. and Rasheed, H.A., 2006. Tension stiffening model for concrete beams reinforced with steel and FRP bars. Journal of Materials in Civil Engineering, 18(6), pp.831-841.

Noh, S.-Y., Lee, C.-Y. and Lee, K.-M., 2006. Deep Beam Design Using Strut-Tie Model, pp. 673–678.

Osman, B. H. Wu, E., Ji, B. and Abdulhameed S. S., 2017. Repair of Pre-cracked Reinforced Concrete (RC) Beams with Openings Strengthened Using FRP Sheets Under Sustained Load. *International Journal of Concrete Structures and Materials*, 11(1), pp. 171–183.

Pauw, A., 1960. Static modulus of elasticity of concrete as affected by density. ACI Jorunal, Proceedings, [e-journal] 57(12), pp.679-687. https://doi.org/10.14359/8040.

Rai, P., 2021. Non-Linear Finite Element Analysis of RC Deep Beam Using CDP Model. *Advances in Technology Innovation*, 6(1), pp. 01–10.

Raja, R. S., Kumar B. S. C. and Monica, A., 2019. Comparitive study on behaviour of deep beams. *International Journal of Recent Technology and Engineering*, 7(6C2), pp. 210–214.

Salamy, M.R., Kobayashi H. and Unjoh, Sh., 2005. Experimental and analytical study on reinforced concrete deep beams. *Asian hournal of civil engineering, 6, pp. 487-499.*

Shah, A., Haq, E. and Khan, S., 2011. Analysis and design of disturbed regions in concrete structures.*Procedia Engineering*, 14, pp. 3317–3324.

Shahbazpanahi, S. Karim, H. Abdullah, W. and Mosavi*, M*., 2021. Crack propagation modeling of strengthening of RC deep beams with CFRP plates. *Preprints*,1.

Shubhangi, M. and Reddy, K. R. C., 2014. Analysis of deep beam- A parametric study using Finite Element Method. *International Conference on Advances in Engineering & Technology*, pp. 34–39.

Suresh, G. S. and Kulkarni, S., 2016. Experimental study on behaviour of RC deep beams. *International Research Journal of Engineering and Technology (IRJET)*, 03(08), pp. 676–679.

Wahlgren, N. and Bailleul, N., 2016. Experimental analysis of limitations in the strut-and-tie method. Division of Structural Engineering.

Wahalathantri, B.L., 2012. Damage assessment in reinforced concrete flexural members using modal strain energy based method (Doctoral dissertation, Queensland University of Technology).

Yousif, J. L., 2016. Structural Behavior of Indirectly Loaded Deep Beams with and without Web Opening. Ph. D thesis, Huazhong University of Science & Technology Wuhan 430074.

Yang, K. H. Eun, H. C, and Chung, H. S. H. S., 2006. The influence of web openings on the structural behaviour of reinforced high-strength concrete deep beams. *Engineering Structures,* 28, pp. 1825-1834

Zhang, J. H., Li , S.S., Xie, W. and Guo, Y.D., 2020.Experimental study on shear capacity of high strength reinforcement concrete deep beams with small shear span-depth ratio.*Materials*, 13(5).

Zhang, N. and Tan, K. H., 2007.Size effect in RC deep beams: Experimental investigation and STM verification.*Engineering Structures*, 29(12), pp. 3241–3254.

APPENDICES

Appendix A: Shear Capacity Calculation Step

Reference	Calculation step	Remark
	For Reference Beam, R01	
	<u>Beam detail</u>	
	Beam overall depth, d: 350mm	
	Beam thickness, b_w: 80 mm	
	Beam full span length, l: 1330mm	
	Beam shear span length, a: 350mm	
	Beam effective depth, d_{eff}: 308mm	
	Shear span to effective depth ratio, a/d_{eff}:	
	350mm/308mm = 1.14	
	Shear span to depth ratio, a/d: 350mm/350mm	
	= 1.0	
	Concrete compressive strength, f'_c: 25.9MPa	
	Shear reinforcement diameter, d_v: 6mm	
	Shear reinforcement area, A_v: 113.10mm^2 for (2	
	legs and 2 shear links each side)	
	Shear reinforcement yield strength, f_{yv}: 425MPa	
	(for R6 shear link)	
	Steel plate width, w_b: 52.5mm	
	Angle between strut and tie	
	$\theta_s = tan^{-1}\left(\frac{0.9d}{a}\right)$	
	$\theta_s = tan^{-1}(\frac{0.9(308mm)}{350mm})$	
	$= 38.38\circ$	
	Concrete efficiency factor	
	$v = (1.8 - 38\varepsilon_1)(f'_c)^{-1/3}$	

Zwicky and Vogel (2006)	ε_1 is the tensile strain in the concrete in the direction of tension tie with suggested value of 0.00008. $v = (1.8 - 38(0.00008))(25.9MPa)^{-1/3}$ $= 0.607349235$ MPa	
Chetchotisak *et al* (2014)	**Width of prismatic strut** *Equation 3.12* $w_s = \sqrt{(kd)^2 + (w_b)^2}$ k = 0.3 according to classic bending theory and the bending theory formula proposed by Dhahir and Nadir (2020). $w_s = \sqrt{(kd)^2 + (w_b)^2}$ $\quad = \sqrt{(0.3*308mm)^2 + (52.5mm)^2}$ $\quad = 106.27$mm	
Chetchotisak *et al* (2014)	*Equation 3.13* $w_s = kd$ $\quad = 0.3*308mm$ $\quad = 92.4$mm **Shear capacity of deep beam** $V_n = vf'_c sin\theta_s b_w w_s + A_h f_{yh} tan\theta_s + A_v f_{yv}$ $\quad = 0.607*25.9MPa*sin(38.38°)*$ $80mm*106.27mm + 0 +$ $113.10mm^2 425MPa$ $\quad = 131.21$kN ∴ Failure load $= 2*V_n = 262.4$kN $V_n = vf'_c sin\theta_s b_w w_s + A_h f_{yh} tan\theta_s + A_v f_{yv}$ $\quad = 0.607*25.9MPa*sin(38.38°)*$ $80mm*92.4mm + 0 + 113.10mm^2 425MPa$ $\quad = 120.37$kN ∴ Failure load $= 2*V_n = 240.75$kN	For w_s = 106.27mm For w_s = 92.4mm

Reference	Calculation step	Remark
	For Control Beam, C01	
	Beam detail	
	Beam overall depth, d: 350mm	
	Beam thickness, b_w: 80 mm	
	Beam full span length, l: 1330mm	
	Beam shear span length, a: 245mm	
	Beam effective depth, d_{eff}: 308mm	
	Shear span to effective depth ratio, a/d_{eff}: 245mm/308mm = 0.8	
	Shear span to depth ratio, a/d: 245mm/350mm = 0.7	
	Concrete compressive strength, f'$_c$: 25.9MPa	
	Shear reinforcement diameter, d_v: 6mm	
	Shear reinforcement area, A_v: 113.10mm^2 for (2 legs and 2 shear links each side)	
	Shear reinforcement yield strength, f_{yv}: 425MPa (for R6 shear link)	
	Steel plate width, w_b: 52.5mm	
	Angle between strut and tie	
	$\theta_s = tan^{-1}\left(\frac{0.9d}{a}\right)$	
	$\theta_s = tan^{-1}(\frac{0.9(308mm)}{245mm})$	
	$= 48.53\circ$	
Zwicky and Vogel (2006)	**Concrete efficiency factor**	
	$v = (1.8 - 38\varepsilon_1)(f'_c)^{-1/3}$	
	ε_1 is the tensile strain in the concrete in the direction of tension tie with suggested value of 0.00008.	

Chetchotisak *et al* (2014) Chetchotisak *et al* (2014)	$v = (1.8 - 38(0.00008))(25.9MPa)^{-1/3}$ $= 0.607349235$ MPa **Width of prismatic strut** *Equation 3.12* $w_s = \sqrt{(kd)^2 + (w_b)^2}$ k = 0.3 according to classic bending theory and the bending theory formula proposed by Dhahir and Nadir (2020). $w_s = \sqrt{(kd)^2 + (w_b)^2}$ $= \sqrt{(0.3*308mm)^2 + (52.5mm)^2}$ $= 106.27$mm *Equation 3.13* $w_s = kd$ $= 0.3*308mm$ $= 92.4$mm **Shear capacity of deep beam** $V_n = vf'_c sin\theta_s b_w w_s + A_h f_{yh} tan\theta_s + A_v f_{yv}$ $= 0.607*25.9MPa*sin(48.53 \circ)*$ $80mm*106.27mm + 0 + 113.10mm^2*$ $425MPa$ $= 148.39$kN $\therefore$ Failure load $= 2*V_n = 296.77$kN $V_n = vf'_c sin\theta_s b_w w_s + A_h f_{yh} tan\theta_s + A_v f_{yv}$ $= 0.607*25.9MPa*sin(48.53 \circ)*$ $80mm*92.4mm + 0 + 113.10mm^2*$ $425MPa$ $= 135.31$kN $\therefore$ Failure load $= 2*V_n = 270.61$kN	For $w_s =$ 106.27mm For $w_s =$ 92.4mm

Reference	Calculation step	Remark
	For Test Beam, SVD-0.85	
	<u>Beam detail</u>	
	Beam overall depth, d: 350mm	
	Beam thickness, b_w: 80 mm	
	Beam full span length, l: 1330mm	
	Beam shear span length, a: 297.5mm	
	Beam effective depth, d_{eff}: 308mm	
	Shear span to effective depth ratio, a/d_{eff}: 297.5mm/308mm = 0.97	
	Shear span to depth ratio, a/d: 297.5mm/350mm = 0.85	
	Concrete compressive strength, f'_c: 25.9MPa	
	Shear reinforcement diameter, d_v: 6mm	
	Shear reinforcement area, A_v: 113.10mm^2 for (2 legs and 2 shear links each side)	
	Shear reinforcement yield strength, f_{yv}: 425MPa (for R6 shear link)	
	Steel plate width, w_b: 52.5mm	
	Angle between strut and tie	
	$\theta_s = tan^{-1}\left(\frac{0.9d}{a}\right)$	
	$\theta_s = tan^{-1}(\frac{0.9(308mm)}{297.5mm})$	
	$= 42.98\circ$	
	Concrete efficiency factor	
	$v = (1.8 - 38\varepsilon_1)(f'_c)^{-1/3}$	
Zwicky and Vogel (2006)	ε_1 is the tensile strain in the concrete in the direction of tension tie with suggested value of 0.00008.	

Chetchotisak *et al* (2014) Chetchotisak *et al* (2014)	$v = (1.8 - 38(0.00008))(25.9MPa)^{-1/3}$ $= 0.607349235$ MPa **Width of prismatic strut** *Equation 3.12* $w_s = \sqrt{(kd)^2 + (w_b)^2}$ k = 0.3 according to classic bending theory and the bending theory formula proposed by Dhahir and Nadir (2020). $w_s = \sqrt{(kd)^2 + (w_b)^2}$ $\quad = \sqrt{(0.3 * 308mm)^2 + (52.5mm)^2}$ $\quad = 106.27$mm *Equation 3.13* $w_s = kd$ $\quad = 0.3 * 308mm$ $\quad = 92.4$mm **Shear capacity of deep beam** $V_n = vf'_c sin\theta_s b_w w_s + A_h f_{yh} tan\theta_s + A_v f_{yv}$ $\quad = 0.607 * 25.9MPa * sin(42.98 °) *$ $80mm * 106.27mm + 0 + 113.10mm^2 *$ $425MPa$ $\quad = 139.35$kN ∴ Failure load = 2*V_n = 278.70kN $V_n = vf'_c sin\theta_s b_w w_s + A_h f_{yh} tan\theta_s + A_v f_{yv}$ $\quad = 0.607 * 25.9MPa * sin(42.98 °) *$ $80mm * 92.4mm + 0 + 113.10mm^2 *$ $425MPa$ $\quad = 127.45$kN ∴ Failure load = 2*V_n = 254.89kN	 For w$_s$ = 106.27mm For w$_s$ = 92.4mm

Reference	Calculation step	Remark
	For Test Beam, SVD-0.55	
	<u>Beam detail</u>	
	Beam overall depth, d: 350mm	
	Beam thickness, b_w: 80 mm	
	Beam full span length, l: 1330mm	
	Beam shear span length, a: 192.5mm	
	Beam effective depth, d_{eff}: 308mm	
	Shear span to effective depth ratio, a/d_{eff}:	
	192.5mm/308mm = 0.63	
	Shear span to depth ratio, a/d: 192.5mm/350mm	
	= 0.55	
	Concrete compressive strength, f'$_c$: 25.9MPa	
	Shear reinforcement diameter, d_v: 6mm	
	Shear reinforcement area, A_v: 113.10mm^2 for (2	
	legs and 2 shear links each side)	
	Shear reinforcement yield strength, f_{yv}: 425MPa	
	(for R6 shear link)	
	Steel plate width, w_b: 52.5mm	
	<u>Angle between strut and tie</u>	
	$\theta_s = tan^{-1}\left(\frac{0.9d}{a}\right)$	
	$\theta_s = tan^{-1}(\frac{0.9(308mm)}{192.5mm})$	
	$= 55.22°$	
Zwicky and Vogel (2006)	**<u>Concrete efficiency factor</u>**	
	$v = (1.8 - 38\varepsilon_1)(f'_c)^{-1/3}$	
	ε_1 is the tensile strain in the concrete in the	
	direction of tension tie with suggested value of	
	0.00008.	

	$v = (1.8 - 38(0.00008))(25.9 MPa)^{-1/3}$ $= 0.607349235$ MPa	
Chetchotisak *et al* (2014)	**Width of prismatic strut** *Equation 3.12* $w_s = \sqrt{(kd)^2 + (w_b)^2}$ k = 0.3 according to classic bending theory and the bending theory formula proposed by Dhahir and Nadir (2020). $w_s = \sqrt{(kd)^2 + (w_b)^2}$ $\quad = \sqrt{(0.3 * 308mm)^2 + (52.5mm)^2}$ $\quad = 106.27$mm	
Chetchotisak *et al* (2014)	*Equation 3.13* $w_s = kd$ $\quad = 0.3 * 308mm$ $\quad = 92.4$mm	
	Shear capacity of deep beam $V_n = vf'_c sin\theta_s b_w w_s + A_h f_{yh} tan\theta_s + A_v f_{yv}$ $\quad = 0.607 * 25.9 MPa * sin(55.22 \circ) *$ $80mm * 106.27mm + 0 + 113.10mm^2 *$ $425 MPa$ $\quad = 158.03$kN $\therefore$ Failure load $= 2*V_n = 316.05$kN	For w_s = 106.27mm
	$V_n = vf'_c sin\theta_s b_w w_s + A_h f_{yh} tan\theta_s + A_v f_{yv}$ $\quad = 0.607 * 25.9 MPa * sin(55.22 \circ) *$ $80mm * 92.4mm + 0 + 113.10mm^2 *$ $425 MPa$ $\quad = 143.69$kN $\therefore$ Failure load $= 2*V_n = 287.37$kN	For w_s = 92.4mm

Reference	Calculation step	Remark
	For Test Beam, SVD-0.4	
	<u>Beam detail</u>	
	Beam overall depth, d: 350mm	
	Beam thickness, b_w: 80 mm	
	Beam full span length, l: 1330mm	
	Beam shear span length, a: 140mm	
	Beam effective depth, d_{eff}: 308mm	
	Shear span to effective depth ratio, a/d_{eff}:	
	140mm/308mm = 0.45	
	Shear span to depth ratio, a/d: 140mm/350mm	
	= 0.4	
	Concrete compressive strength, f'$_c$: 25.9MPa	
	Shear reinforcement diameter, d_v: 6mm	
	Shear reinforcement area, A_v: 113.10mm^2 for (2	
	legs and 2 shear links each side)	
	Shear reinforcement yield strength, f_{yv}: 425MPa	
	(for R6 shear link)	
	Steel plate width, w_b: 52.5mm	
	Angle between strut and tie	
	$\theta_s = tan^{-1}\left(\frac{0.9d}{a}\right)$	
	$\theta_s = tan^{-1}(\frac{0.9(308mm)}{140mm})$	
	$= 63.20°$	
Zwicky and Vogel (2006)	**Concrete efficiency factor**	
	$v = (1.8 - 38\varepsilon_1)(f'_c)^{-1/3}$	
	ε_1 is the tensile strain in the concrete in the	
	direction of tension tie with suggested value of	
	0.00008.	

Chetchotisak *et al* (2014)	$v = (1.8 - 38(0.00008))(25.9MPa)^{-1/3}$ $= 0.607349235$ MPa **Width of prismatic strut** *Equation 3.12* $w_s = \sqrt{(kd)^2 + (w_b)^2}$ k = 0.3 according to classic bending theory and the bending theory formula proposed by Dhahir and Nadir (2020). $w_s = \sqrt{(kd)^2 + (w_b)^2}$ $\quad = \sqrt{(0.3 * 308mm)^2 + (52.5mm)^2}$ $\quad = 106.27$mm	
Chetchotisak *et al* (2014)	*Equation 3.13* $w_s = kd$ $\quad = 0.3 * 308mm$ $\quad = 92.4$mm **Shear capacity of deep beam** $V_n = vf'_c sin\theta_s b_w w_s + A_h f_{yh} tan\theta_s + A_v f_{yv}$ $\quad = 0.607 * 25.9MPa * sin(63.20°) *$ $80mm * 106.27mm + 0 + 113.10mm^2 *$ $425MPa$ $\quad = 167.56$kN ∵ Failure load = 2*V_n = 355.11kN $V_n = vf'_c sin\theta_s b_w w_s + A_h f_{yh} tan\theta_s + A_v f_{yv}$ $\quad = 0.607 * 25.9MPa * sin(55.22°) *$ $80mm * 92.4mm + 0 + 113.10mm^2 *$ $425MPa$ $\quad = 151.97$kN ∵ Failure load = 2*V_n = 303.94kN	For w$_s$ = 106.27mm For w$_s$ = 92.4mm

Appendix B: Models Captured Results
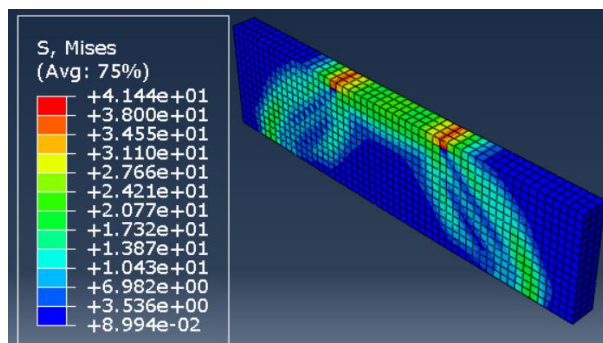
Figure B-1: Concrete Von Mises Stress Contour of R01
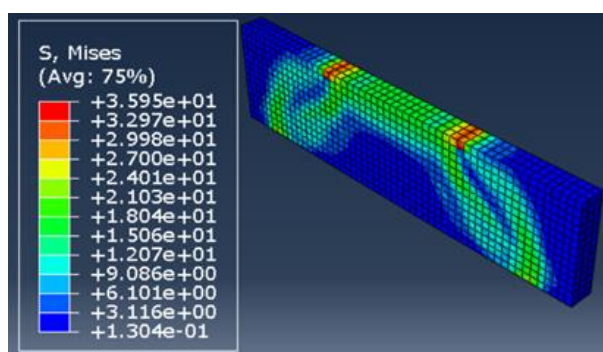
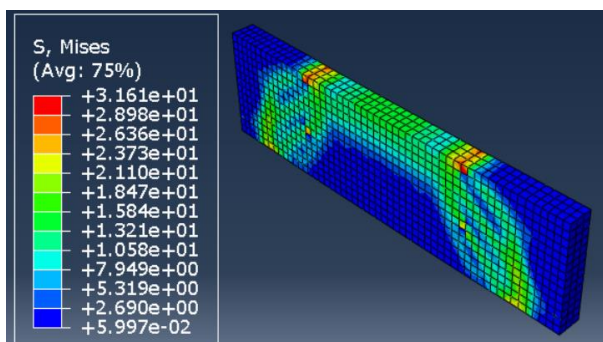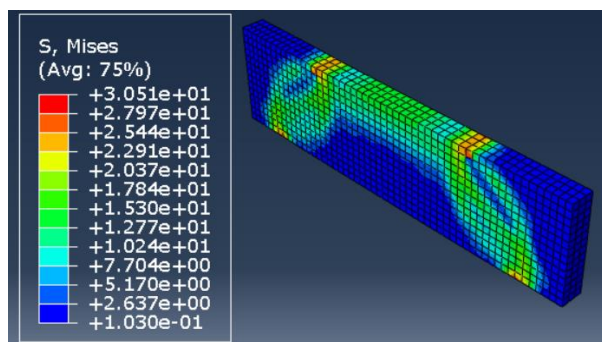Figure B-2: Concrete Von Mises Stress Contour of SVD-0.85
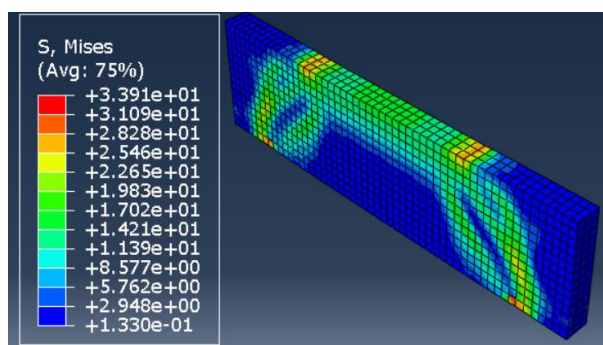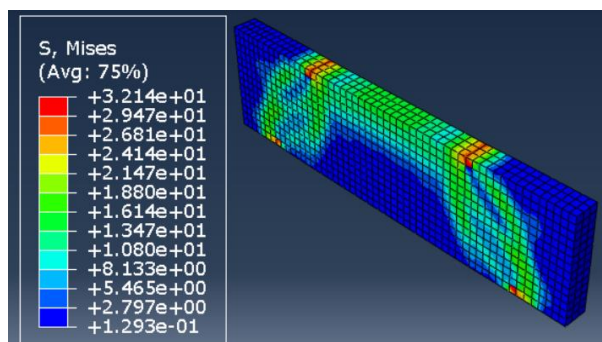

Figure B-3: Concrete Von Mises Stress Contour of C01
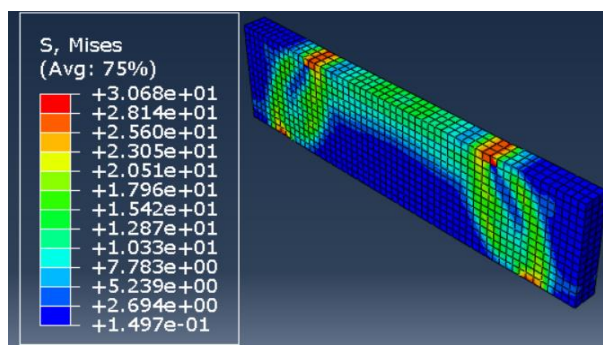
Figure B-4: Concrete Von Mises Stress Contour of SVD-0.55
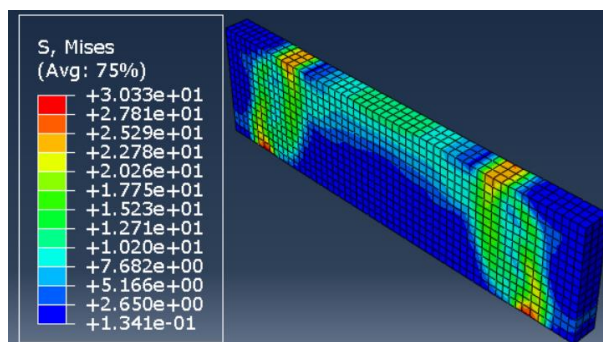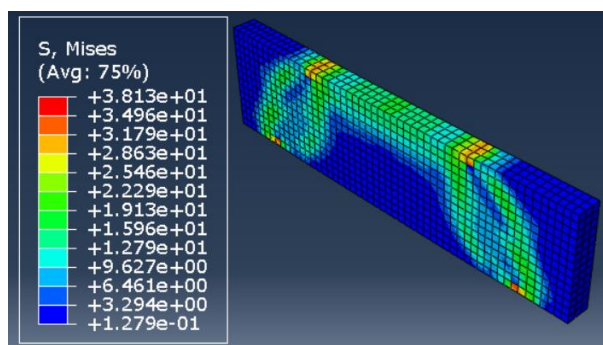

Figure B-5: Concrete Von Mises Stress Contour of SVD-0.4
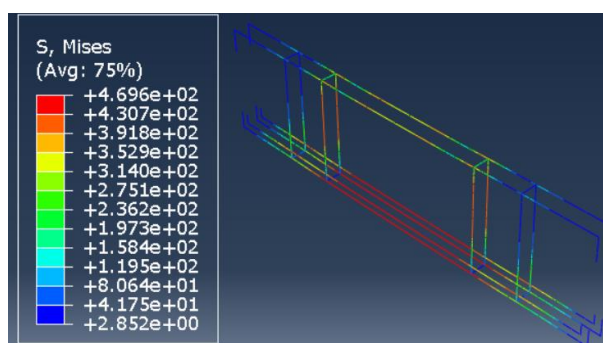
Figure B-6: Reinforcement cage Von Mises Stress Contour of R01
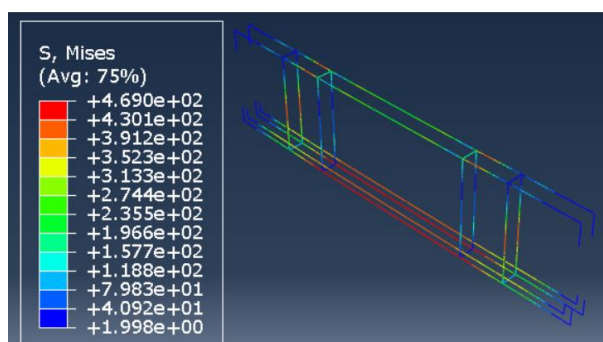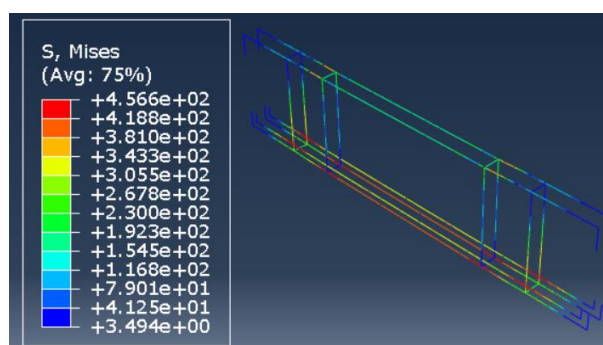

Figure B-7: Reinforcement cage Von Mises Stress Contour of SVD-0.85
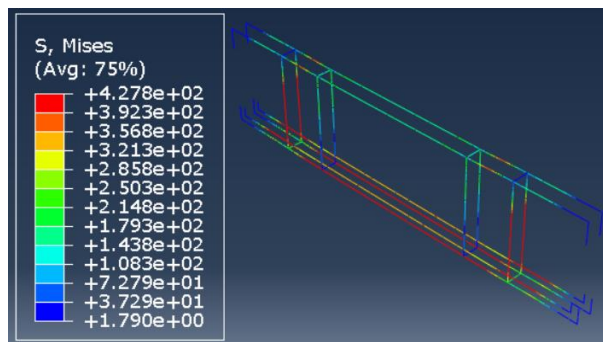
Figure B-8: Reinforcement cage Von Mises Stress Contour of C01
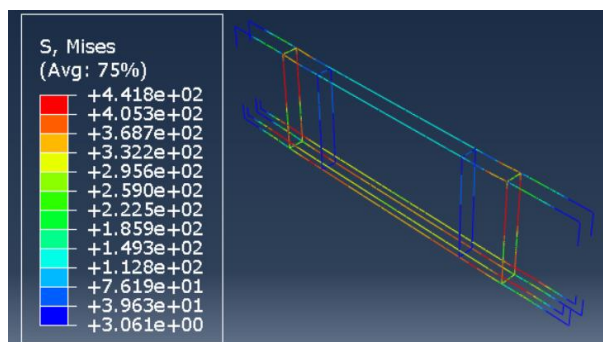
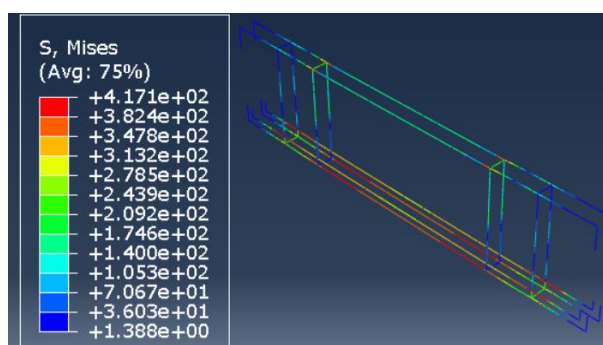

Figure B-9: Reinforcement cage Von Mises Stress Contour of SVD-0.55
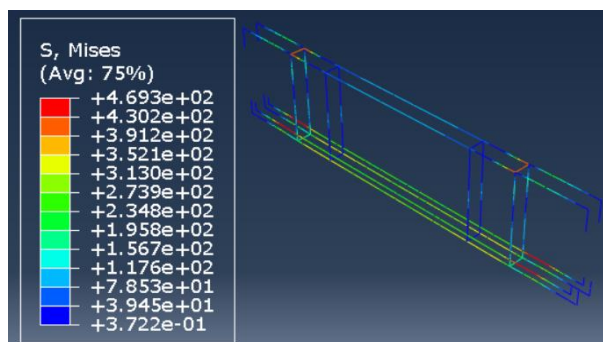
Figure B-10: Reinforcement cage Von Mises Stress Contour of SVD-0.4
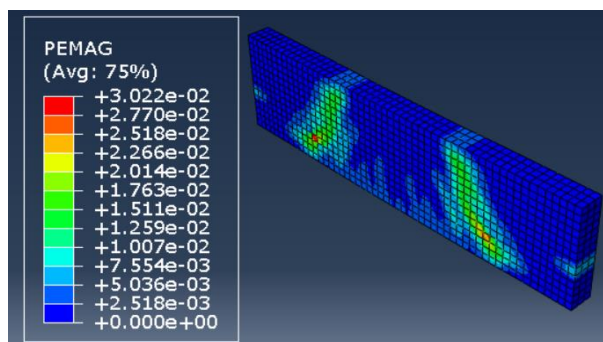
Figure B-11: PEMAG Diagram of R01
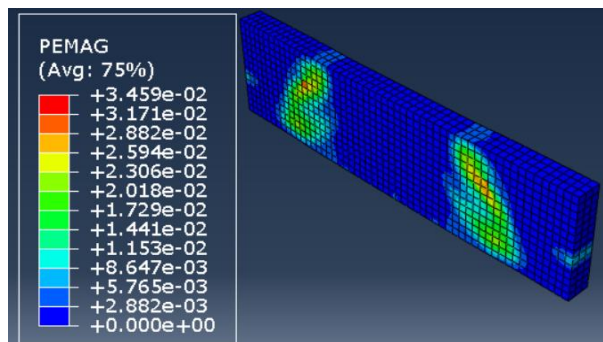
Figure B-12: PEMAG Diagram of SVD-0.85
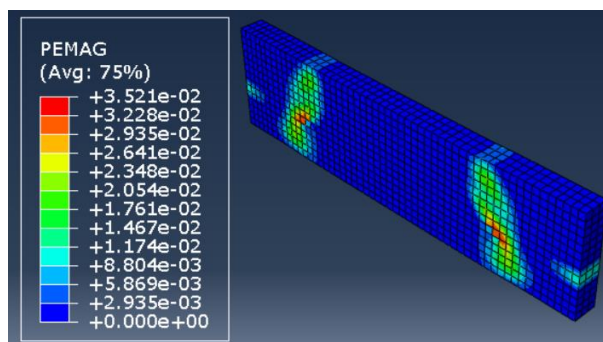
Figure B-13: PEMAG Diagram of C01
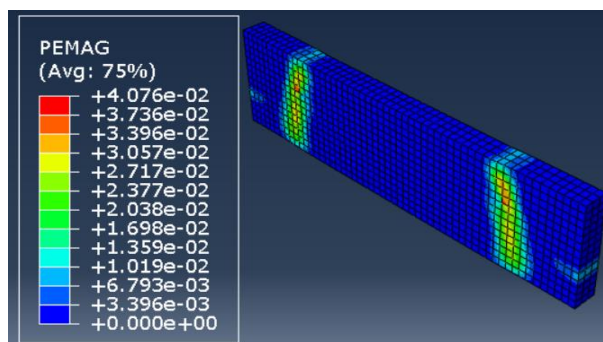
Figure B-14: PEMAG Diagram of SVD-0.55
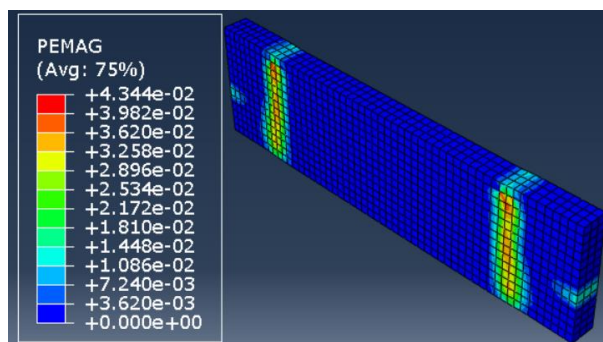
Figure B-15: PEMAG Diagram of SVD-0.4
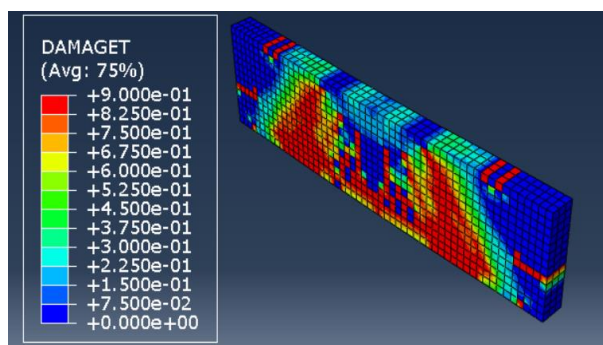
Figure B-16: Tension Damage Contour of R01
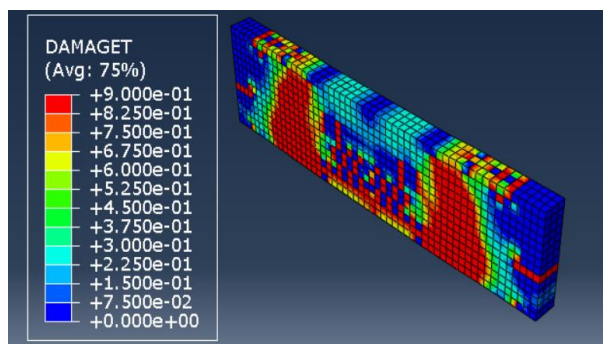
Figure B-17: Tension Damage Contour of SVD-0.85
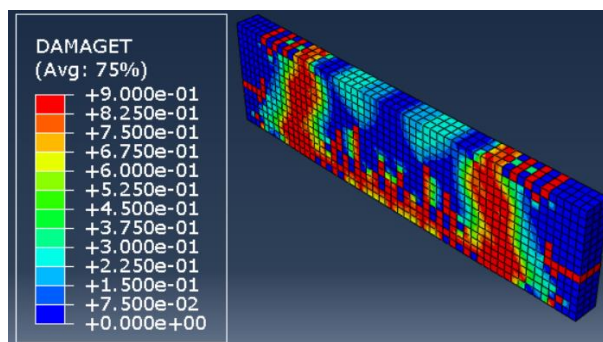
Figure B-18: Tension Damage Contour of C01
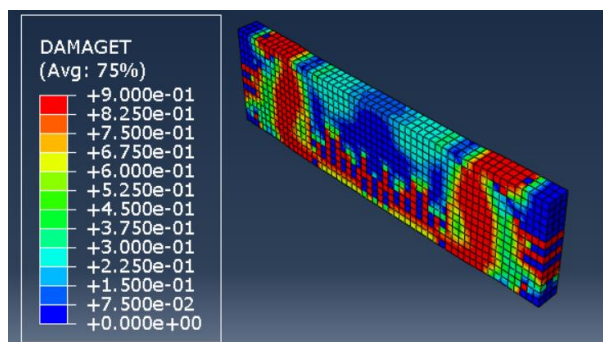
Figure B-19: Tension Damage Contour of SVD-0.55
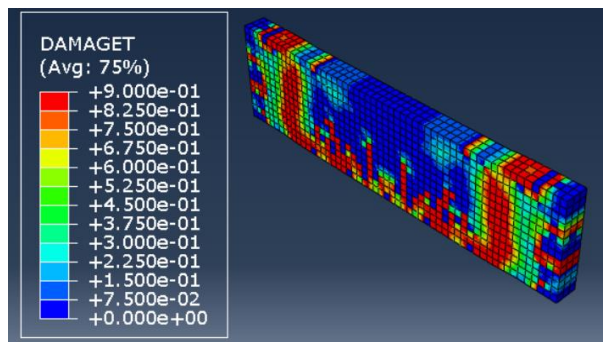
Figure B-20: Tension Damage Contour of SVD-0.4
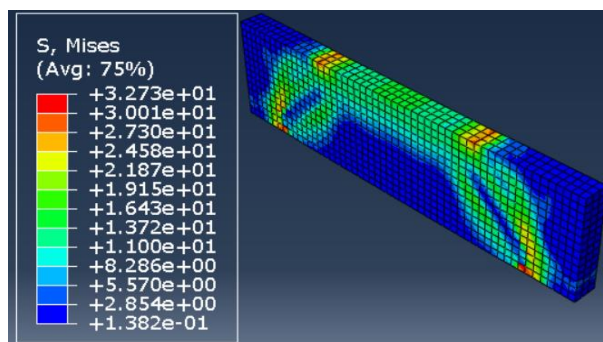
Figure B-21: Concrete Von Mises Stress Contour of SLR-T13
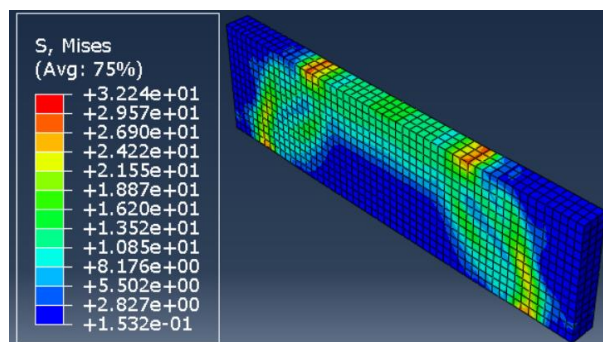
Figure B-22: Concrete Von Mises Stress Contour of SLR-T16
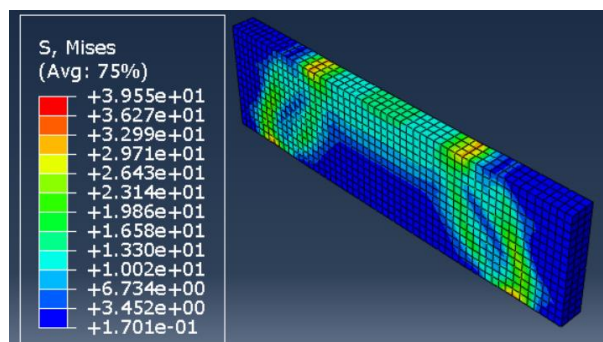
Figure B-23: Concrete Von Mises Stress Contour of SLR-T20
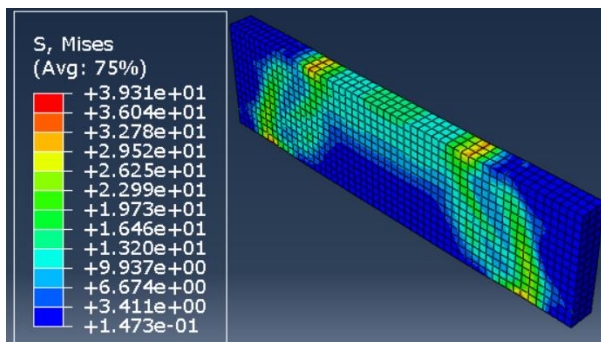
Figure B-24: Concrete Von Mises Stress Contour of SLR-T22
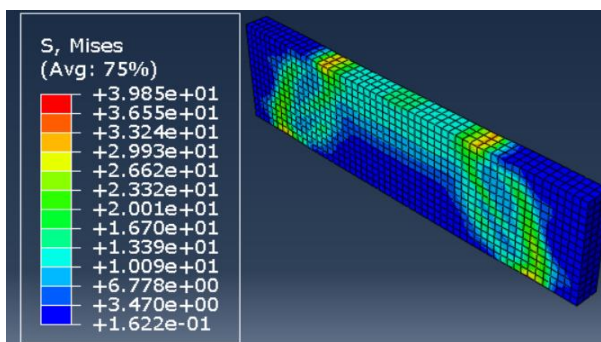
Figure B-25: Concrete Von Mises Stress Contour of SLR-T25
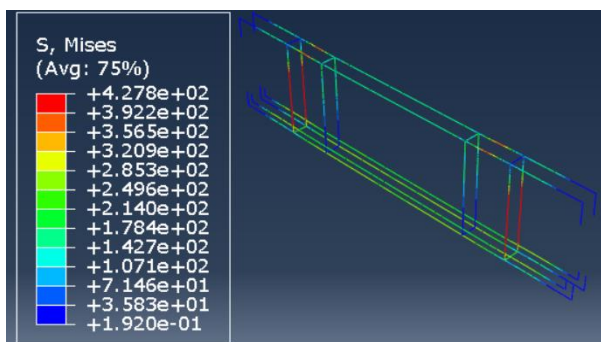
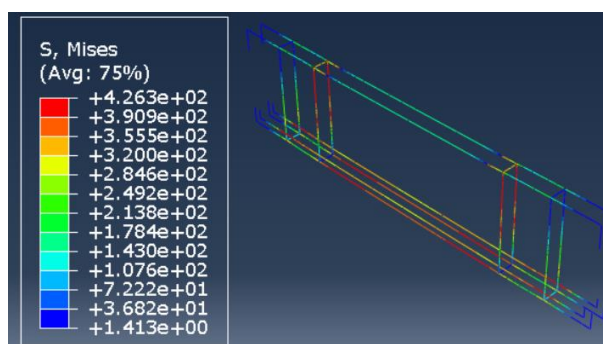Figure B-26: Reinforcement cage Von Mises Stress Contour of SLR-T13
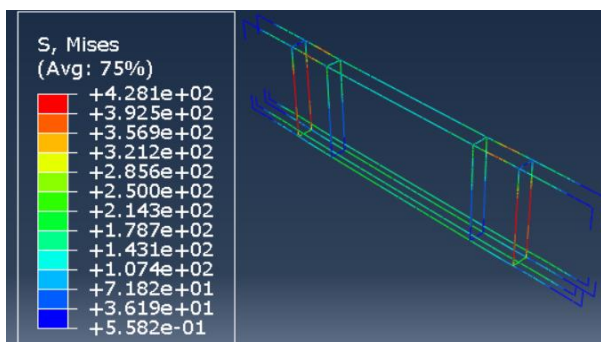
Figure B-27: Reinforcement cage Von Mises Stress Contour of SLR-T16
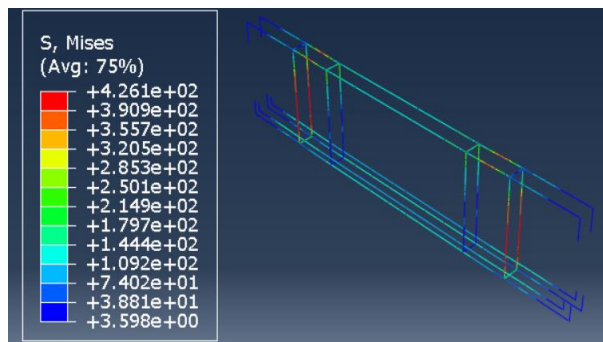
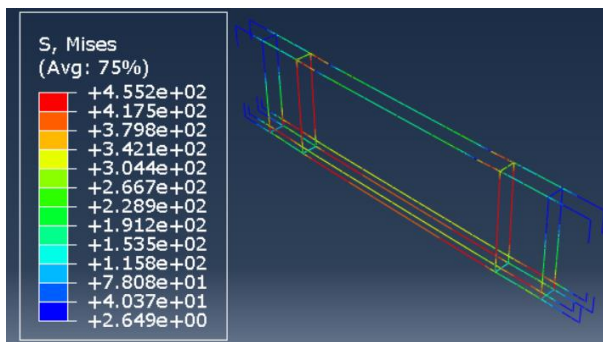Figure B-28: Reinforcement cage Von Mises Stress Contour of SLR-T20
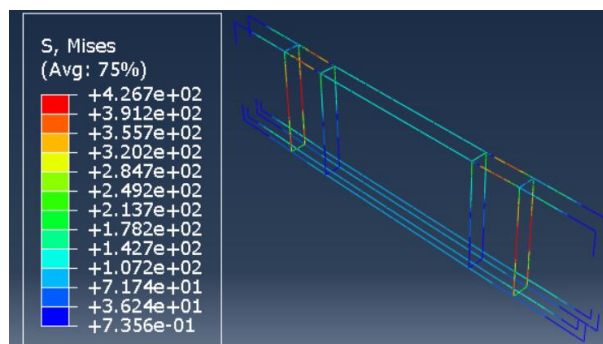
Figure B-29: Reinforcement cage Von Mises Stress Contour of SLR-T22
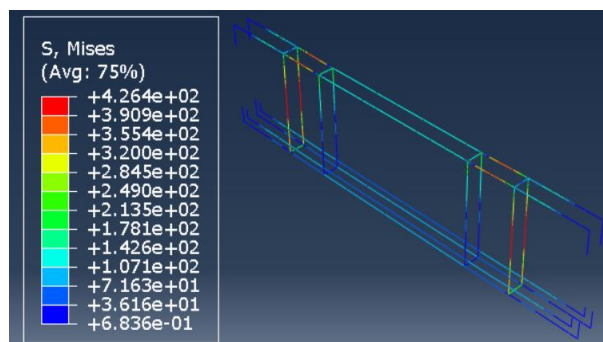
Figure B-30: Reinforcement cage Von Mises Stress Contour of SLR-T25
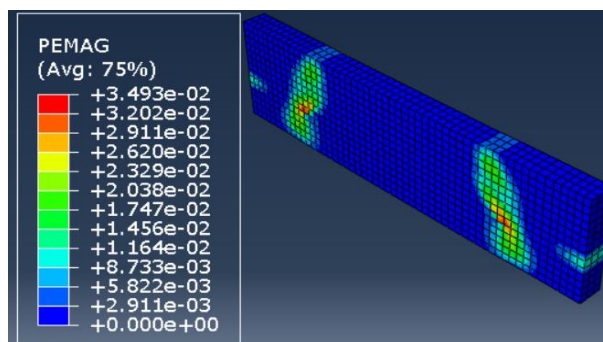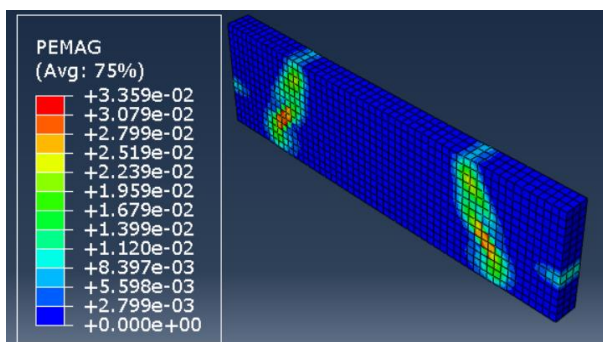

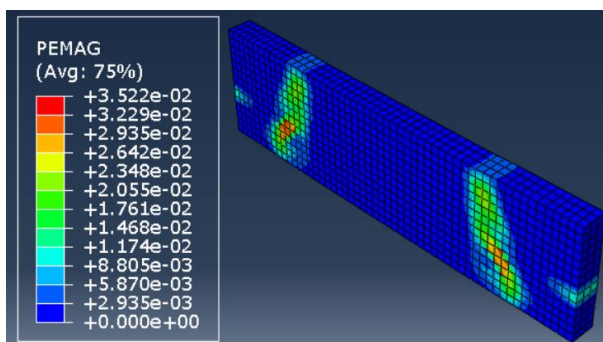Figure B-31: PEMAG Diagram of SLR-T13
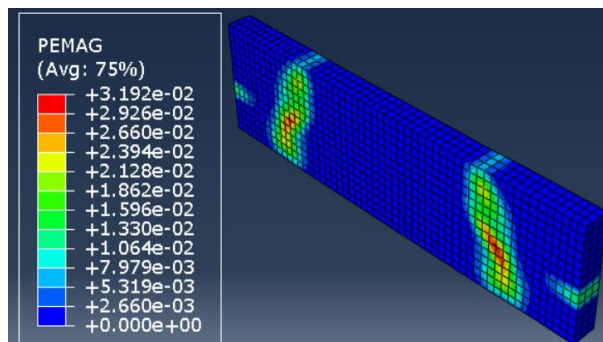
Figure B-32: PEMAG Diagram of SLR-T16
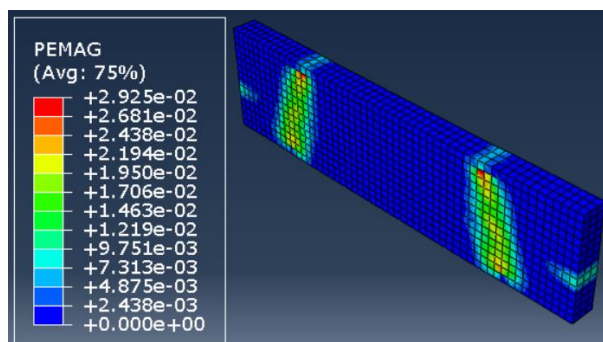
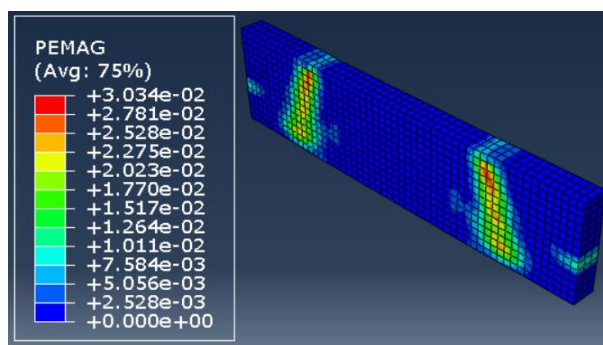Figure B-33: PEMAG Diagram of SLR-T20
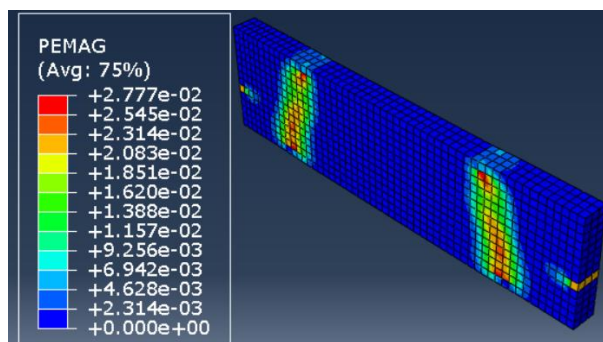
Figure B-34: PEMAG Diagram of SLR-T22
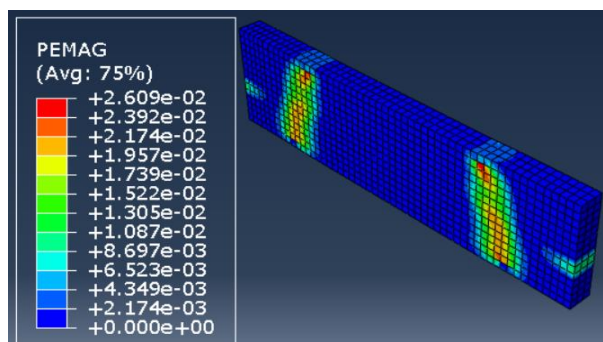
Figure B-35: PEMAG Diagram of SLR-T25
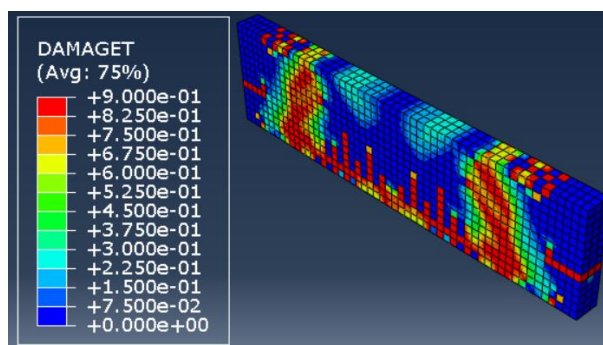
Figure B-36: Tension Damage Contour of SLR-T13
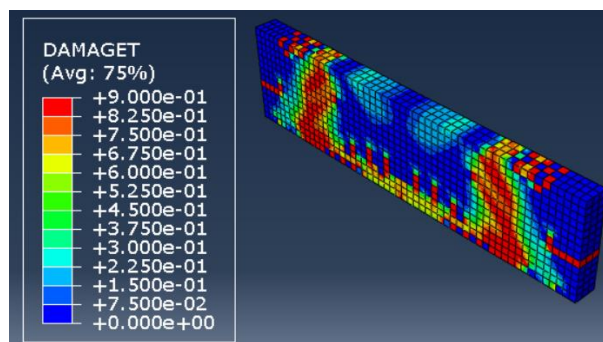
Figure B-37: Tension Damage Contour of SLR-T16
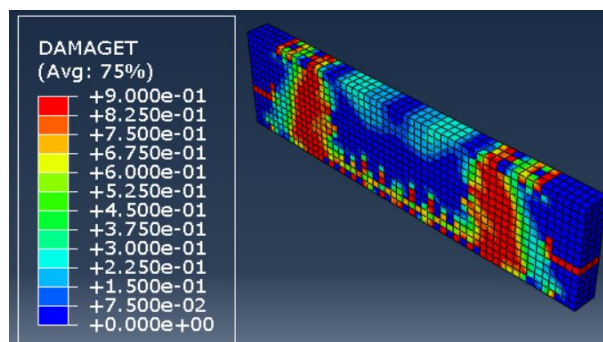
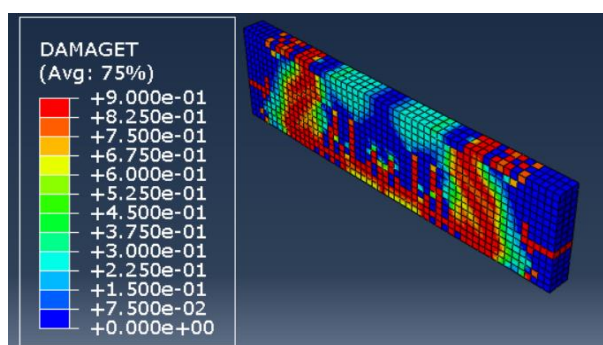
Figure B-38: Tension Damage Contour of SLR-T20
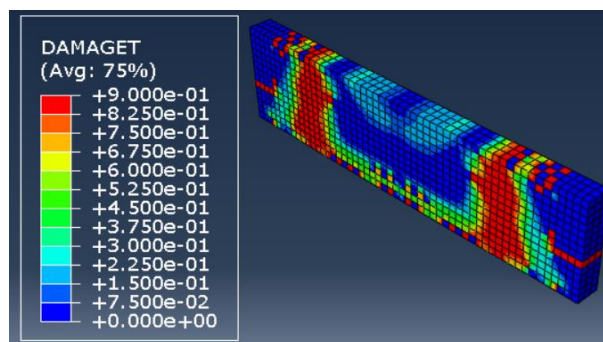
Figure B-39: Tension Damage Contour of SLR-T22
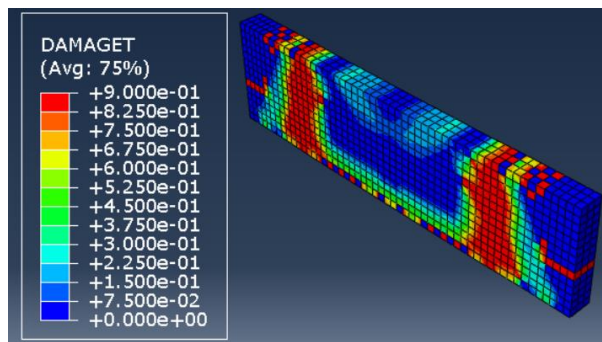
Figure B-40: Tension Damage Contour of SLR-T25

Figure B-41: Concrete Von Mises Stress Contour of SVL-375 mm

Figure B-42: Concrete Von Mises Stress Contour of SVL-400 mm

Figure B-43: Concrete Von Mises Stress Contour of SVL-425 mm

Figure B-44: Concrete Von Mises Stress Contour of SVL-425 mm

Figure B-45: Reinforcement cage Von Mises Stress Contour of SVL-375 mm

Figure B-46: Reinforcement cage Von Mises Stress Contour of SVL-400 mm

Figure B-47: Reinforcement cage Von Mises Stress Contour of SVL-425 mm

Figure B-48: Reinforcement cage Von Mises Stress Contour of SVL-450 mm
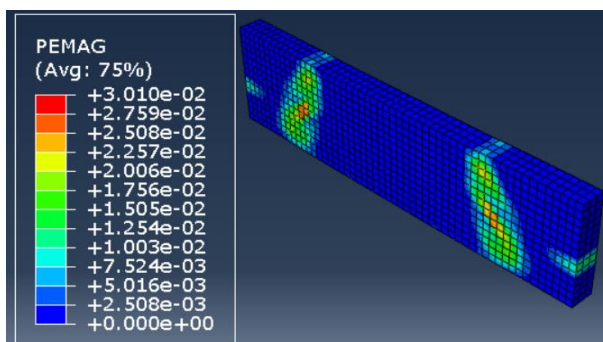
Figure B-49: PEMAG Diagram of SVL-375 mm

Figure B-50: PEMAG Diagram of SVL-400 mm

Figure B-50: PEMAG Diagram of SVL-425 mm

Figure B-51: PEMAG Diagram of SVL-450 mm

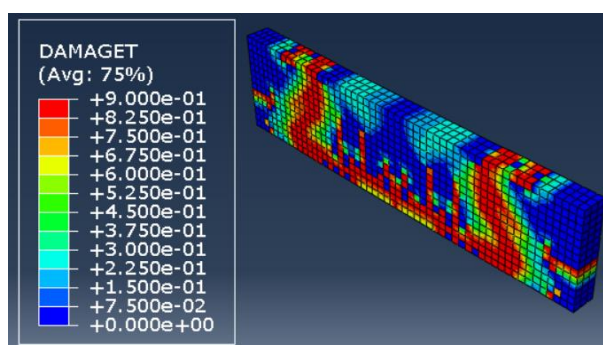
Figure B-52: Tension Damage Contour of SVL-375 mm

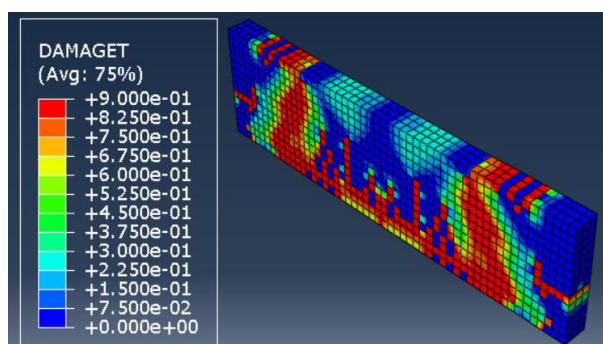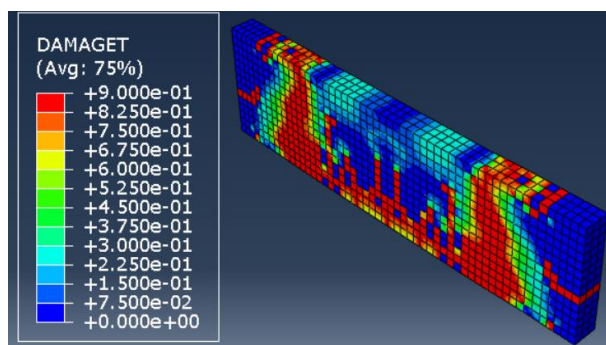Figure B-53: Tension Damage Contour of SVL-400 mm

Figure B-54: Tension Damage Contour of SVL-425 mm

Figure B-55: Tension Damage Contour of SVL-450 mm